Vol. 122 No. 1 March 1, 1980
(Computer Techniques and Optimization, Vol. 4 No. 1)
ISSN 0378-4304

ANALYTICA CHIMICA ACTA

International journal devoted to all branches of analytical chemistry

COMPUTER TECHNIQUES AND OPTIMIZATION

ELSEVIER SCIENTIFIC PUBLISHING COMPANY

ANALYTICA CHIMICA ACTA

International journal devoted to all branches of analytical chemistry
Revue internationale consacrée à tous les domaines de la chimie analytique
Internationale Zeitschrift für alle Gebiete der analytischen Chemie

PUBLICATION SCHEDULE FOR 1980 (incorporating the section on Computer Techniques and Optimization).

	J	F	M	A	M	J	J	A	S	O	N	D
Analytica Chimica Acta	113/1 113/2	114	115	116/1	116/2	117	118/1	118/2	119	120/1	120/2	121
Section on Computer Techniques and Optimization			122/1			122/2			122/3			122/4

Scope. *Analytica Chimica Acta* publishes original papers, short communications, and reviews dealing with every aspect of modern chemical analysis, both fundamental and applied. The section on *Computer Techniques and Optimization* is devoted to new developments in chemical analysis by the application of computer techniques and by interdisciplinary approaches, including statistics, systems theory and operation research. The section deals with the following topics: Computerized acquisition, processing and evaluation of data. Computerized methods for the interpretation of analytical data including chemometrics, cluster analysis, and pattern recognition. Storage and retrieval systems. Optimization procedures and their application. Automated analysis for industrial processes and quality control. Organizational problems.

Submission of Papers. Manuscripts (three copies) should be submitted as designated below for rapid and efficient handling:

Papers from the Americas to: Professor Harry L. Pardue, Department of Chemistry, Purdue University, West Lafayette, IN 47090, U.S.A.

Papers from all other countries to: Dr. A. M. G. Macdonald, Department of Chemistry, The University, P.O. Box 363, Birmingham B15 2TT, England.

For the section on *Computer Techniques and Optimization:* Dr. J. T. Clerc, Universität Bern, Pharmazeutisches Institut, Sahlistrasse 10, CH-3012 Bern, Switzerland.

American authors are recommended to send manuscripts and proofs by INTERNATIONAL AIRMAIL.

Information for Authors. Papers in English, French and German are published. There are no page charges. Manuscripts should conform in layout and style to the papers published in this Volume. Authors should consult Vol. 111, p. 343 for detailed information. Reprints of this information are available from the Editors or from: Elsevier Editorial Services Ltd., Mayfield House, 256 Banbury Road, Oxford OX2 7DE (Great Britain).

Reprints. Fifty reprints will be supplied free of charge. Additional reprints (minimum 100) can be ordered. An order form containing price quotations will be sent to the authors together with the proofs of their article.

Advertisements. Advertisement rates are available from the publisher.

Subscriptions. Subscriptions should be sent to: Elsevier Scientific Publishing Company, P.O. Box 211, 1000 AE Amsterdam, The Netherlands. The section on *Computer Techniques and Optimization* can be subscribed to separately.

Publication. *Analytica Chimica Acta* (including the section on *Computer Techniques and Optimization*) appears in 10 volumes in 1980. The subscription for 1980 (Vols. 113–122) is Dfl. 1390.00 plus Dfl. 160.00 (postage) (total approx. U.S. $756.00). The subscription for the *Computer Techniques and Optimization* section only (Vol. 122) is Dfl. 139.00 plus Dfl. 16.00 (postage) (total approx. U.S. $75.50). Journals are sent automatically by airmail to the U.S.A. and Canada at no extra cost and to Japan, Australia and New Zealand for a small additional postal charge. All earlier volumes (Vols. 1–112) except Vols. 23 and 28 are available at Dfl. 150.00 (U.S. $73.00), plus Dfl. 10.00 (U.S. $5.00) postage and handling, per volume.

Claims for issues not received should be made within three months of publication of the issue, otherwise they cannot be honoured free of charge.

Customers in the U.S.A. and Canada who wish to obtain additional bibliographic information on this and other Elsevier journals should contact Elsevier/North Holland Inc., Journal Information Center, 52 Vanderbilt Avenue, New York, NY 10017. Tel: (212) 867-9040.

ANALYTICA CHIMICA ACTA
VOL. 122 (1980)
(Computer Techniques and Optimization, Vol. 4)

ANALYTICA CHIMICA ACTA

International journal devoted to all branches of analytical chemistry

COMPUTER TECHNIQUES AND OPTIMIZATION

VOL. 4 1980

ELSEVIER SCIENTIFIC PUBLISHING COMPANY

Anal. Chim. Acta, Vol. 122 (1980)

Printed in The Netherlands.

Analytica Chimica Acta, 122 (1980) 1—26
Computer Techniques and Optimization

COMPUTER IMPLEMENTATION OF SIMULATION MODELS FOR NON-LINEAR, NON-IDEAL CHROMATOGRAPHY

Part 1. Fundamental Mathematical Considerations

J. C. SMIT and H. C. SMIT*

Laboratory for Analytical Chemistry, University of Amsterdam, Nieuwe Achtergracht 166, 1018 WV Amsterdam (The Netherlands)

E. M. DE JAGER

Institute of Applied Mathematics, University of Amsterdam, Roetersstraat 15, Amsterdam (The Netherlands)

(Received 25th May 1979)

SUMMARY

A proper mathematical model is essential for understanding processes in chromatographic columns. In this paper two models are developed, a discrete and a continuous model, both describing the behaviour of mass transport in chromatographic columns, with linear or non-linear distribution isotherms and with or without longitudinal dispersion. The discrete model is used for computer simulations of chromatographic problems. The mathematical expressions are derived from physical fundamentals in such a way that computer implementation is feasible without great problems. To check the correctness of the numerical solutions, exact solutions of parts of the continuous model are derived. The influence of the choice of explicit difference schemes on the numerical solution is discussed.

Accurate knowledge of mass transport in columns can be very valuable in many fields of chromatography, particularly in studies of the influence of all possible column parameters in chromatographic separation and in several kinds of optimization (resolution, analysis time, costs, etc.). In research of new techniques like correlation chromatography [1], knowledge of column response on several input signals, both stochastic and deterministic, is also valuable. In preparative chromatography, where sample concentrations in the mobile phase become large, the conventional description of analytical peaks at zero concentration is no longer valid and non-linear isotherms are introduced. With the formulation of a chromatographic model, a non-linear partial differential equation is obtained for which in most cases exact solutions are unknown.

With the increasing use of digital computers in analytical laboratories, simulation of these problems is carried out to avoid rather complicated mathematical methods. Unless precautions are taken, this approach will often lead to time-consuming simulation programs without obtaining really reliable

results. Furthermore, it must be realized that the development of a simulation model causes a lot of programming work with technical problems as well as scientific requirements.

An important part of simulation is checking the results, wherever possible with the exact solutions. For this purpose, the chromatographic theories used were based on the original work of DeVault [2] and Wilson [3], who described a continuous mathematical model in non-linear ideal liquid chromatography. Many other workers based their models on the previous work of DeVault to describe gas, ion-exchange and partition chromatography with finite concentrations [4—7]. Of great importance is the suggestion to use the method of characteristics for obtaining exact solutions of the ideal non-linear chromatography problem [8], in mathematics defined as a Cauchy problem. This solution technique is used on a large scale in gas dynamics and fluid mechanics [9—12].

STRATEGY AND OBJECTIVES

The base of a "simulation model" is the formulation of objectives and strategy. The starting point is the "physical reality" which can be converted to a verbal model depending on the objectives of the experiment. Since the verbal model is an abstraction of the physical reality, differences between the model and reality may arise. Simplifications of the model are limited by the admissibility of mapping errors. The representation of the physical reality into a verbal model will never be a one-to-one mapping. The final aim is to arrive at a manipulative computer implementation, starting from the verbal model (Fig. 1). The first abstraction of the verbal model (in this case a mass

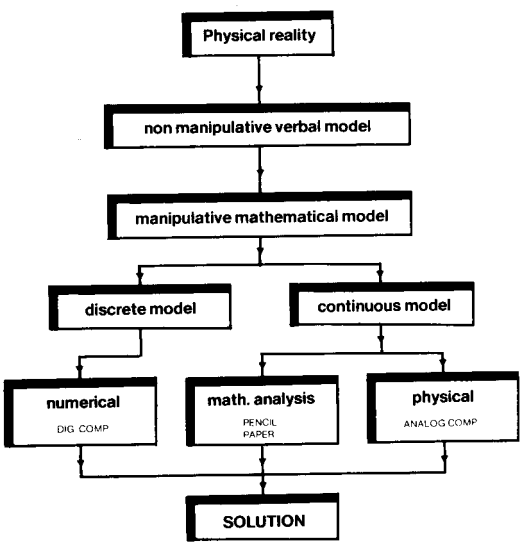

Fig. 1. Flow diagram of the simulation procedure.

conservation law) depends on the choice of the "description technique". An integral form is obtained by using a mathematical one. The next step is the conversion of the conservation (integral) form to a continuity (differential or difference) conservation form.

For the solution of the mathematical model in differential or difference equation form, a choice can be made between several solution techniques. First, there are analytical solution techniques. Of course, in general the evaluation of a complete solution of the mathematical problem makes simulation superfluous. Nevertheless, complete solutions of parts of the mathematical problem can be used to check the simulation results. The implementation of the mathematical model in a system with easily manipulative physical components with the same mathematical properties is called a physical solution technique. A well-known example is the solution of differential or difference equations by an analog computer. In the numerical solution technique the digital computer is the main tool. The execution of the solution technique can be considered as a numerical experiment, realized by a computer or calculating algorithm. "Simulation" of a physical reality means the realization of the solution by means of a numerical or physical solution technique.

THE VERBAL MODEL AND CONTINUOUS MATHEMATICAL MODELS

Simplifications

Before the verbal model is formulated the simplifications according to nonlinear chromatography with longitudinal dispersion must be considered. A theoretical homogeneous column model with an infinite length is considered, defined as an interval $-\infty < z < +\infty$; the cross-section is independent of z with area A. Furthermore a mobile and a stationary phase can be distinguished. The chromatographic detector is considered as an infinitely small cross-sectional area on $z = L$ with the same characteristics of a column segment, measuring the sample concentration in the mobile phase C^m and the sample concentration in the stationary phase C^s together. The column temperature is invariant in time and place. The equilibrium between the two phases is thermodynamically reversible. The equilibrium concentrations between stationary and mobile phase may be described by an expression $C^s = f(C^m)$ (distribution isotherm), where the functional dependence is invariant with time and place.

To describe a general model for chromatographic mass transport the term distribution isotherm is used for solution equilibria as well as for adsorption equilibria. The averaged linear velocity of the moving phase is constant along the length and cross-section of the column (the fluid is incompressible). The axial molecular diffusion and the eddy mixing effect are represented by a single parameter D, where D is assumed to be independent of the fluid velocity. No dispersion occurs in the stationary phase.

Verbal and mathematical models

The verbal model consists of the formulation of a mass conservation law

of a sample in a fixed domain G with the distinction of a mobile phase and a stationary phase, and a partition of solute or sample material among the two phases. The conservation law asserts that in a fixed domain G with volume $A(z_2 - z_1)$ the rate of change of a total amount of solute is equal to the solute flux at the boundaries of the domain. This leads to the general mathematical formulation of the mass conservation law in divergence form [13]

$$\frac{\partial}{\partial t}\int_{z_1}^{z_2} C^t(t,z)A \, dz = -\int_{z_1}^{z_2} A \cdot \operatorname{div} J(t,z) dz \tag{1}$$

where C^t denotes the total solute concentration, $J(t,z)$ the mass flux, and A the cross-sectional area of the column. Considering a point (t,z) in the neighbourhood of which C^t and the flux J have continuous partial derivatives, integration and differentiation can be interchanged; because eqn. (1) is valid for all z_1 and z_2 in a sufficiently small neighbourhood of z, integration can be omitted, which results in the so-called differential conservation law

$$\partial C^t(t,z)/\partial t = -\partial J(t,z)/\partial z \tag{2}$$

In the model, transport will occur only in the cross-sectional fraction ϵA, which means that the flux $J(t,z)$ will be

$$J(t,z) = C^m(t,z)\langle v\rangle\epsilon - D\epsilon\,[\partial C^m(t,z)]/\partial z \tag{3}$$

where $C^m(t,z)$ denotes the solute concentration in the mobile phase, ϵ the fraction of the cross-sectional area occupied by the fluid stream, $\langle v\rangle$ the average fluid velocity over the corresponding cross-sectional area, and D the already defined dispersion coefficient of the solute in the mobile phase.

With the expression

$$C^t = (1 - \epsilon)C^s + \epsilon C^m \tag{4}$$

where C^s is the solute concentration in the stationary phase, and $(1 - \epsilon)$ is the fraction of the cross-section occupied by the stationary phase, we find

$$\epsilon C^m = C^t/\{1 + [(1 - \epsilon)C^s/\epsilon C^m]\} \tag{5}$$

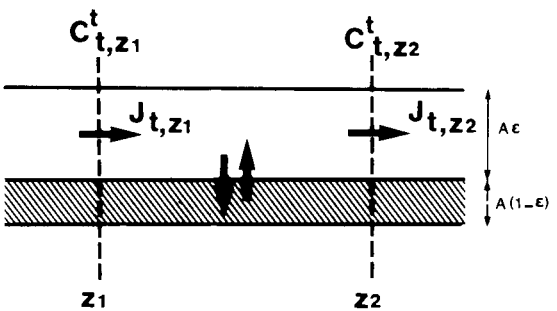

Fig. 2. Schematic representation of a column segment.

Substituting eqn. (5) into eqn. (3) gives the mass flux in terms of C^t, i.e.

$$J(t,z) = V^*C^t(t,z) - \frac{\partial}{\partial z}\{D^*C^t(t,z)\} \tag{6}$$

where $V^* = \langle v\rangle/[1 + (1 - \epsilon/\epsilon)(C^s/C^m)]$

and $D^* = D/[1 + (1 - \epsilon/\epsilon)(C^s/C^m)]$

Here V^* is the generally accepted definition of the migration velocity. Now the mass transport equation can be found by substituting eqn. (6) into (2)

$$\partial C^t(t,z)/\partial t = -\partial V^*C^t(t,z)/\partial z + \partial^2 D^*C^t(t,z)/\partial z^2 \tag{7}$$

The derived expression is an appropriate mathematical model describing mass transport in columns with non-linear distribution isotherms. One of the advantages of this model is that it retains the divergence form, which is extremely useful for numerical simulations.

Using $\partial V^*C^t/\partial z = \epsilon\langle v\rangle\, \partial C^m/\partial z = [\epsilon\langle v\rangle\, dC^m/dC^t]\, [\partial C^t/\partial z]$, and the relation (4), and similarly for the second term of the right-hand side of (7), we obtain

$$\partial C^t(t,z)/\partial t = -V^{**}\, \partial C^t(t,z)/\partial z + (\partial/\partial z)\{D^{**}\, \partial C^t(t,z)/\partial z\} \tag{8}$$

where $V^{**} = \langle v\rangle/1 + [(1 - \epsilon/\epsilon)dC^s/dC^m]$

and $D^{**} = D/1 + [(1 - \epsilon/\epsilon)dC^s/dC^m]$

By substituting eqns. (4) and (3) into (2) a mathematical expression can be derived in mobile phase concentrations

$$\partial C^m(t,z)/\partial t = -V^{**}\, \partial C^m(t,z)/\partial z + D^{**}\, \partial^2 C^m(t,z)/\partial z^2 \tag{9}$$

Equation (9) is the same as that derived by Huber and Gerritse [14] and earlier workers in this field. In the dispersionless case ($D^{**} = 0$) two partial differential equations which are the same in mathematical sense are obtained.

As to the use of eqns. (8) and (9) for C^t and C^m, it is important to note that these equations are valid only as long as C^t and C^m can be continuously differentiated. However, it is well known that the solutions in the dispersionless case ($D^{**} = 0$) may exhibit discontinuities (shocks) and in that case one needs the mass conservation law (eqn. (1)) to establish the velocity of propagation of the discontinuity (see also eqns. (69) and (70)). Since for non-linear distribution isotherms there is a time-dependent exchange of concentrations between the mobile and the stationary phase, there is no mass conservation law for C^m or C^s. Therefore, in a mathematical model for the dispersionless case, eqn. (8) with $D^{**} = 0$ is to be preferred to eqn. (9) with $D^{**} = 0$.

Moreover, a useful check for numerical results is provided by the relation

$$\frac{\partial}{\partial t}\int_{-\infty}^{+\infty} C^t(t,z)dz = 0 \tag{10}$$

a formula which does not hold for $C^m(t,z)$.

Finally, eqn. (9) is, in contrast to eqn. (8), not in divergence form and so it is less appropriate for numerical calculations than the equation for C^t (see below).

A DISCRETE MATHEMATICAL MODEL

Discretization errors of the model

A discrete mathematical model may be derived directly from the verbal model. In this case however, another approach is possible, namely to replace the differential operators in eqn. (7) by difference operators; thus

$$\Delta C^t/h = -\nabla V^* C^t/l + \delta^2 D^* C^t/l^2 \tag{11}$$

In this equation Δ denotes a forward difference operator, ∇ a backward difference operator, δ a central difference operator, and h and l are Δt and Δz, respectively.

These operators are defined by

$$\left.\begin{aligned} \Delta C^t &= C^t(t+h,z) - C^t(t,z) \\ \nabla C^t &= C^t(t,z) - C^t(t,z-l) \\ \delta C^t &= C^t\left(t,z+\tfrac{1}{2}l\right) - C^t\left(t,z-\tfrac{1}{2}l\right) \\ \delta^2 C^t &= C^t(t,z+l) - 2C^t(t,z) + C^t(t,z-l) \end{aligned}\right\} \tag{12}$$

To check the linear numerical model, which implies a linear distribution isotherm, V^* and D^* should be independent of the concentration. If $V^* = V_c$ and $D^* = D_c$, then the transport may be described by the differential equation

$$\partial C^t/\partial t = -V_c\, \partial C^t/\partial z + D_c\, \partial^2 C^t/\partial z^2 \tag{13}$$

and given initial and boundary conditions.

Although this initial value problem can be solved in closed mathematical form, e.g. by means of a so-called elementary solution, a numerical solution of this problem is also very useful, because the discretization procedure, without careful precautions, often involves the introduction of errors which are not directly recognizable. Experience with discretization procedures in solving a linear initial value problem may be of great value for numerical procedures applied to non-linear initial value problems.

Apart from such considerations it will appear in Part 2 of this series that the numerical treatment of the initial value problem (eqn. 13) leads to interesting results. A Taylor series expansion gives

$$\frac{\Delta C^t}{h} = \frac{\partial C^t}{\partial t} + \frac{\partial^2 C^t}{\partial t^2}\cdot\frac{h}{2} + \frac{\partial^3 C^t}{\partial t^3}\cdot\frac{h^2}{6} + \cdots\cdots \tag{14}$$

$$\frac{\nabla C^t}{l} = \frac{\partial C^t}{\partial z} - \frac{\partial^2 C^t}{\partial z^2}\cdot\frac{l}{2} + \frac{\partial^3 C^t}{\partial z^3}\cdot\frac{l^2}{6} - \cdots\cdots \tag{15}$$

$$\frac{\delta^2 C^t}{l^2} = \frac{\partial^2 C^t}{\partial z^2} + \frac{\partial^4 C^t}{\partial z^4} \cdot \frac{l^2}{12} + \cdots\cdots \tag{16}$$

Substituting eqn. (13) into (14) and changing the order of differentiation, the result will be

$$\frac{\Delta C^t}{h} = -V_c \frac{\partial C^t}{\partial z} + D_c \frac{\partial^2 C^t}{\partial z^2} + \frac{h}{2}\frac{\partial}{\partial z}\left\{-V_c \frac{\partial C^t}{\partial t}\right\} + \frac{h}{2}\frac{\partial^2}{\partial z^2}\left\{D_c \frac{\partial C^t}{\partial t}\right\} + \cdots\cdots \tag{17}$$

By substituting again eqn. (13) into (17) and replacing all partial derivatives by differences by means of eqns. (15) and (16), we obtain

$$\frac{\Delta C^t}{h} = -V_c \frac{\nabla C^t}{l} + \left(D_c - V_c \cdot \frac{l}{2} + V_c^2 \frac{h}{2}\right)\frac{\delta^2 C^t}{l^2} + \cdots\cdots \tag{18}$$

The numerical dispersion $\left(-V_c \cdot \frac{l}{2} + V_c^2 \frac{h}{2}\right)$ can only be reduced to zero by a proper choice of l and h in a first-order approach. It is easy to see that in that case we obtain the condition

$$V_c = l/h \tag{19}$$

Propagation of errors in the statistical moments

To describe errors in the computer algorithm, from the point of view of the application to chromatography, it suffices to consider a rectangular pulse as initial condition. As chromatographic results are mostly characterized by statistical moments, the correctness of the algorithm will be investigated in relation to the exactness of the moments obtained in the discrete model. Many workers in this field have studied the behaviour of the statistical moments with more or less simplified models [15—18]. Substituting eqn. (12) into (11) and supposing that the distribution isotherm is linear, a first-order approach gives

$$y_n^{k+1} = y_n^k + h\{\alpha y_{n+1}^k + \beta y_n^k + \gamma y_{n-1}^k\} \tag{20}$$

where $y_n^{k+1} = C^t(t + h,z)$, $y_{n+1}^k = C^t(t,z + l)$, $y_n^k = C^t(t,z)$, $y_{n-1}^k = C^t(t,z - l)$, $\alpha = D_c/l^2$, $\beta = -V_c/l - 2D_c/l^2$, and $\gamma = V_c/l + D_c/l^2$.

Introducing the weighting function

$$w_m = \begin{cases} 0 & m < -1 \\ \alpha & m = -1 \\ \beta & m = 0 \\ \gamma & m = +1 \\ 0 & m > +1 \end{cases}$$

eqn. (20) may be written as

$$y_n^{k+1} = y_n^k + h \sum_{m=-\infty}^{+\infty} y_{n-m}^k \, w_m \tag{21}$$

The summation on the right-hand side is a convolution of the two sequences $\{w_n\}$ and $\{y_n^k\}$ defined by

$$\{y_n^k\} * \{w_n\} = \sum_{m=-\infty}^{+\infty} y_m^k \, w_{n-m} \tag{22}$$

where $*$ denotes the convolution operator, as usual.
So the algorithm can easily be written as

$$y_n^{k+1} = y_n^k + h\,\{y_n^k\} * \{w_n\} \tag{23}$$

The j^{th} statistical moment of the place function y^{k+1} for $j \geqslant 1$ is defined as

$$m_j(y^{k+1}) = \sum_{n=-\infty}^{+\infty} n^j y_n^{k+1} = m_j(y^k) + h \sum_{n=-\infty}^{+\infty} n^j \{y_n^k\} * \{w_n^k\} \tag{24}$$

and for $j = 0$, $m_0(y^{k+1}) = \sum_{n=-p}^{+\infty} y_n^{k+1}$.

The change in the statistical moment of the place function after a single step $\Delta t = h$ will now be

$$m_j(y^{k+1}) - m_j(y^k) = h \cdot m_j(y_n^k * W_n) \tag{25}$$

Substituting eqn. (22) into (25), with $p = n - m$, gives

$$m_j(y^{k+1}) - m_j(y^k) = h \sum_{p=-\infty}^{+\infty} \left\{ w_p^k \cdot \sum_{m=-\infty}^{+\infty} (p+m)^j y_m^k \right\} \tag{26}$$

After some calculations we obtain

$$\left.\begin{aligned}
m_0(y^{k+1}) - m_0(y^k) &= h(m_0(y^k) \cdot m_0(w)) \\
m_1(y^{k+1}) - m_1(y^k) &= h(m_0(y^k) \cdot m_1(w) + m_1(y^k) \cdot m_0(w)) \\
m_2(y^{k+1}) - m_2(y^k) &= h(m_0(y^k) \cdot m_2(w) + 2m_1(y^k) \cdot m_1(w) \\
&\quad + m_2(y^k) \cdot m_0(w)) \\
m_3(y^{k+1}) - m_3(y^k) &= h(m_0(y^k) \cdot m_3(w) + 3m_1(y^k) \cdot m_2(w) \\
&\quad + 3m_2(y^k) \cdot m_1(w) + m_3(y^k) \cdot m_0(w)) \\
m_4(y^{k+1}) - m_4(y^k) &= h(m_0(y^k) \cdot m_4(w) + 4m_1(y^k) \cdot m_3(w) \\
&\quad + 6m_2(y^k) \cdot m_2(w) + 4m_3(y^k) \cdot m_1(w) + m_4(y^k) \cdot m_0(w))
\end{aligned}\right\} \tag{27}$$

With the definition of the normalized moment $\mu_j(y^k) = m_j(y^k)/m_0(y^k)$ for $j \geqslant 0$, and the central or reduced moment $\tilde{\mu}_j(y^k) = \Sigma_{n=-\infty}^{+\infty} (n - \mu_1)^j y_n^k$ for $j \geqslant 1$, and $m_0(w) = 0$, tedious calculations give the following results

$$\left.\begin{aligned}
\Delta\mu_0(y) &= m_0(w) = 0 \\
\Delta\mu_1(y) &= h \cdot m_1(w) \\
\Delta\tilde{\mu}_2(y) &= h \cdot m_2(w) - h^2 m_1^2(w) \\
\Delta\tilde{\mu}_3(y) &= h \cdot m_3(w) - 3h^2 m_1(w) m_2(w) + 2h^3 m_1^3(w) \\
\Delta\tilde{\mu}_4(y) &= h \cdot m_4(w) - 4h^2 m_1(w) m_3(w) + 6h^3 m_1^2(w) m_2(w) - 3h^4 m_1^4(w)
\end{aligned}\right\} \tag{28}$$

The change in the statistical moments of $\{y_n^h\}$ is fully described by the weighting function w and is independent of k. Equation (28) can be used to study several kinds of discretization procedures in the z-direction and provides a tool to compare the numerical results with the exact solutions of the initial value problem (eqn. 13) for which solutions can be obtained by Laplace transformation of eqn. (13) (see refs. 15—17). From eqn. (28) and the weighting function (eqn. 20) the comparison shown in Table 1 can be obtained. With condition (19) a correct second moment can be found, but the third central moment is still incorrect.

Differentiating the Newton Backward and the Stirling formula [19] we obtain the well-known formulae

$$\frac{\partial y}{\partial z} = \frac{1}{l}\left(\nabla y - \frac{1}{2}\nabla^2 y + \frac{1}{3}\nabla^3 y - \frac{1}{4}\nabla^4 y\right) \tag{29}$$

and

$$\frac{\partial^2 y}{\partial z^2} = \frac{1}{l}\left(\delta^2 y - \frac{1}{12}\delta^4 y\right) \tag{30}$$

Substituting the results into eqn. (7), it is possible to obtain, similarly as in eqn. (20), the weighting function for a fourth-order approach in the z-direction

$$\left.\begin{aligned} w_{-2} &= -D_c\, l_1 \\ w_{-1} &= +16D_c\, l_1 \\ w_0 &= -30D_c\, l_1 - 25V_c\, l_2 \\ w_{+1} &= +16D_c\, l_1 + 48V_c\, l_2 \\ w_{+2} &= -D_c\, l_1 - 36V_c\, l_2 \\ w_{+3} &= +16V_c\, l_2 \\ w_{+4} &= -3V_c\, l_2 \end{aligned}\right\} \tag{31}$$

where $l_1 = 1/12l^2$ and $l_2 = 1/12l$

The moments of the weighting function are

$$\left.\begin{aligned} m_0(w) &= 0 \\ m_1(w) &= V_c\, h/l \\ m_2(w) &= 2D_c\, h/l^2 \\ m_3(w) &= 0 \\ m_4(w) &= 0 \end{aligned}\right\} \tag{32}$$

Use of eqn. (28) gives the comparison in Table 2. Obviously, a higher-order approach in the z-direction only is not a way to solve the numerical dispersion problem. Instability (negative concentrations) is another undesirable effect.

TABLE 1

A comparison of the change in statistical moments of a computer algorithm with the theoretical changes; the distribution isotherm is linear; first-order approach in the z-direction and also in the t-direction

	Computer algorithm	Exact math. solution
$\Delta\mu_0(y)$	0	0
$\Delta\mu_1(y)$	$V_c\frac{h}{l}$	$V_c\frac{h}{l}$
$\Delta\tilde{\mu}_2(y)$	$2D_c\frac{h}{l^2}+V_c\frac{h}{l}-V_c^2\frac{h^2}{l^2}$	$2D_c\frac{h}{l^2}$
$\Delta\tilde{\mu}_3(y)$	$V_c\frac{h}{l}-3h^2\left(\frac{V_c}{l}\right)\left(\frac{2D_c}{l^2}+\frac{V_c}{l}\right)+2h^3\left(\frac{V_c^3}{l^3}\right)$	0

TABLE 2

A comparison of the change in statistical moments of a computer algorithm with the theoretical changes; the distribution isotherm is linear; fourth-order approach in the z-direction and first-order in the t-direction

	Computer algorithm	Exact math. solution
$\Delta\mu_0$	0	0
$\Delta\mu_1$	$V_c\frac{h}{l}$	$V_c\frac{h}{l}$
$\Delta\tilde{\mu}_2$	$2D_c\frac{h^2}{l^2}-V_c^2\frac{h^2}{l^2}$	$2D_c\frac{h}{l^2}$
$\Delta\tilde{\mu}_3$	$-\left(\frac{V_c}{l}\cdot\frac{2D_c}{l^2}\right)3h^2+2h^3\left(\frac{V_c}{l}\right)^3$	0

Fourth-order Runge Kutta method

Incrementing the order in the t-direction by means of a fourth-order Runge Kutta method, gives the formula

$$y_n^{k+1}=y_n^k+h\cdot\frac{1}{6}\{K_0^k(n)+2K_1^k(n)+2K_2^k(n)+K_3^k(n)\} \tag{33}$$

with

$$\left.\begin{aligned}
K_0^k(n)&=\{y_n^k\}*\{w_n\}\\
K_1^k(n)&=\left\{y_n^k+\frac{1}{2}h\,K_0^k(n)\right\}*\{w_n\}\\
K_2^k(n)&=\left\{y_n^k+\frac{1}{2}h\,K_1^k(n)\right\}*\{w_n\}\\
K_3^k(n)&=\left\{y_n^k+h\,K_2^k(n)\right\}*\{w_n\}
\end{aligned}\right\} \tag{34}$$

Substituting eqns. (34) into (33) results in

$$y_n^{k+1} = y_n^k + hy_n^k * w_n + \frac{1}{2}h^2 y_n^k * w_n * w_n + \frac{1}{6}h^3 y_n^k * w_n * w_n * w_n$$

$$+ \frac{1}{24}h^4 y_n^k * w_n * w_n * w_n * w_n \tag{35}$$

In the same way as was done for eqn. (23) the changes in the statistical moments of y_n^k can be calculated: time-consuming calculations give

$$\left.\begin{aligned} \Delta\mu_0(y) &= m_0(w) = 0 \\ \Delta\mu_1(y) &= h\ m_1(w) \\ \Delta\tilde{\mu}_2(y) &= h\ m_2(w) \\ \Delta\tilde{\mu}_3(y) &= h\ m_3(w) \end{aligned}\right\} \tag{36}$$

Finally substitution into eqn. (36) of the values of $m_j(w)$ $(j = 0,\ldots 3)$ obtained in eqn. (32) by a fourth-order approach in the z-direction gives the correct values of the changes in the statistical moments.

Ideal mixer or theoretical plate model

In chromatographic theory, there are two approaches to describing material transport. One approach is the so-called rate model, based on a differential mass-balance equation and described above; the other approach is the so-called theoretical chamber model. In the latter, a chromatographic column can be visualized as a series of ideal mixers [20]. The concentration can be calculated at any time t in each mixer by

$$C^t(t,n) = C_0^t\ [(t/\tau)^{n-1}/(n-1)!]e^{-t/\tau} \tag{37}$$

where $C^t(t,n)$ denotes the sample concentration at time t in mixer n, C_0^t the initial concentration at time $t = 0$ in the first mixer (all other mixers have at time $t = 0$ concentration zero), τ the mixer time constant l/V_c, n the number of the mixer $n = 1, 2,\ldots..N$, N the total number of mixers, l the mixer width, and V_c the migration velocity, supposing a linear distribution isotherm.

Equation (37) is an expression for a Poisson distribution with fixed parameter t/τ, used in statistics. The statistical moments of this distribution, or in the present case the moments of the concentration profile, will be

$$\mu_1 = \tilde{\mu}_2 = \tilde{\mu}_3 = t/\tau = t\ V_c/l \tag{38}$$

So the change in the moments after a time step $\Delta t = h$ will be

$$\Delta\mu_1 = \Delta\tilde{\mu}_2 = \Delta\tilde{\mu}_3 = h\ V_c/l \tag{39}$$

Returning to the numerical solution of the rate model without dispersion and applying a first-order approach in the z-direction and a fourth-order Runge Kutta approach in the t-direction, the changes in statistical moments are given by eqn. (36). With a weighting function

$$w_m = \begin{cases} 0 & m < 0 \\ -\dfrac{V_c}{l} & m = 0 \\ +\dfrac{V_c}{l} & m = 1 \\ 0 & m > 1 \end{cases} \tag{40}$$

The changes in the statistical moments can now be calculated and they appear to be identical to the moments in eqn. (39). Hence it can be concluded that this numerical procedure is a perfect computer implementation of the ideal mixer model. However, the intention was to implement the rate model and not the ideal mixer model with its inherent numerical dispersion. For studying distortion or dispersion effects in the rate model, this undesirable effect can be minimized relatively by increasing the number of Δz steps. In order to keep the numerical experiment stable (see Convergence and stability), a smaller value of Δt should be chosen; this can lead frequently to inadmissibly large computing time.

Moving coordinates

A pure translation with a minimum numerical dispersion can only be simulated by using infinitely small Δz and Δt values. Drastic reduction of the mentioned undesirable effects can be achieved by introducing a moving coordinate system. The reason for this is, that by using a moving coordinate system it is not necessary to simulate the translation part of the solution, and we are left with the simulation of the distortion originating from physical dispersion and non-linearity effects.

Starting from eqn. (7) a new z-coordinate will now be defined by

$$z = z^* - V_{\text{ref}}t \tag{41}$$

Here, z denotes the new z-coordinate, V_{ref} is an arbitrary constant velocity of the moving coordinate system, and z^* is the old z-coordinate.

Substitution of eqn. (41) into (7) gives

$$\partial C^t(t,z)/\partial t = -\partial/\partial z\,\{(V^* - V_{\text{ref}})C^t(t,z)\} + \partial^2 D^* C^t(t,z)/\partial z^2 \tag{42}$$

To interpret the effect of the moving coordinate system, partial differentiation is necessary:

$$\frac{\partial C^t(t,z)}{\partial t} = -\left\{C^t \frac{dV^*}{dC^t}\right\}\frac{\partial C^t}{\partial z} - \{V^* - V_{\text{ref}}\}\frac{\partial C^t}{\partial z} + \frac{\partial^2 D^* C^t}{\partial z^2} \tag{43}$$

On the right-hand side of eqn. (43), three separate parts can be distinguished. The first and second parts describe, respectively, the non-linear and the linear velocity effects in the transport mechanism, while the third part describes the physical dispersion effect. A proper choice of V_{ref} can reduce the numerical dispersion effects which arise from the second part. In the linear

case, where $V^* = V_c$, a choice of $V_{ref} = V_c$ will reduce this numerical dispersion effect to zero.

In this case the weighting function can be derived from eqn. (42) and calculation, similar to that which follows from eqn. (41), yields

$$w_m = \begin{cases} 0 & m < -1 \\ \dfrac{D_c}{l^2} & m = -1 \\ -(V_c - V_{ref})/l - 2D_c/l^2 & m = 0 \\ +(V_c - V_{ref})/l + D_c/l^2 & m = 1 \\ 0 & m > 1 \end{cases} \tag{44}$$

From eqn. (28), the changes in the statistical moments are

$$\left.\begin{aligned} \Delta\mu_0(y) &= 0 \\ \Delta\mu_1(y) &= 0 \\ \Delta\tilde{\mu}_2(y) &= 2D_c\, h/l^2 \\ \Delta\tilde{\mu}_3(y) &= 0 \end{aligned}\right\} \tag{45}$$

As only the central moments are shift-invariant, only $\Delta\mu_1(y)$ has to be corrected with the shift of the coordinate system. The corrected value will be $\Delta\mu_1(y) = V_c\, h/l$. With a first-order discretization in the z-direction and a fourth-order Runge Kutta approach in the t-direction, all moments are obtained correctly up to the third moment when eqns. (32) and (36) are applied.

Convergence and stability

With the investigation of the convergence of a numerical solution, a measure for the approximation of the solution of a differential equation relative to the exact solution of the differential equation can be obtained by limiting the size of Δz and Δt to zero. The convergence depends only on the choice of the difference scheme. The measure of stability of the solution can be considered as an amplification factor for round-off errors and depends on a so-called "stability criterion". Several authors have discussed the stability and convergence of numerical solutions of certain classes of linear partial differential equations; an extensive review is given by Vliegenthart [21]. In the case of non-linear equations, the problem is in general more complicated and only partially described by Lieberstein [22].

In fact it is very difficult to determine the stability criterion of a non-linear problem. In this paper the linear one will be used. A discussion of the usefulness of this stability criterion for the non-linear equation, governing the mass transport, will be given in Part 2 of this series. Developing the round-off errors $\epsilon(t,z)$ in a complex Fourier series with period $2L$ gives

$$\epsilon(t,z) = \sum_{j=-\infty}^{+\infty} C_j\, e^{iP_j z} \tag{46}$$

where L is a certain interval and $P_j = j\P/L$ and assuming $\epsilon(t,z) = 0$ for $z < -L$ and $z > +L$. Because the round-off errors satisfy the same difference equation as the numerical solution y_n^k, the difference scheme for $\epsilon(t,z)$ is given by eqn. (23) and we obtain

$$\epsilon_n^{k+1} = \epsilon_n^k + h\{\cdots + w_{n+1}\,\epsilon_{n-1}^k + w_n\epsilon_n^k + w_{n-1}\,\epsilon_{n+1}^k + \cdots\} \tag{47}$$

Substitution of eqn. (46) into (47) gives

$$\epsilon_n^{k+1} = \sum_{j=-\infty}^{+\infty} C_j\, e^{iP_j(nl)} + h\left\{\cdots w_{n+1} \sum_{j=-\infty}^{+\infty} C_j\, e^{iP_j(n-1)l} + w_n \sum_{j=-\infty}^{+\infty} C_j\, e^{iP_j(n)l} + w_{n-1} \sum_{j=-\infty}^{+\infty} C_j\, e^{iP_j(n+1)l} + \cdots\right\} \tag{48}$$

Putting

$$\epsilon_n^{k+1} = \sum_{j=-\infty}^{+\infty} C_j\, e^{iP_j(nl)+q_jh} \tag{49}$$

and assuming that the Fourier spectrum of $\epsilon(t,z)$ is white (i.e. C_j is a constant), one gets

$$e^{q_jh} = \xi = 1 + h \sum_{m=-\infty}^{+\infty} w_m\, e^{-iP_j(ml)} \tag{50}$$

The stability criterion can be formulated for any arbitrary weighting function as

$$|\xi| = |1 + hF\{w_m\}| < 1 \tag{51}$$

where $F\{w_m\}$ denotes the discrete Fourier transform of the weighting function [23]. In the case that the weighting function w_m is defined by eqn. (20) it is possible to derive

$$h \cdot F\{w_m\} = -(4h\,D_c/l^2 + 2h\,V_c/l)\sin^2(P_jl/2) - (i\,h/l\,V_c)\sin(P_jl) \tag{52}$$

Applying the criterion (eqn. 51) gives

$$|(1 - 4h\,D_c/l^2 - 2h\,V_c/l)^2 + (h\,V_c/l)^2| < 1 \tag{53}$$

Working out this inequality:

$$h < [4(V_c/l + 2D_c/l^2)]/[4(V_c/l + 2D_c/l^2)^2 + (V_c/l)^2] \tag{54}$$

Introducing moving coordinates, with $V_{ref} = V_c$ the criterion will be

$$h < l^2/2D_c \tag{55}$$

DISCRETE MATHEMATICAL NON-LINEAR MODEL

Difference scheme

Applying the difference operators defined in eqn. (12) to eqn. (7) and introducing a moving coordinate system with an arbitrary chosen constant velocity V_{ref} gives

$$y_n^{k+1} = y_n^k + h\left\{\alpha \frac{y_{n+1}^k}{p_{n+1}^k} + \beta \frac{y_n^k}{p_n^k} + \gamma \frac{y_{n-1}^k}{p_{n-1}^k} + \frac{V_{\text{ref}}}{l}(y_n^k - y_{n-1}^k)\right\} \quad (56)$$

where $p_n^k = 1 + (1 - \epsilon)\, C^s(t,z)/\epsilon\, C^m(t,z)$ with $t = kh$ and $z = nl$, $\alpha = D/l^2$, $\beta = -2D/l^2 - \langle v\rangle/l$ and $\gamma = D/l^2 + \langle v\rangle/l$.

The effect of the non-linearity of the distribution isotherm is represented by the factors p_{n+j}^k ($j = 1, 0, -1$) and depends on the ratio of the mobile phase and the stationary phase concentration.

Compared with the difference schemes of other workers [24, 25], the derived difference scheme (eqn. 56) is still an exact representation of the mass conservation law.

Non-linear moment analysis

To check the algorithm of the non-linear model, eqn. (56) was rewritten as

$$y_n^{k+1} = y_n^k + h\,[\{z_n^k\} * \{w_n\} + (V_{\text{ref}}/l)(y_n^k - y_{n-1}^k)] \quad (57)$$

According to eqn. (5) $z_n^k = y_n^k/p_n^k$ denotes the mobile phase concentration, and $\{w_n\}$ is the weighting function. The change in place function moments can be derived using the same procedure as used in *Propagation of errors in the statistical moments*. The following equations are obtained

$$\Delta m_0(y) = h\,[m_0(z^k)\cdot m_0(w) + (V_{\text{ref}}/l)(m_0(y^k) - m_0(y^k))] = 0 \quad (58)$$

$$\Delta m_1(y) = h\,[m_0(z^k)\cdot m_1(w) - (V_{\text{ref}}/l)\, m_0(y^k)] \quad (59)$$

$$\Delta m_2(y) = h\,[m_0(z^k)m_2(w) + 2m_1(z^k)\cdot m_1(w) - (V_{\text{ref}}/l)(m_1(y^k) + m_0(y^k))] \quad (60)$$

$$\Delta m_3(y) = h\,[m_0(z^k)m_3(w) + 3m_1(z^k)m_2(w) + 3m_2(z)m_1(w) - (V_{\text{ref}}/l)(3m_2(y^k) + 3m_1(y^k) + m_0(y^k))] \quad (61)$$

The equations obtained are too complicated to be useful to check a higher-order approach in the t-direction by means of a Runge Kutta method. To check computer calculations in the case of non-linear distribution isotherms while dispersion is neglected, another strategy was followed based on the suggestion of Huber and Gerritse [14] to reconstruct the isotherms from the peak shape of the elution profiles (see Part 2).

METHOD OF CHARACTERISTICS FOR EXACT SOLUTIONS OF A NON-LINEAR IDEAL CHROMATOGRAPHY

General considerations

To make it possible to check simulation methods as described above, it is desirable to have available a rigorous mathematical solution of at least one representative particular model which exhibits all essential features of the transport phenomena in the chromatography experiments.

In the present case it is possible to obtain an explicit rigorous solution of the differential equation

$$\partial C^t/\partial t + V^{**}(C^t)\,\partial C^t/\partial z = 0, \quad -\infty < z < +\infty, \quad 0 < t \tag{62}$$

with the initial condition

$$C^t(0,z) = C_0^t\{\theta(z) - \theta(z-\delta)\}, \quad -\infty < z < +\infty \tag{63}$$

where θ denotes the Heaviside unit step function, δ is a parameter measuring the geometrical support of the initial concentration, and C_0^t is a positive constant being the value of this concentration.

In this section the explicit solution is derived for the initial value problem (62) and (63) and the results will be used in Part 2 to check the methods of simulation. The derivation of the explicit solution will be obtained with the aid of the so-called method of characteristics. A brief general description of this method which will be applied consecutively to the initial value problem is given below.

The general initial value problem is

$$\partial u/\partial t + a(u)\,\partial u/\partial x = 0, \quad -\infty < x < +\infty, \quad t > 0 \tag{64}$$

(where $a(u)$ is an integratable function of u) with the initial condition

$$u(0,x) = u_0(x) \tag{65}$$

By integrating $a(u)$ eqn. (64) may be written in divergence form

$$\partial u/\partial t + f(u)\,\partial/\partial x = 0 \tag{66}$$

with

$$f(u) = \int_0^u a(u')\mathrm{d}u' \tag{67}$$

We assume that $a(u)$ increases for increasing u and hence $f(u)$ is convex. The case of $a(u)$ decreasing and $f(u)$ concave is quite similar. A characteristic is a curve along which the differential operator $\partial/\partial t + a(u)\,\partial/\partial x$ is a differentiation in the direction of the tangent to the curve. This means that the solution of eqns. (64) and (65) is constant along the characteristics of which the slope is given by $\mathrm{d}x/\mathrm{d}t = a(u)$, with u constant. It follows that the characteristics are straight lines and the characteristic through the point $(0,\bar{x})$ is given by the equation $t = x - \bar{x}/a(u_0(\bar{x}))$. If $u_0(x)$ is an increasing continuous function of x for all values of x, the solution of the initial value problem is readily given; the characteristics through the points $(0,\bar{x})$ diverge and the solution u is constant along each characteristic with value $u_0(\bar{x})$ (see Fig. 3).

A complication arises whenever $u_0(x)$ does not increase for all values of x. If $u_0(x)$ increases for $x < x_1$ and decreases for $x > x_1$, the characteristics diverge for $x < x_1$, but converge for $x > x_1$ (see Fig. 4). The consequence is that characteristics intersect and so at points of intersection the solution becomes multivalued. This is not acceptable from the physical point of view. To overcome this difficulty the concept of solution in generalized sense is introduced. The differentiations in eqn. (66) are taken in the so-called weak

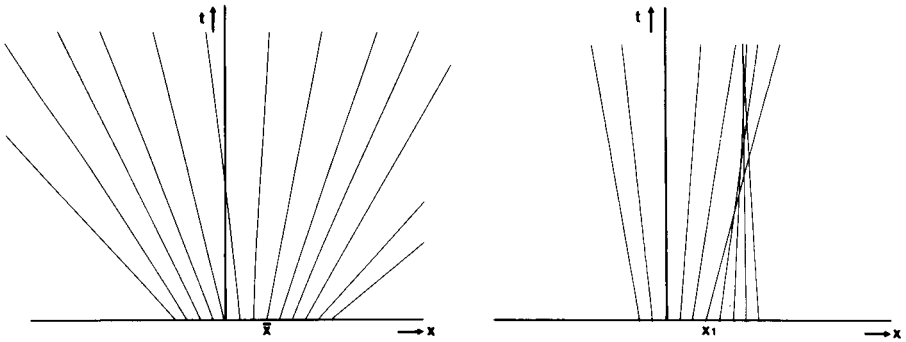

Fig. 3. Diverging fan of characteristics.

Fig. 4. Fan of characteristics, partially converging.

sense, which means that the solution should not satisfy eqns. (66) and (67) but the equation

$$\int_0^{\infty}\int_{-\infty}^{+\infty}\left[\frac{\partial\phi}{\partial t}(t,x)\,u(t,x)+\frac{\partial\phi}{\partial x}(t,x)\cdot f\{u(t,x)\}\right]\mathrm{d}t\,\mathrm{d}x+\int_{-\infty}^{+\infty}\phi(0,x)u_0(x)\,\mathrm{d}x=0 \quad (68)$$

where $\phi(t,x)$ is any continuously differentiatable function with bounded support in the region $t \geqslant 0$. Equation (68) is formally obtained by multiplying eqn. (66) by $\phi(t,x)$ and integrating consecutively by parts. Equation (68) is a generalization of eqns. (66) and (67) in so far as any differentiatable solution of (66) and (67) is also a solution of (68). However, whereas eqns. (66) and (67) do not allow discontinuous solutions, eqn. (68) does. Curves across which the generalized solution u is discontinuous are known as shock-curves (shock-waves).

Interpreting eqn. (66) as a conservation law for mass transport with flux $f(u)$ the mass balance for a fixed interval $[a,b]$ is

$$\int_a^b u(t,x)\mathrm{d}x\,\Big|_{t_1}^{t_2}=\int_{t_1}^{t_2}[f\{u(t,a)\}-f\{u(t,b)\}]\mathrm{d}t \quad (69)$$

Suppose that the shock-curve is given by

$$x = s(t) \quad (70)$$

and that $s(t)$ can be differentiated with an integratable derivative. We consider now a fixed interval $[a,b]$ with $a \leqslant s(t) \leqslant b$ for say $t_1 \leqslant t \leqslant t_2$; the mass balances for the intervals $[a,s(t)]$ and $[s(t),b]$ may be expressed as

$$\int_a^{s(t)} u(t,x)\mathrm{d}x\,\Big|_{t_1}^{t_2}=\int_{t_1}^{t_2}[f\{u(t,a)\}-f\{u(t,s_-(t))\}+u(t,s_-(t))\,\mathrm{d}s/\mathrm{d}t]\mathrm{d}t$$

and

$$\int_{s(t)}^b u(t,x)\mathrm{d}x\,\Big|_{t_1}^{t_2}=\int_{t_1}^{t_2}[f\{u(t,s_+(t))\}-f\{u(t,b)\}-u(t,s_+(t))\,\mathrm{d}s/\mathrm{d}t]\mathrm{d}t$$

where $u(t,s_-(t))$ and $u(t,s_+(t))$ denote respectively the value of u at the left-hand side and the right-hand side of the shock. Adding the latter two equalities and subtracting the result from eqn. (69) gives

$$\int_{t_1}^{t_2} [f\{u(t,s_-(t))\} - f\{u(t,s_+(t))\} - \{u(t,s_-(t)) - u(t,s_+(t))\}\, ds/dt]dt = 0$$

which is valid for any interval $[t_1,t_2]$. Hence the so-called jump relation is obtained

$$[u\{t,s_-(t)\} - u\{t,s_+(t)\}]\, ds/dt = f\{u(t,s_-(t))\} - f\{u(t,s_+(t))\} \tag{71}$$

A price has to be paid for the generalization allowing discontinuous solutions to be accepted. This stems from the fact that eqn. (68) is not uniquely solvable. A simple example is provided by $f(u) = u^2/2$ and $u_0(x) = \theta(x)$. The method of characteristics gives immediately $u \equiv 0$ for $x < 0$, and $u \equiv 1$ for $x > t$ (see Fig. 5). This solution does not determine the value of u in the wedge $0 \leqslant x \leqslant t$. This gap can be filled in two ways, namely

$u(x,t) = 0$ for $0 \leqslant x < t/2$; $u(x,t) = 1$ for $t/2 < x \leqslant t$, or by

$u(x,t) = x/t$ for $0 \leqslant x \leqslant t$

Both solutions satisfy the generalized equation (68), the first being discontinuous across the line $t = 2x$ and the second being continuous for all t and x. In the first solution the slope of the straight shock-curve was chosen in accordance with the jump relation (71).

In order to obtain uniqueness of the solution — which is a physical requirement — an extra condition must be imposed on the solution u; this condition is known as the entropy condition. There are several formulations of this condition which are equivalent; the formulation which is perhaps most attractive for physicists is that the shock should be stable. This results in the condition that the two characteristics issuing from a point on the shock-curve lie on either side of the shock-curve (see Fig. 6), or in formula

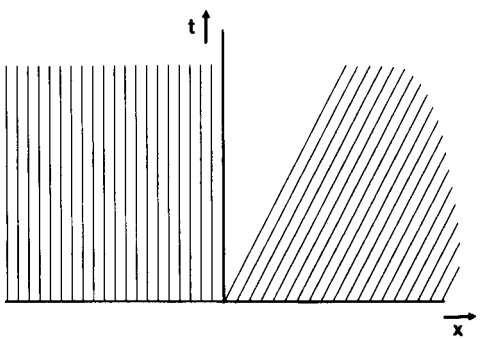

Fig. 5. Wedge with undetermined solutions.

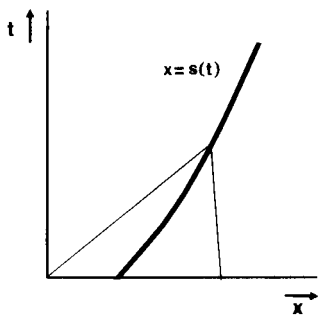

Fig. 6. Shock-wave supported by intersection of characteristics.

$$a\{u(t,s_-(t))\} > \mathrm{d}s/\mathrm{d}t > a\{u(t,s_+(t))\} \tag{72}$$

Because a has been assumed to increase this means that across a shock there is also the relation $u(t,s_-(t)) > u(t,s_+(t))$. It follows that in the example the discontinuous solution should be dismissed as a physically acceptable solution. The solution $u(t,x) = x/t$ for $0 \leqslant x \leqslant t$ is known as a so-called expansion. This may be interpreted as follows. The initial condition $u(0,x) = \theta(x)$ may be looked on as the limit for $\delta \to 0$ ($\delta > 0$) of the initial condition $u(0,x) \equiv 0$ for $x \leqslant 0$, $u(0,x) \equiv x/\delta$ for $0 \leqslant x \leqslant \delta$, $u(0,x) \equiv 1$ for $x \geqslant \delta$. Constructing the characteristics from these initial data gives a diverging family of characteristics which becomes in the limit for $\delta \to 0$ a diverging fan of characteristics, called an expansion fan, in which the solution changes continuously from zero to one according to the formula $u = x/t$ for $0 \leqslant x \leqslant t$ (see Fig. 7). This short introduction gives enough theoretical background to solve the model problem for the concentration C^t. For more details of this theory, refs. 10, 11, 13 should be consulted.

The initial value problem for C^t with Langmuir non-linearity

The initial value problem for C^t reads as

$$\partial C^t/\partial t + V^{**}(C^t)\,\partial C^t/\partial z = 0, \quad -\infty < z < +\infty, \quad t > 0 \tag{73}$$

with

$$C^t(0,z) = C^t_0\,[\theta(z) - \theta(z-\delta)], \quad -\infty < z < +\infty \tag{74}$$

where

$$V^{**}(C^t) = \mathrm{d}\{V^*(C^t)C^t\}/\mathrm{d}C^t = C^t\,\mathrm{d}V^*(C^t)/\mathrm{d}C^t + V^*(C^t) \tag{75}$$

and

$$V^*(C^t) = \langle v\rangle/[1 + (1-\epsilon/\epsilon)C^s/C^m] \tag{76}$$

C^s and C^m are the concentrations in the stationary and mobile phases, respectively, which constitute the total concentration C^t according to $C^t = \epsilon C^m + (1-\epsilon)C^s$ and which are assumed to be correlated to each other by the Langmuir isotherm

$$C^s = AC^m/(1 + BC^m) \tag{77}$$

where A and B are positive constants. Hence

$$C^t = \epsilon C^m + (1-\epsilon)\,AC^m/(1 + BC^m) \tag{78}$$

From eqns. (75) and (76), it follows that $V^{**}(C^t)$ may be expressed as

$$V^{**}(C^t) = \mathrm{d}\{\epsilon\langle v\rangle C^m\}/\mathrm{d}C^t = \epsilon\langle v\rangle\,\mathrm{d}C^m/\mathrm{d}C^t$$

or with the aid of

$$\mathrm{d}C^t/\mathrm{d}C^m = \epsilon + (1-\epsilon)\,\mathrm{d}C^s/\mathrm{d}C^m = \epsilon + (1-\epsilon)\,A/(1 + BC^m)^2$$

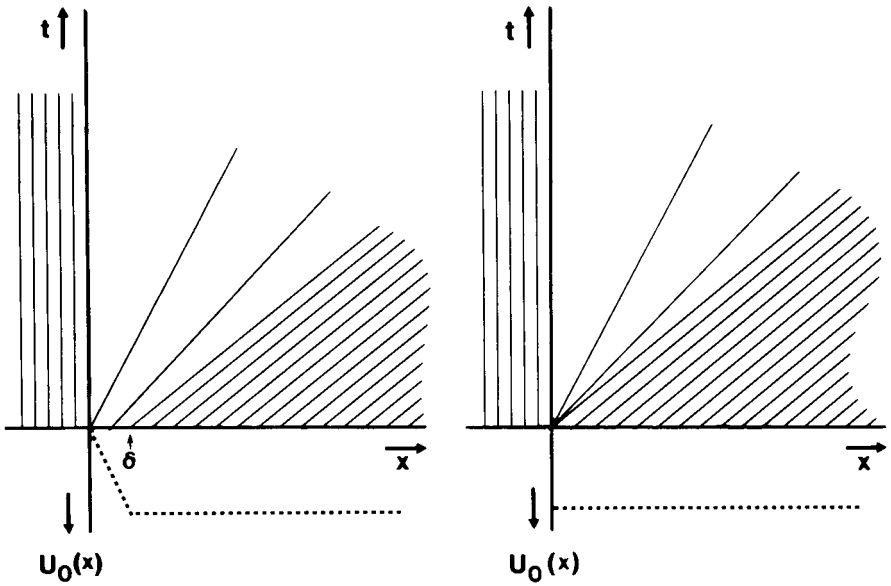

Fig. 7. Wedge filled with diverging fan of characteristics.

$$V^{**}(C^t) = \langle v\rangle \Big/ \left[1 + \left(\frac{1-\epsilon}{\epsilon}\right)\frac{dC^s}{dC^m}\right] = \langle v\rangle \Big/ \left[1 + \left(\frac{1-\epsilon}{\epsilon}\right)\frac{A}{(1+BC^m)^2}\right] \tag{79}$$

Because $V^{**}(C^t)$ is an increasing function of C^m and C^m an increasing function of C^t, it follows that $V^{**}(C^t)$ is an increasing function of C^t and the theory of the preceding section may be applied to the initial value problem (73), (74).

The partial solution with straight shock-wave

From the initial condition (74) it follows that the characteristics issuing from the points $(0,z)$ of the initial line have the slopes $1/V^{**}(0)$ for $z < 0$, $1/V^{**}(C_0^t)$ for $0 < z < \delta$, and again $1/V^{**}(0)$ for $z > \delta$; because according to eqn. (79) the value of $V^{**}(C_0^t)$ is larger than that of $V^{**}(0)$ the characteristics issuing from the points z with $0 < z < \delta$ intersect with those issuing from the points z with $z > \delta$ (see Fig. 8).

Consider first the region $0 \leqslant t \leqslant T_0$, where T_0 is the t-ordinate of the point of intersection of the characteristics $t = z/V^{**}(C_0^t)$ and $t = z - \delta/V^{**}(0)$. The theory yields immediately that

$$\left.\begin{aligned} &C^t(t,z) \equiv 0 \text{ for } z < V^{**}(0)t \\ &C^t(t,z) \equiv C_0^t \text{ for } V^{**}(C_0^t)t < z < V^{**}(0)t + \delta, \quad 0 \leqslant t \leqslant T_0 \\ &C^t(t,z) \equiv 0 \text{ for } z > V^{**}(C_0^t)t + \delta \end{aligned}\right\} \tag{80}$$

The function $C^t(t,z)$ is not yet determined in the wedge BAC, i.e. in the region $V^{**}(0)t < z < V^{**}(C_0^t)t$, $0 \leqslant t \leqslant T_0$, and in the wedge CDE, i.e. in the region

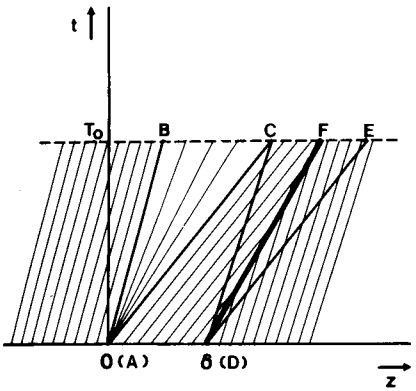

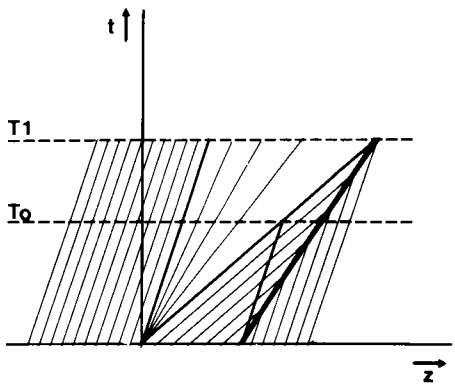

Fig. 8. Intersection of characteristics with a rectangular initial condition.

Fig. 9. Intersection of characteristics and the shock-wave with a rectangular initial condition.

$V^{**}(0)t + \delta < z < V^{**}(C_0^t)t + \delta$, $0 \leqslant t \leqslant T_0$. In the first, there are, strictly speaking, no characteristics issuing from the initial line and in the second one the characteristics intersect (compare Fig. 8). The value of $C^t(t,z)$ in the first wedge is obtained by constructing, as discussed above, an expansion fan. In the second wedge with intersecting characteristics, the function $C^t(t,z)$ is obtained by constructing a shock-wave as follows.

According to the jump relation (71), which is valid because C^t satisfies the conservation law (69) and from eqn. (75), the shock-curve $z = s(t)$ with a jump from $C^t \equiv C_0^t$ to $C^t \equiv 0$ is represented by the equation

$$(C_0^t - 0)\, ds/dt = V^*(C_0^t)C_0^t - V^*(0)\cdot 0 \quad \text{or} \quad ds/dt = V^*(C_0^t)$$

and hence the shock is given by the straight line

$$z = V^*(C_0^t)t + \delta \tag{81}$$

An easy check with the aid of eqns. (76), (77) and (79) gives $V^{**}(0) < V^*(C_0^t) < V^{**}(C_0^t)$, and so the shock is a straight line DF lying between DC and DE (see Fig. 8). For $0 \leqslant t \leqslant T_0$ the result is that $C^t(t,z) \equiv C_0^t$ between DC and DF and $C^t(t,z) \equiv 0$ at the right-hand side of DF. It follows from eqn. (81) that the shock migrates with the velocity $V^*(C_0^t)$, i.e. the velocity as defined by eqn. (6). This phenomenon has also been found in experimental results with break-through curves [14]. The concentration distribution in the expansion fan can now be calculated. In the expansion fan, according to the theory of characteristics, $z = V^{**}(C^t)t$ or according to eqn. (79)

$$\frac{z}{t} = [\langle v\rangle(1 + BC^m)^2] \Big/ \left[(1 + BC^m)^2 + \left(\frac{1-\epsilon}{\epsilon}\right)A\right]$$

Solving C^m and substituting the result into eqn. (78) gives

$$C^t(t,z) = \frac{\epsilon}{B}\left[\left\{\left(\frac{1-\epsilon}{\epsilon}\right)A - 1\right\} + \left(\frac{1-\epsilon}{\epsilon}A\right)^{1/2} \cdot \frac{2z - t\langle v\rangle}{[z(t\langle v\rangle - z)]^{1/2}}\right] \tag{82}$$

valid for $V^{**}(0)t \leqslant z \leqslant V^{**}(C_0^t)t, \quad 0 \leqslant t \leqslant T_0$.

Because the concentration remains constant along the characteristics, as long as these do not intersect a shock-curve, the solution valid for $0 \leqslant t \leqslant T_0$ may be extended to values of t with $0 \leqslant t \leqslant T_1$, where T_1 is the t-ordinate of the point of intersection of the characteristic $z = V^{**}(C_0^t)t$ and the shock-curve $z = V^{*}(C_0^t)t + \delta$ (see Fig. 9).
It follows that

$$T_1 = \delta/[V^{**}(C_0^t) - V^{*}(C_0^t)] \tag{83}$$

Summarizing the above results, for $0 \leqslant t \leqslant T_1$:

$$\left.\begin{aligned} &C^t(t,z) \equiv 0 \text{ for } z \leqslant V^{**}(0)t \\ &C^t(t,z) \text{ is given by eqn. (82) for } V^{**}(0)t \leqslant z \leqslant V^{**}(C_0^t)t \\ &C^t(t,z) \equiv C_0^t \text{ for } V^{**}(C_0^t)t \leqslant z < V^{*}(C_0^t)t + \delta \\ &C^t(t,z) \equiv 0 \text{ for } V^{*}(C_0^t)t + \delta < z \end{aligned}\right\} \tag{84}$$

For $t > T_1$ the characteristics in the expansion fan intersect the line $z = V^{*}(C_0^t)t + \delta$, which represents the shock-wave for $0 \leqslant t \leqslant T_1$. The shock-curve cannot be continued as a straight line in the same direction, because $C^t(t,z)$ would decrease along $z = V^{*}(C_0^t)t + \delta$ for increasing values of t with $t \geqslant T_1$. Keeping constant the value of the slope ds/dt of the shock-curve would violate the jump condition (eqn. 71), i.e.

$$(C^t - 0)\, ds/dt = V^{*}(C^t)C^t - V^{*}(0) \cdot 0 \quad \text{or} \quad ds/dt = V^{*}(C^t) \tag{85}$$

The extension of the shock-curve is calculated below and the result is used to give the $C^t(t,z)$ distribution for $t \geqslant T_1$.

The continued solution with curved shock-wave

The shock-curve $z = s(t)$ satisfies, according to the jump relation (85) the differential equation

$$dz/dt = ds/dt = V^{*}(C^t) \quad \text{for} \quad t \geqslant T_1 \tag{86}$$

The initial condition for the curved shock is obtained from the fact that the total shock-curve should be continuous; thus

$$s(T_1) = V^{*}(C_0^t)T_1 + \delta \tag{87}$$

On the other hand for any point (t,z) on the shock

$$\frac{z}{t} = V^{**}(C^t) \tag{88}$$

where (t,z) is the point of intersection of the shock and the characteristic $z = V^{**}(C^t)t$ in the expansion fan. Thus the extended shock-wave is obtained

by eliminating C^t from eqns. (86) and (88). By again using eqns. (76), (77) and (79):

$$V^*(C^t) = \langle v\rangle \Big/ \left[1 + \left(\frac{1-\epsilon}{\epsilon}\right)\frac{A}{1+BC^m}\right]$$

and

$$V^{**}(C^t) = \langle v\rangle \Big/ \left[1 + \left(\frac{1-\epsilon}{\epsilon}\right)\frac{A}{(1+BC^m)^2}\right] = z/t$$

Solving $(1 + BC^m)$ from the latter equation as a function of z/t and substituting the result into the former, $V^*(C^t)$ is obtained as a function of z/t.

Substituting this last result into eqn. (86) gives, after an easy calculation, the following differential equation for the extended shock-curve

$$\frac{dz}{dt} = \langle v\rangle \Big/ \left[1 + \left[A\,\frac{1-\epsilon}{\epsilon}\right]^{1/2}\left[\langle v\rangle\frac{t}{z} - 1\right]^{1/2}\right] \tag{89}$$

with the initial condition

$$z(T_1) = V^*(C_0^t)T_1 + \delta \tag{90}$$

Putting $z = \langle v\rangle x$ and $t = x + \tau$ we get the simple equation

$$\frac{d\tau}{dx} = \left[A\left(\frac{1-\epsilon}{\epsilon}\right)\right]^{1/2}\left[\frac{\tau}{x}\right]^{1/2}$$

Integration and the use of the initial condition (90) yields for the extended shock-curve the implicit relation

$$\left[A\left(\frac{1-\epsilon}{\epsilon}\right)\right]^{1/2}\cdot z^{1/2} - \{\langle v\rangle\, t - z\}^{1/2}$$

$$= \left[A\left(\frac{1-\epsilon}{\epsilon}\right)\right]^{1/2}\{V^*(C_0^t)T_1 + \delta\}^{1/2} - \{(\langle v\rangle - V^*(C_0^t))T_1 - \delta\}^{1/2}, \quad t \geqslant T_1 \tag{91}$$

For t and z going to infinity we get asymptotically

$$\frac{z}{t} = \langle v\rangle \Big/ \left[1 + A\left(\frac{1+\epsilon}{\epsilon}\right)\right] = V^{**}(0) = V^*(0) \tag{92}$$

and hence the slope of the shock-curve approaches at infinity that of the characteristic $z = V^{**}(0)t$ as was to be expected.

It follows immediately from eqns. (91) and (92) that the curved part of the shock-wave is a parabola with axis parallel to the line $z/t = V^{**}(0)$. For actual computations it is preferable to use a parametrization of eqn. (91). Putting

$$\left[A\cdot\frac{1-\epsilon}{\epsilon}\right]^{1/2}\{V^*(C_0^t)T_1 + \delta\}^{1/2} - \{(\langle v\rangle - V^*(C_0^t))T_1 - \delta\}^{1/2} = \rho^{1/2} \tag{93}$$

and

$$A\left(\frac{1-\epsilon}{\epsilon}\right) = \gamma \tag{94}$$

the parametrization may be given by

$$\left.\begin{aligned} z &= \frac{\rho}{\gamma} \cdot \cosh^4 p \\ t &= \frac{\rho}{\langle v\rangle}\left(\frac{1}{\gamma} \cdot \cosh^4 p + \sinh^4 p\right) \end{aligned}\right\} \tag{95}$$

with $\operatorname{arc\,cos}\, h\left[\frac{\gamma}{\rho}\{V^*(C_0^t)T_1 + \delta\}\right]^{1/4} \leqslant p < \infty$

Another useful representation of the shock-wave is given by

$$\left(A \cdot \frac{1-\epsilon}{\epsilon} + 1\right) z - \langle v\rangle\, t = \rho^{1/2}\left\{\left[A \cdot \frac{1-\epsilon}{\epsilon}\right]^{1/2} z^{1/2} + (\langle v\rangle\, t - z)^{1/2}\right\}$$

or

$$z - V^{**}(0)t = \rho^{1/2}\left\{\left[A \cdot \frac{1-\epsilon}{\epsilon}\right]^{1/2} z^{1/2} + (\langle v\rangle\, t - z)^{1/2}\right\} \Big/ \left[1 + A\left(\frac{1-\epsilon}{\epsilon}\right)\right] \tag{96}$$

Because $C^t(t,z) \equiv 0$ for $z \leqslant V^{**}(0)t$ and for points at the right-hand side of the shock, the expression (96) gives for any point $(t,z(t))$ in the shock-curve the width of the expansion fan for $t \geqslant T_1$. Denoting this width by $L(t)$:

$$L(t) = \rho^{1/2}\left[\left\{A \cdot \frac{1-\epsilon}{\epsilon}\right\}^{1/2} \{z(t)\}^{1/2} + \{\langle v\rangle\, t - z(t)\}\right]^{1/2} \Big/ \left[1 + A\left(\frac{1-\epsilon}{\epsilon}\right)\right] \tag{97}$$

where $(t,z(t))$ is a point on the shock-curve with $t \geqslant T_1$.
For $t \to \infty$, eqn. (91) gives

$$z(t) = s(t) = V^{**}(0)t + 0(t^{1/2})$$

where 0(big Landau symbol) denotes s if t is of the order $t^{1/2}$, which means $s(t)/t^{1/2}$ is bounded as $t \to \infty$. Dividing by t gives $z(t)/t = V^{**}(0) + 0(t^{-1/2})$, and it follows with the aid of $V^{**}(0) = \langle v\rangle/[1 + (1-\epsilon)A/\epsilon]$, that for $t \to \infty$

$$L(t) = 2t^{1/2}\left[\langle v\rangle\, A\left(\frac{1-\epsilon}{\epsilon}\right)\rho\right]^{1/2} \Big/ \left[1 + A\left(\frac{1-\epsilon}{\epsilon}\right)\right]^{3/2} + 0(t^{-1/2}) \tag{98}$$

Hence the width of the expansion fan is asymptotically $0(t^{1/2})$ for $t \to \infty$ and therefore on account of mass conservation

$$C^t(t,z) = 0(t^{-1/2}) \text{ for } t \to \infty \tag{99}$$

which is in accordance with a well-known theorem regarding non-linear mass transport [10].

Using eqn. (82) we may summarize the results of this section as follows; we have for $t \geqslant T_1$

$$\left.\begin{aligned} &C^t(t,z) \equiv 0 \text{ for } z \leqslant V^{**}(0)t \\ &C^t(t,z) \text{ is represented by eqn. (82) for } V^{**}(0)t \leqslant z < V^{**}(0)t + L(t) \\ &C^t(t,z) \equiv 0 \text{ for } z > V^{**}(0)t + L(t) \end{aligned}\right\} \quad (100)$$

where $L(t)$ is to be determined from eqns. (95) and (97). The eqns. (84) and (100) give the complete solution $C^t(t,z)$ of the non-linear ideal model problem (see also Fig. 10).

With the obtained place functions or elution functions computer algorithms can be checked (also with use of statistical moments).

CONCLUSIONS AND DISCUSSION

With the assumed simplifications the mathematical model for non-linear mass transport in columns will be described in the most simple way by eqn. (7). This equation is also the most suitable form as starting point for numerical simulation experiments.

Introduction of moving coordinates reduces the undesirable but unavoidable numerical dispersion effects to a minimum. Furthermore, the described method of characteristics should be a good procedure to check the numerical experiments, but it is undoubtedly an important solution technique for dispersionless non-linear mass transport with arbitrary initial value functions. Concave or convex isotherms, however, simplify this procedure, and research has to be done for the chromatographic interesting field of sigmoidal iso-

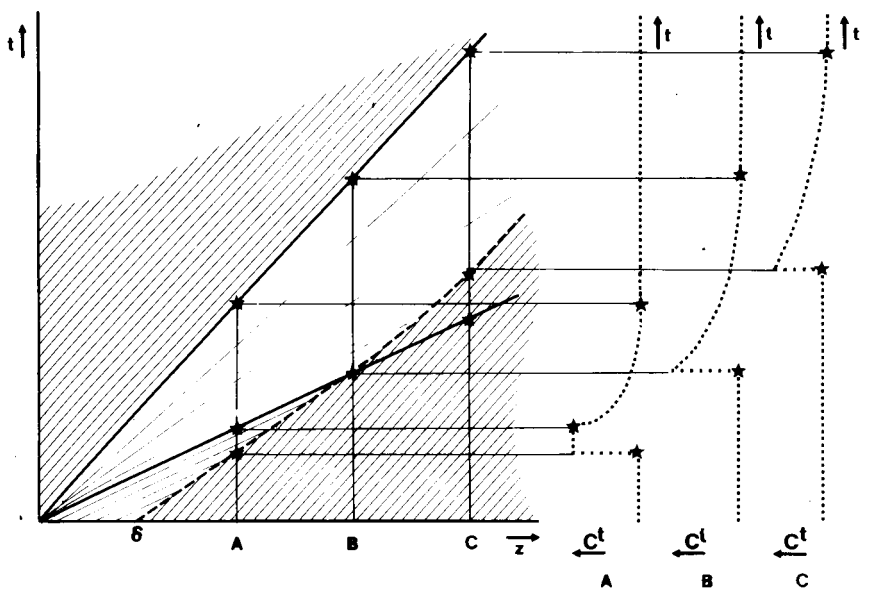

Fig. 10. Construction of elution profiles by means of the method of characteristics.

therms. For checking numerical results in the case of a Langmuir non-linearity, eqn. (100) is useful in describing both place and time functions. With this assumption, it is rather simple to calculate elution curves and at this moment possibilities are being investigated to calculate higher moments to characterize elution profiles for several kinds of isotherms.

The authors thank Professor Dr. J. F. K. Huber, Drs. P. Wilders and Dr. J. W. Reyn for valuable discussions during the preparation of the last section of this paper.

REFERENCES

1 H. C. Smit, Chromatographia, 3 (1970) 515.
2 D. Devault, J. Am. Chem. Soc., 65 (1943) 532.
3 J. Wilson, J. Am. Chem. Soc., 62 (1940) 1583.
4 J. C. Giddings, Dynamics of Chromatography, Dekker, New York, 1965.
5 G. Guiochon and L. Jacob, Chromatogr. Rev., 14 (1971) 77.
6 G. Klein and F. Helfferich, Multicomponent Chromatography, Dekker, New York, 1970.
7 H. Vink, J. Chromatogr., 15 (1964) 488; 18 (1965) 25; 20 (1965) 305; 25 (1966) 71.
8 L. Jacob and G. Guiochon, J. Chromatogr., 65 (1972) 19.
9 B. L. Rozhdenstvenskiy and N. M. Yanenko, Systems of Quasilinear Equations and their Applications to Gas Dynamics (U.S. Army Publ.), Nauka, Moscow, 1968, p. 634.
10 P. D. Lax, Comm. Pure Appl. Math., 7 (1954) 159; 10 (1957) 537.
11 A. Jeffrey, Quasilinear Hyperbolic Systems and Waves; Research Notes in Mathematics, Vol. 5, Pitman, London, 1976.
12 M. van Dyke, Perturbation Methods in Fluid Mechanics, Parabolic Press, Stanford, CA, 1975.
13 P. D. Lax, Regional Conference Series in Applied Mathematics, Vol. 11. SIAM Publications, Philadelphia, 1973.
14 J. F. K. Huber and R. G. Gerritse, J. Chromatogr., 58 (1971) 137.
15 E. Kučera, J. Chromatogr., 19 (1965) 237.
16 O. Grubner, A. Zikonova and M. Ralek, J. Chromatogr., 28 (1967) 209.
17 M. Kubin, Collect. Czech. Chem. Commun., 30 (1965) 1104.
18 D. A. McQuarrie, J. Chem. Phys., 38 (1963) 437.
19 F. Scheid, Schaum's Outline of Theory and Problems of Numerical Analysis, McGraw-Hill, New York, 1971.
20 A. J. P. Martin and R. L. M. Synge, Biochem. J., 35 (1941) 1358.
21 A. C. Vliegenthart, Thesis, Delft University of Technology, The Netherlands (1971).
22 H. Melvin Lieberstein, A Course in Numerical Analysis, Harper and Row, New York, 1969.
23 E. Oram Brigham, The Fast Fourier Transform, Prentice-Hall, London, 1974.
24 F. T. Dunckhorst and G. Houghton, Ind. Eng. Chem. Fundam., 5 (1966) 93.
25 K. Yamaoka and T. Makagawa, J. Chromatogr., 103 (1975) 221.

Analytica Chimica Acta, 122 (1980) 27—40
Computer Techniques and Optimization

A THEORY OF MEASUREMENT WITH APPLICATIONS TO SPECTROMETRY

JOHN C. HELMER

Varian Assoc., 611 Hansen Way, Palo Alto, CA 94303 (U.S.A.)

(Received 7th August 1979)

SUMMARY

An analytic function operating on experimental data is optimized for making the most accurate measurement of a parameter of the expected data, under the conditions of non-stationary shot noise. The value of the parameter is obtained by equating the operation on experimental data with the same operation on the expected data which contains the parameter as an unknown value. If the operation is represented by a weighting function, the form of the optimum weighting function depends on the initial transformation of the experimental data by the measuring instrument. The optimum weighting function always contains the derivative of the expected signal with respect to the unknown parameter, divided by the time-dependent variance of the received signal. Weighting functions for the logarithmic output of a spectrophotometer are described. The superiority over least-squares curve-matching is shown. A method for determination of peak position by optimum slope measurement is derived. In general, the optimum weighting function is not a matched filter. The optimum result is the same for center-of-gravity measurements. The optimum parameter measurement is equivalent to a least-squares error minimization weighted by the inverse variance or mean-square noise level. This variance weighting is significant in photometric measurements limited by shot noise or other measurements described by Poisson statistics, such that the mean-square noise level varies with time. The form of the optimum filter, for non-white, non-stationary noise is derived.

This study began with the question of how to estimate a chemical reaction rate from an optical absorbance measurement. A common procedure is to make a least-squares fit of a theoretical curve to the absorbance data. The reaction rate is then given by the slope of the fitted curve.

An alternative approach would be to pass the absorbance data through a digital filter whose output would directly give the desired slope. This approach is closely related to least-squares curve-fitting. Savitzky and Golay [1] have derived the properties of filters which produce least-squares matching of polynomials to the input data. These are not optimum filters in terms of signal-to-noise ratio but they can often be close to optimum [2].

Optimum or "matched" filters were first discussed in relation to the detection of signals in radar. If $v(t)$ is a measured signal, including noise, and $h(t)$ is a function generated by the measuring system, the output measurement M can be defined by

$$M = \int_{-\infty}^{\infty} h(t)v(t)\mathrm{d}t \qquad (1)$$

If $\sigma^2(M)$ is the variance of M, produced by white noise, then the signal-to-noise ratio, $\langle M\rangle/\sigma(M)$, is maximized by the choice $h(t) = k\langle v(t)\rangle = ks(t)$, where $s(t)$ is the expected value of $v(t)$, and k is an arbitrary constant: then $h(t) = ks(t)$ is known as the matched filter. $ks(t)$ is known beforehand; for example, by the pulse shape. This measurement provides the most sensitive detection of small signals $s(t)$.

From the above, it is not surprising that if $s(t) = Au(t)$, the most accurate estimate of the amplitude A is obtained from the output of a matched filter $h(t) = u(t)$. This result holds only when the noise amplitude is independent of time. In photometric measurements employing a photomultiplier tube, the accuracy is often limited by shot noise which varies with the square root of the signal amplitude. The matched filter is no longer optimum for this case; nor is it optimum for estimating the value of a parameter which is not a linear factor of $s(t)$.

An illustration of the methods used is to calculate the signal-to-noise voltage ratio R that results from boxcar integration over a single peak. This is of importance in determining the loss or gain in sensitivity that may be incurred, for example, by increasing the resolution (reducing peak width) at the expense of sample size. The comparison of packed g.c. columns with capillary g.c. columns is relevant to this issue. Similar questions occur in other analytic techniques.

Let $n(t)$ be the noise voltage. The measured signal is $v(t) = s(t) + n(t)$. The mean-square noise voltage is its variance $\sigma^2(n)$. This results from passing white noise through a preamplifier of bandwidth $B = (2\pi\tau_c)^{-1}$ Hz, where τ_c is approximately the correlation time of the noise. Since $\sigma^2(n)$ is proportional to bandwidth, it is related to the correlation time by $\tau_c\sigma^2(n) = \text{const}$. This constant may be identified as the spectral noise power density. It characterizes the strength of the white noise source.

The peak area measurement is given by $A = \int_0^T v(t)\,dt$, where T is the width of a boxcar chosen to encompass most of the peak. If $\langle\ \rangle$ denotes expected value, then the variance of A is given by

$$\sigma^2(A) = \langle(\int_0^T n(t)\,dt)^2\rangle = \tau_c T\sigma^2(n) \tag{2}$$

The result on the right-hand side is obtained in the following way. The integral squared is evaluated as a double integral with argument $n(t_1)n(t_2)\,dt_1dt_2$. Let $t_2 = x + t_1$ and integrate the expression $n(t_1)n(x + t_1)\,dx$. Since $\langle n(t_1)n(x + t_1)\rangle$ is non-zero only for $x < \tau_c$, this first integral yields $\sigma^2(n)\tau_c$. The second integral then yields the final result.

The signal-to-noise area ratio can be defined by

$$R = \langle A\rangle/\sigma(A) = \int_0^T s(t)\,dt/(T\tau_c)^{1/2}\sigma(n) \tag{3}$$

This shows that sensitivity is lost if the instrumental and sampling changes are such that the peak area decreases faster than the square root of the peak width $T^{1/2}$.

This analysis is in time space as opposed to frequency space, an approach that is motivated by the use of microprocessors. It is possible to store data over a time interval T. The problem is how to operate on these data to extract the information, i.e. the values of parameters. With microprocessors any linear operator $h(t)$ in eqn. (1) may be easily implemented. An excursion into frequency space is undesirable if it can be avoided.

Many books have been written on statistical signal detection and parameter estimation. The subject is often treated as a branch of mathematics, with the consequence that reduction to practice is difficult. For the most part, the development given here is not available in the listed references. Parts of it may be found. The closest work appears to be in the books by Fedorov [3] and Scheffe [4]; both these authors emphasize variance weighting, and use matrix algebra to obtain their results. The current relevance of this subject to analytical chemistry is evidenced by a recent report [5].

The present approach is developed with integral calculus. An unusually simple derivation of the optimum condition is given. The most important conclusion is the significance of variance weighting when the noise variance is time-dependent. This paper should make the theory of measurement more accessible to spectroscopists and others in the analytical field who wish to have the greatest accuracy in their measurements.

USE OF VARIANCE CALCULATIONS

Texts on the theory of statistical measurement tend not to use the concept of signal-to-noise ratio as an optimum criteria. Discussions begin with the criteria developed by Bayes (1763). These depend on attaching conditional information to the measurement output. If costs and other conditional information are not involved, the method of "maximum likelihood" is used. The probability distribution function for the measurement is then determined and its amplitude is maximized, a procedure that depends on knowing the exact form of the distribution function.

Regardless of the theoretical foundations, a spectroscopist can easily measure the signal-to-noise ratio. From a computational standpoint, the calculation of signal-to-noise ratio is an order of magnitude easier than the computation of maximum likelihood. This is because the signal-to-noise ratio is obtained from the first and second moments of the distribution function, which can be calculated from assumed moments of the input signal without knowing the form of the distribution itself. To ensure the value of moment analysis, it is only necessary to assume that the distribution function is of reasonable shape.

Signal-to-noise ratios are calculated in the following way. Suppose that a detector gives a noisy, time-dependent signal $v(t)$, which has an expected value $\langle v(t) \rangle = s(t)$ and a variance $\sigma^2(v)$. This signal is handled with an unspecified (analytic) function $F[v(t),t]$ and value M is measured:

$$M = \int_0^T F(v,t)\,dt \qquad (4)$$

The variance of M, denoted by $\sigma^2(M)$, is calculated in the following way. Since the variance of a sum is equal to the sum of the variances, the variance of M is equal to the integral of the variance of F. If $F(v,t)$ is linear over a range of about $4\sigma^2(v)$, then $\sigma^2(F) = [\partial F(s,t)/\partial s]^2\sigma^2(v)$. If F is a non-linear function, this requires a suitably high input signal-to-noise ratio [6]. This approximation is realistic because it is often necessary to make the most accurate possible measurement under conditions of good signal-to-noise ratio. In contrast, much of the literature on statistical signal detection is focused on conditions of marginal detection.

The appearance of a correlation time τ_c is rationalized in eqn. (2). Otherwise, one notes that at most T/τ_c uncorrelated samples can be acquired in time T from a single channel. If these are summed, then $1/\tau_c$ appears in the integral approximation of the sum and the variance. If the measurement is then multiplied by τ_c to get the present form, the variance must be multiplied by τ^2_c.

With these considerations, $\sigma^2(M)$, the expected value $\langle M\rangle$, and the derivative of the expected value are calculated with respect to an unknown parameter c appearing in $s(t) = s(c,t)$:

$$\sigma^2(M) = \tau_c \int_0^T [\partial F(s,t)/\partial s]^2\sigma^2(v)\,dt$$

$$\langle M\rangle = \int_0^T F(s,t)\,dt \tag{5}$$

$$d\langle M\rangle/dc = \int_0^T [\partial F(s,t)/\partial s](ds/dc)\,dt$$

The value of c in $s(c,t)$ is determined by equating the measurement and its expected value, and solving for c: thus $M = \langle M\rangle$. But different measurements have different values of M, because of noise. This gives rise to a variance $\sigma^2(c) \equiv (\Delta c)^2$. It is clear that $(\Delta c)^2$ is given by the equation $\sigma^2(M) = (\Delta c)^2 \cdot (d\langle M\rangle/dc)^2$. This can be solved for $(\Delta c)^{-2}$, by substituting eqn. (5):

$$(\Delta c)^{-2} = \{\int_0^T [\partial F(s,t)/\partial s](ds/dc)dt\}^2/\{\tau_c \int_0^T [\partial F(s,t)/\partial s]^2\sigma^2(v)\,dt\} \tag{6}$$

If eqn. (6) is multiplied by c^2 the parameter signal-to-noise power ratio is obtained. However, since c is assumed to have a specific value, its inclusion as a multiplier of eqn. (6) is superfluous.

Minimizing the parameter variance

The problem is now to choose the form of $\partial F(s,t)/\partial s$ which maximizes eqn. (6). The integral of F in eqn. (4) then defines the optimum measurement. Equation (6) may be maximized by variational methods [7].

Rather than complete this derivation for $\partial F/\partial s$, it is instructive to consider an example by Benjamin [8], which is attractively simple. The coherent signals from two antennae which have expected signal and incoherent noise

amplitudes given by s_1, n_1 and s_2, n_2 are added using weighting factors a_1 and a_2. The resultant signal-to-noise power ratio R is given by

$$R = (a_1 s_1 + a_2 s_2)^2/(a_1^2 n_1^2 + a_2^2 n_2^2) \tag{7}$$

a_1 and a_2 may be chosen to maximize R such that their values have the relationship $a_2/a_1 = (s_2/n_2^2)/(s_1/n_1^2)$. Note that each a can be chosen to depend only on the signal it multiplies. With this substitution the maximum value of R is given by

$$R_{\max} = (s_1^2/n_1^2 + s_2^2/n_2^2)^2/(s_1^2/n_1^2 + s_2^2/n_2^2) = (s_1^2/n_1^2) + (s_2^2/n_2^2) \tag{8}$$

By induction, if we wish to maximize an expression of the form

$$R = (\sum a_i s_i)^2/\sum a_i^2 n_i^2 \tag{9}$$

then the terms under the summation signs in the numerator and denominator are equated. Thus $a_i^2 n_i^2 = a_i s_i$, or $a_i = s_i/n_i^2$ and $R_{\max} = \Sigma(s_i^2/n_i^2)$. Considering the exact correspondence between eqns. (9) and (6), it can be seen that Δc is minimized if F obeys the relation

$$\partial F(s,t)/\partial s = (\mathrm{d}s/\mathrm{d}c)/\sigma^2(v) \tag{10}$$

such that

$$(\Delta c)^{-2} = \int_0^T [(\mathrm{d}s/\mathrm{d}c)^2/\tau_c \sigma^2(v)]\mathrm{d}t \tag{11}$$

The time variation of $\sigma^2(v)$ has a significant influence on F, and for shot noise $\sigma^2(v)$ is proportional to $s(t)$. From eqn. (4) and $M = \langle M \rangle$, the measurement equation takes the form

$$\int_0^T F(v,t)\mathrm{d}t = \int_0^T F(s,t)\mathrm{d}t \tag{12}$$

The solution for $\partial F/\partial s$ in eqn. (10) can take various forms. If $\sigma^2(v) = \text{const.}$ and $s = \exp(ct)$, for example, then $\partial F(s,t)/\partial s = ts$, and $F(s,t) = ts^2/2$. To implement this solution requires squaring the input signal. Alternatively the function $ts(c,t)$ can be considered as a function only of time, if first a particular value $c = c_1$ is chosen and is not allowed to vary. Then we obtain $F(s,t) = ts(c_1,t)s(c,t)$. Now the expression $ts(c_1,t)$ becomes a weighting function on both $s(c,t)$ and $v(t)$, and is relatively easy to implement. An error in c is incurred because the blind estimate c_1 is of different value. This leads to an iterative solution, in which c_1 is replaced by the value determined for c and the solution is repeated. When precise estimates are to be made, a rough estimate is often available beforehand. Perhaps only one iteration is needed, since the calculated estimate will be insensitive to moderate deviations from the optimum weighting function.

When the expected signal is a linear function of the unknown parameters, as in polynomial curve-fitting, and $\sigma^2(v) = \text{const.}$, then $\partial F/\partial s$ is independent of c and the problem of the initial estimate is avoided. For shot noise, $\sigma^2(v)$ is proportional to s, and the initial estimate must be included in $\sigma^2(v)$ as

well. However, it can happen that the c-dependent part of ds/dc is cancelled by $\sigma^2(v)$, and the initial estimate is not needed in this case.

It is now assumed that $F(v,t)$ is of the form $F(v,t) = h(t)G(v)$, where $G(v)$ is a known function. $G(v)$ represents an initial transformation by the measuring instrument, and this may be the only form in which the signal is available. For example, in a spectrophotometer, $G(v) = \log(v)$. Then from eqn. (10) the solution for $h(t)$ is

$$h(t) = (ds/dc)/(dG(s)/ds)\sigma^2(v) \tag{13}$$

From the relations $ds/dc = (dG(s)/dc)/(dG(s)/ds)$ and $\sigma^2(G) = (dG(s)/ds)^2\sigma^2(v)$, we obtain $h(t) = (dG(s)/dc)/\sigma^2(G)$. Thus the form of the solution is the same, either in signal space, $G(s) = s$, or in the transformed G space.

Corresponding to eqn. (12), the measuring equation now takes the form

$$\int h(t)G(v)\,dt = \int h(t)G(s)\,dt \tag{14}$$

where the parameter c in $s(c,t)$ [and only in $G(s)$ in eqn. (14)] is varied to obtain equality.

Let the expected signal be given by $s(t) = Au(t)$, in which the shape $u(t)$ is known and an estimate of the amplitude A is required. Since A is a linear parameter, $ds/dA = u(t)$ is independent of A. Also it is assumed that the signal is shot-noise limited, such that $\sigma^2(v) = s(t)$. Then from eqn. (13) with $c = A$ and $G(s) = s$:

$$h(t) = \text{const.}/A = \text{const.} \tag{15}$$

It is normally convenient to disregard constant factors multiplying F or $h(t)$, as these cancel out in the expression of eqn. (6). In other words, the signal-to-noise ratio is unchanged by linear gain. Equation (15) is equally well represented by $h(t) = 1$. Thus the most accurate measurement of the amplitude A is obtained by direct integration of the incoming signal, or a simple count of the number of arriving photons in a photon beam.

In contrast, if $\sigma^2(v) = \text{const.}$, then $h(t) = u(t)$, which is the matched-filter solution.

The accuracy given by eqn. (11) appears to agree with the lower bound of the Cramer—Rao inequality for the case of Gaussian noise [9]. It is unclear whether eqn. (11) is equal to this lower bound in general.

Multiple parameters

The previous discussion has shown how to estimate the value of a single parameter. More often the values of several parameters are unknown. If their values are entirely unknown, the position is difficult. If reasonable initial values are available, then an accurate measurement can be made. This is because measurement accuracy is not very sensitive to deviations from the optimum weighting function, as discussed following eqn. (12).

Thus when multiple parameters are involved and their values are roughly known, an accurate value for each is obtained by the single-parameter estimation process, in which the rough values of all parameters are used as

required in the single-parameter weighting function. There are as many weighting functions $h(t)$ and as many measurements M as there are unknown parameters. An iterative solution is indicated, in which the rough parameter values are replaced in the weighting functions by the last estimated values. Only one stored record of the raw data $v(t)$ is needed.

Allowing for the input filter

This analysis has been simplified by assuming that the input bandwidth of the measuring system does not distort the signal. The input bandwidth determines the value of the correlation time τ_c. If the measuring system is nonlinear then this bandwidth must be limited to achieve sufficient signal-to-noise ratio at the input terminals as discussed preceding eqn. (5). Otherwise, the input filter can be considered as part of the total system filter specified by $h(t)$ in eqn. (13). If $g(t)$ is the impulse response of the input filter, a new weighting function $h_1(t)$ can be calculated so that, in combination, they give the desired response. For example, if $G(v) = v$, then $h_1(t)$ is given by solution of the integral equation, $h(x) = \int h_1(t)g(t-x)\mathrm{d}t$. For simplicity, we continue to assume that the input filter does not distort the signal.

NOISE IN A RATIOING SPECTROPHOTOMETER

A high-precision spectrophotometer has an optical sample channel and an optical reference channel. These two channels are time-multiplexed onto a single detector, the logarithm is taken of each signal, and the two are subtracted. This gives the log of the signal ratio. The ratio provides normalization for changes in lamp intensity and solvent transmission. Each channel also adds noise to the measurement.

The signals at the output of the photodetector are $v_1(t)$ and $v_2(t)$, with expected values $s_1(t)$ and $s_2(t)$, and variances $\sigma^2(v_1)$ and $\sigma^2(v_2)$, respectively. $v_1(t)$ is sampled and integrated over a time interval t_1 and $v_2(t)$ over an interval t_2. These intervals are so short that the expected values and variances are constant within them. The wide bandwidth of the detector circuit provides a noise correlation time $\tau_c \ll t_1, t_2$. Then the sampling circuit has outputs u_1 and u_2 with the following properties:

$$
\begin{aligned}
u_1(t) &= \int_0^{t_1} v_1(t+x)\,\mathrm{d}x & u_2 &= \int_{t_1}^{t_1+t_2} v_2(t+x)\,\mathrm{d}x \\
\sigma^2(u_1) &= \tau_c t_1 \sigma^2(v_1) & \sigma^2(u_2) &= \tau_c t_2 \sigma^2(v_2) \\
\langle u_1 \rangle &= t_1 s_1 & \langle u_2 \rangle &= t_2 s_2
\end{aligned}
\tag{16}
$$

where $\langle u_1 \rangle$ is the expected value of u_1, etc. The total sampling time per cycle is $t_s = t_1 + t_2$.

A measurement M is defined with the following properties:

$$
M = \int_0^T h(t)[\ln(u_1/u_2) - \ln(t_1/t_2)]\,\mathrm{d}t/t_s
$$

$$\sigma^2(M) = \int_0^T h^2(t)\{[\sigma^2(u_1)/t_1^2 s_1^2] + [\sigma^2(u_2)/t_2^2 s_2^2]\}\,dt/t_s$$

$$\langle M\rangle = \int_0^T h(t)\ln(s_1/s_2)\,dt/t_s \tag{17}$$

$$d\langle M\rangle/dc = \int_0^T h(t)\,d[\ln(s_1/s_2)]/dc\,dt/t_s$$

In the above, $\sigma^2(M)$ is calculated from a generalization of eqn. (5) by using the additive properties of variance [6]. It is assumed that the parameter c to be estimated is a function of the signal ratio s_1/s_2. The next step is to choose $h(t)$ to minimize the variance $(\Delta c)^2$ in the equation

$$\sigma^2(M) = (\Delta c)^2(d\langle M\rangle/dc)^2 \tag{18}$$

By previous analysis, the integrands of $d\langle M\rangle/dc$ and $\sigma^2(M)$ are equated; this yields

$$h(t) = \{d[\ln(s_1/s_2)]/dc\}/\{[\tau_c\sigma^2(v_1)/t_1 s_1^2] + [\tau_c\sigma^2(v_2)/t_2 s_2^2]\} \tag{19}$$

such that from eqn. (18)

$$(\Delta c)^{-2}_{max} = \int_0^T \{d(\ln(s_1/s_2))/dc]^2 dt/t_s\}/\{[\tau_c\sigma^2(v_1)/t_1 s_1^2] + [\tau_c\sigma^2(v_2)/t_2 s_2^2]\} \tag{20}$$

Normally it is chosen that $t_1 = t_2$. But under the constraint that $t_1 + t_2 = t_s$ = const., the sum term has a minimum with respect to changes in t_1. This occurs when

$$t_1/t_2 = [\sigma(v_1)/s_1]/[\sigma(v_2)/s_2] \tag{21}$$

Thus the sampling time per channel should be proportional to the noise-to-signal amplitude ratio in the channel.

For shot noise, this result has been given by Janossy [10] in the analysis of ratio measurements, for which the optimum occurs at $t_1/t_2 = (s_2/s_1)^{1/2}$. The result is of some value for measuring high absorbance, in which $s_1 \ll s_2$. As compared with the usual case $t_1 = t_2$, the maximum advantage to be obtained is a reduction in $\sigma^2(M)$ by a factor of two. This is evident by assuming that one signal is so strong that its noise contribution is negligible (as a percentage). Then the weak signal can be sampled for a maximum time t_s, which is twice as long.

For shot noise, v_1 and v_2 are electron fluxes (number per second) emitted from a photocathode. These represent the incident photon flux reduced by the quantum yield of the photocathode. For normally high photon fluxes, the following multiplication may be considered noiseless [11]. In a time τ_c the number of electrons $v\tau_c$ emitted by the photocathode has a variance $\sigma^2(v\tau_c) = s\tau_c$. From this, it can be concluded that $\sigma^2(v) = s/\tau_c$. For the case $t_1 = t_2$, we then obtain from eqn. (19), dropping τ_c/t_1:

$$h(t) = [(1/s_1) + (1/s_2)]^{-1}\,d[\ln(s_1/s_2)]/dc \tag{22}$$

Case 1. Let $s_1 = 1$, $s_2 = e^{-ct}$; then $h(t) = t/(1 + e^{ct})$. Although c is unknown, its value can be visually estimated from the raw data and used in $h(t)$. An accurate value of c is that value in the ratio s_1/s_2 which then produces equality in the measurement equation $\langle M \rangle = M$.

Case 2. In Case 1, it is assumed that both the time $t = 0$ at which the rate c becomes active and the value s_1/s_2 at $t = 0$ are known. In general these are unknown, although the time origin can be hidden in the initial value of s_1/s_2. Thus it is necessary to take $s_1 = 1$ and $s_2/s_1 = Ae^{-ct}$, where both A and c must be estimated. The expected data generated by the spectrophotometer are $\ln(s_1/s_2) = ct - \ln A$. If it is assumed that the spectrophotometer is a single-beam instrument, which is achieved by using a noiseless reference beam, $\sigma^2(v_1) = 0$ in eqn. (19), and $t_2 = t_s$, then the weighting functions for estimating c and A are given respectively by $h_c(t) = te^{-c_1 t}$ and $h_A(t) = e^{-c_1 t}$. Here c_1 is the first estimated value of c, and constant multipliers have been dropped. Although measurement time is finite, the result of integration from $t = 0$ to $t = \infty$ is taken for example. This yields the measuring equations

$$(2c/c_1^3) - (\ln A/c_1^2) = \int_0^\infty te^{-c_1 t}\ln(t_s/u_2)\,dt \tag{23}$$

$$(c/c_1^2) - (\ln A/c_1) = \int_0^\infty e^{-c_1 t}\ln(t_s/u_2)\,dt$$

from which the solution for c is

$$c = c_1^2 \int_0^\infty (c_1 t - 1)e^{-c_1 t}\ln(t_s/u_2)\,dt \tag{24}$$

The rate c is therefore obtained by integrating the raw data $\ln(t_s/u_2)$ multiplied by a function $(c_1 t - 1)\exp(-c_1 t)$. The deviation of this function from the Savitzky—Golay method [1], which uses a linear ramp, is evident.

For slope measurement, it will be shown later that the unbiased, least-squares theory of polynomial curve-fitting leads to a weighting function $h(t) = t$. For Case 2, the accuracy obtainable with the ideal weighting function $h(t) = t\exp(-c_1 t)$ can be compared with the accuracy obtained for $h(t) = t$. Using the single-beam shot noise case of eqn. (17), $\sigma^2(u_1) = 0$, $\sigma^2(u_2) = t_2 s_2$, $t_2 = t_s$, eqn. (18) yields

$$(\Delta c)^{-2} = \{\int_0^T h(t)[d(\ln(s_1/s_2))/dc]dt\}^2 / \int_0^T h^2(t)dt/s_2 \tag{25}$$

where T is the integration time. The accuracy $(\Delta c)^2$ obtained with the two $h(t)$ functions vs. T is compared in Fig. 1. Because the noisy part of the data is overweighted by a linear ramp, this method should not exceed a measuring time T of about 3.5 time-constants. In contrast, the ideal measurement makes use of all the data and achieves a significant improvement in accuracy. The best measurement requires integration to at least five time-constants, or an absorbance of 2.2.

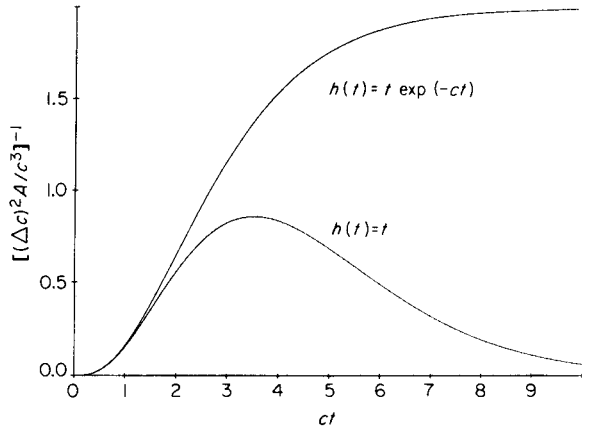

Fig. 1. Measurement accuracy $[(\Delta c)^2 A/c^3]^{-1}$ obtained with the least-squares weighting function $h(t) = t$, compared to the ideal weighting function $h(t) = t\exp(-ct)$.

MEASUREMENT OF PEAK POSITION

Peak position can be treated as a parameter, in which case the previous analysis applies. In this section the peak position is defined operationally, as the point of zero slope on a measurement in which the experimental peak is correlated with a sliding weighting function. $G(v(t))$ is defined as a function of the experimental data $v(t)$; $v(t)$ has an expected value $s(t)$ and a variance $\sigma^2(v)$. If $h(t-x)$ is the weighting function, and $\mathrm{d}M/\mathrm{d}x$ is the desired measurement, then

$$M(x) = \int_{-\infty}^{\infty} G(v(t))h(t-x)\,\mathrm{d}t \tag{26}$$

and the following relationships hold

$$\mathrm{d}M/\mathrm{d}x = \int G(v)(\mathrm{d}h/\mathrm{d}x)\,\mathrm{d}t$$

$$\sigma^2(\mathrm{d}M/\mathrm{d}x) = \tau_c \int [\mathrm{d}G(s)/\mathrm{d}s]^2(\mathrm{d}h/\mathrm{d}x)^2\sigma^2(v)\,\mathrm{d}t \tag{27}$$

$$\langle \mathrm{d}M/\mathrm{d}x\rangle = \int G(s)(\mathrm{d}h/\mathrm{d}x)\,\mathrm{d}t$$

$$\mathrm{d}\langle \mathrm{d}M/\mathrm{d}x\rangle/\mathrm{d}x = \int G(s)(\mathrm{d}^2h/\mathrm{d}x^2)\,\mathrm{d}t$$

At any chosen slope $\mathrm{d}M/\mathrm{d}x$, the position x is uncertain by an amount Δx, given by

$$\sigma^2(\mathrm{d}M/\mathrm{d}x) = (\Delta x)^2[\mathrm{d}(\langle \mathrm{d}M/\mathrm{d}x\rangle)/\mathrm{d}x]^2 \tag{28}$$

That is, if we go to a position x where the slope is expected to be $\langle \mathrm{d}M/\mathrm{d}x\rangle$, the difference is corrected by following the curvature to the chosen value of slope.

The general conditions for validity of this equation are difficult to deter-

mine. For simple spectroscopic peak shapes of time-width T, it is sufficient that $[\tau_c\sigma^2(v)/Ts^2]^{1/2} \ll 1$, where $s/\sigma(v)$ is the signal-to-noise ratio at the peak center. Conservation of peak shape requires that $\tau_c/T \ll 1$. Then the analysis is valid for rather noisy signals.

The expression for $d(\langle dM/dx\rangle)/dx$ does not have the standard form needed for optimization, e.g. $d\langle M\rangle/dc$ in eqn. (5). The standard form can be obtained if $h(t)$ is restricted such that at $t = \pm\infty$, $dh/dt = 0$. With the substitution $dh/dx = -dh/dt$, integration by parts yields the expression

$$d[\langle dM/dx\rangle]/dx = \int [dG(s)/dt](dh/dt)dt \tag{29}$$

Then eqn. (28) can be rewritten in the form

$$(\Delta x)^{-2} = \{\int (dG(s)/dt)(dh/dt)dt\}^2/\{\tau_c \int [dG(s)/ds]^2(dh/dt)^2\sigma^2(v)dt\} \tag{30}$$

It follows that $(\Delta x)^2$ is minimized when

$$dh/dt = [dG(s)/dt]/[dG(s)/ds]^2\sigma^2(v) = [ds/dt]/[\sigma^2(v)dG(s)/ds] \tag{31}$$

Thus far, the value of dM/dx which is to be measured has not been specified. The solution specifies $h(t - x)$ which minimizes the uncertainty in the location of dM/dx. This at the same time determines the value of $\langle dM/dx\rangle$, from eqns. (27) and (31):

$$\langle dM/dx\rangle = \int_{-\infty}^{\infty} \{[G(s)ds/dt]/[\sigma^2(v)dG/ds]\}dt \tag{32}$$

If $\sigma^2(v)$ is either constant or a function of s, then the integrand in eqn. (32) can be expressed as a function of s alone and integrated over ds. If the initial and final values of s are zero, and the integrand is single-valued, it must be that $\langle dM/dx\rangle = 0$. The commonest case is $G(s) = s$, for which $dh/dt = (ds/dt)/\sigma^2(v)$.

For thermal noise, $\sigma^2(v) = \text{const.}$, and the most precise position measurement occurs when $h(t - x)$ coincides with $s(t)$, such that $\langle dM/dx\rangle = 0$. The case when $h(t) = s(t)$ is called the matched-filter solution. The correlation of $h(t - x)$ with $s(t)$ produces a function $M(x)$ which is symmetric about and peaked at $x = 0$, regardless of the initial symmetry of $s(t)$. If shot noise is used instead of thermal noise for the above case, then $\sigma^2(v) = s$, and $h(t) = \ln s(t)$.

In a different photometric problem, the logarithmic weighting function has been obtained by Reiffen and Sherman [12], using the method of maximum likelihood.

The improvement in accuracy in measuring the peak position by the correlation process compared to the accuracy of measurement on the unfiltered peak, depends on whether the curvature of the unfiltered peak is dominated by noise or by signal. If the latter case which requires an initially high signal-to-noise ratio is considered, then the accuracy of measurement $(\Delta t)^{-1}$ on a Gaussian-shaped peak of width T (full width at half maximum) is improved by a factor of about $0.5(T/\tau_c)^{3/2}$.

An alternative method of peak location is to measure the peak center of

gravity. In effect, the peak is multiplied by a function which has the value -1 for $t < x$ and $+1$ for $t > x$. The location is marked by the value x for which the integral is zero. In general, the problem is to establish the function $h(t-x)$ which will provide the most accurate value of x for a specified value of $M(x)$. The previous analysis gives the answer if dM/dx is replaced by M and dh/dx by h. The answer is

$$h(t) = [ds/dt]/[\sigma^2(v)\,dG(s)/ds] \tag{33}$$

Thus if $G(s) = s$ and $\sigma^2(v) = \text{const.}$, the most accurate "center of gravity" measurement is obtained by correlating the peak with its expected time-derivative. This is not a new method, as only the language associated with the previous analysis has been changed. The analytical result remains the same.

THE CONNECTION WITH LEAST-SQUARES CURVE FITTING

When an expected or assumed function $s(t)$ is matched to experimental data $v(t)$ by the method of least squares, the requirement is that $\int_0^T [v(t)-s(t)]^2 dt$ be minimized. If $s(t) = s(c,t)$ contains parameters c which are to be estimated, then the derivative of this integral with respect to each c must be zero. Taking the derivative and equating the two parts of the integrand yields

$$\int_0^T v(t)[ds(c,t)/dc]\,dt = \int_0^T s(c,t)[ds(c,t)/dc]\,dt \tag{34}$$

If the previous example, in which $s(t) = ct - \ln A$, is used, then $ds/dc = t$. Thus the slope estimate is obtained by employing the weighting function t in the measurement equation.

If $v(t)$ is a Gaussian variable with variance $\sigma^2(t)$, then the logarithm of the likelihood that $s(t)$ is the expected value of the measurements $v(t)$ is given by $-\int_0^T [v(t) - s(t)]^2/2\sigma^2(t)\,dt$. If $s(t)$ is a function of parameters c, the likelihood is maximized by minimizing this integral with respect to each parameter c. This is equivalent to the method of least squares when $\sigma^2(t)$ is a constant. If $\sigma^2(t)$ is independent of the parameters c, then in the same way as eqn. (34):

$$\int_0^T v(t)[ds(c,t)/dc]/dt/\sigma^2(t) = \int_0^T s(c,t)\,[ds(c,t)/dc]\,dt\,/\sigma^2(t) \tag{35}$$

This is now compared with the measurement equation (eqn. 12). By expansion, $F(v) = F(s) + (v - s)dF/ds$; the optimum solution (eqn. 10) is then used for dF/ds. Then eqn. (12) becomes identical with eqn. (35). Thus it is proven that a variance-weighted, least-squares parameter estimation is equivalent to the method of the optimum weighting function. For shot noise, $\sigma^2(t)$ also depends on the parameter values, which must remain fixed in $\sigma^2(t)$ during the variational process. This leads to an iterative solution. Otherwise $\sigma^2(t)$ might be measured from the record of $v(t)$. With this restriction, eqns. (10) and (12) are also equivalent to the method of maximum likelihood for Gaussian signals, although these equations include no assumption about the form of the probability distribution for $v(t)$.

SOLUTION FOR NON-WHITE, NON-STATIONARY NOISE

When the noise source is non-white, a more general analysis is required. The signal is defined as $v(t) = s(t) + n(t)$. The expected signal is $s(t) = s(c,t)$ with an unknown parameter c, and $n(t)$ is a random noise function such that $\langle n(t)\rangle = 0$. If $F(v)$ is an analytic operation on v, the measurement is defined as $M = \int_0^T F(v(t))\mathrm{d}t$. The variation in M from noise $n(t)$ is, in the linear approximation,

$$\Delta M = \int_0^T [\mathrm{d}F(s(t))/\mathrm{d}s]n(t)\,\mathrm{d}t \tag{36}$$

From this the variance can be constructed:

$$\sigma^2(M) = \int_0^T [\mathrm{d}F(s(t))/\mathrm{d}s] \int_0^T [\mathrm{d}F(s(t_1))/\mathrm{d}s]\langle n(t)n(t_1)\rangle \mathrm{d}t_1\mathrm{d}t \tag{37}$$

Also we have

$$\mathrm{d}\langle M\rangle/\mathrm{d}c = \int_0^T [\mathrm{d}F(s(t))/\mathrm{d}s](\mathrm{d}s/\mathrm{d}c)\,\mathrm{d}t \tag{38}$$

The value of c is obtained by equating the expected measurement with the actual measurement. The resulting variance $(\Delta c)^2$ is given by $(\Delta c)^2 = \sigma^2(M)/(\mathrm{d}\langle M\rangle/\mathrm{d}c)^2$. As before, the function F which minimizes $(\Delta c)^2$ is given by equating the integrands under $\mathrm{d}t$ in eqns. (37) and (38). Thus, F is given by the solution of an integral equation:

$$\int_0^T [\mathrm{d}F(s(t_1))/\mathrm{d}s]\langle n(t)n(t_1)\rangle \mathrm{d}t_1 = \mathrm{d}s/\mathrm{d}c \tag{39}$$

When $n(t)$ is produced by white noise, this expression is equivalent to eqn. (27).

If the noise properties were stationary in time, it would be possible to use the Wiener—Khintchine theorem that relates the noise autocorrelation function to the spectral noise power density $\rho(\omega)$. Then for ergodic noise the time and ensemble averages are equal, and

$$\langle n(t)n(t+\tau)\rangle = \int_{-\infty}^{\infty} \rho(\omega)\mathrm{e}^{i\omega\tau}(\mathrm{d}\omega/2\pi) \tag{40}$$

where $\langle\ \rangle$ denotes the ensemble average. With the proper interpretation it is still possible to use this expression for non-stationary shot noise, which varies with the signal amplitude. Specifically, $\rho(\omega) = \rho(\omega,t)$ is obtained from the shot noise that would be observed at a fixed amplitude of the expected signal which occurs at time t. In such problems it is customary to approximate the expected signal by a series of stair-steps, such that the noise is stationary on each step [12]. When the expected signal varies slowly compared to the noise, it is clear that $\langle n(t)n(t+\tau)\rangle$ exists and is approximately described by $\rho(\omega,t)$ as defined.

For a shot-noise-limited signal with an expected amplitude of unity, the noise spectral power density is described by $\rho_0(\omega)$. Then if $A(t)$ is the ex-

pected amplitude, $\rho(\omega,t) = A(t)\rho_0(\omega)$. Letting $t_1 = t + \tau$ and $dt_1 = d\tau$, eqns. (39) and (40) then give

$$\int_0^T \{dF[s(t+\tau)]/ds\} \int_{-\infty}^{\infty} \rho_0(\omega) e^{i\omega\tau} (d\omega/2\pi) d\tau = [ds(t)/dc]/A(t) \tag{41}$$

Since $\langle n(t)n(t+\tau)\rangle = \langle n(t)n(t-\tau)\rangle$, the left-hand side is recognized as a convolution integral whose Fourier transformation is the product of the transforms of its functions. If the symbol $\mathcal{F}$ denotes the Fourier transform, the solution is

$$\mathcal{F}[dF(s)/ds] = (1/\rho_0(\omega))\mathcal{F}[(ds/dc)/A(t)] \tag{42}$$

If $dF/ds = h(t)$ with transform $H(\omega)$, and c is a linear parameter such that $ds/dc = u(t)$, with transform $U(\omega)$, and $A(t) = \text{const.}$, then this solution reduces to the better-known case for stationary, non-white noise [2],

$$H(\omega) = U(\omega)/\rho(\omega) \tag{43}$$

which in turn reduces to the matched filter when $\rho(\omega) = \text{const.}$

REFERENCES

1 A. Savitzky and E. Golay, Anal. Chem., 36 (1964) 1627.
2 R. R. Ernst, in J. Haugh (Ed.), Advances in Magnetic Resonance, Vol. 2, Academic Press, New York, 1966.
3 V. V. Fedorov, Theory of Optimal Experiments, Academic Press, New York, 1972.
4 H. Scheffe, The Analysis of Variance, Wiley, New York, 1959, Chap. 1.
5 T. A. Brubaker, R. Tracy and C. L. Pomernacki, Anal. Chem., 50 (1978) 1017A.
6 C. Eisenhard and M. Zelen, in E. Condon and H. Odishaw (Eds.), Handbook of Physics, McGraw-Hill, New York, 1958, Part 1, Chap. 12.
7 W. B. Davenport, Jr. and W. L. Root, Random Signals and Noise, McGraw-Hill, New York, 1958, p. 223.
8 R. Benjamin, Modulation Resolution and Signal Processing in Radar/Sonar and Related Systems, Pergamon Press, Oxford, 1966, p. 119.
9 C. W. Helstrom, Statistical Theory of Signal Detection, 2nd edn., Pergamon Press, Oxford, 1968, p. 265.
10 L. Jánossy, Theory and Practice of the Evaluation of Measurements, Clarendon Press, Oxford, 1965, p. 337.
11 RCA Photomultiplier Manual, RCA Corp., Harrison, NJ, 1970, p. 56.
12 B. Reiffen and H. Sherman, Proc. IEEE, 51 (1963) 1316.

Analytica Chimica Acta, 122 (1980) 41—46
Computer Techniques and Optimization

COMPUTER-AIDED N.M.R. SPECTRA INTERPRETATION
Part 1. An Artificial Intelligence System

M. VIDA

Central N.M.R. Laboratory, Slovak Technical University, 880 37 Bratislava (Czechoslovakia)

(Received 19th July 1979)

SUMMARY

Some desirable hardware and software features of an artificial intelligence system tailored to the needs of a modern computerized n.m.r. laboratory are discussed. A system corresponding to this idea is described.

Molecular structure elucidation is one of the most rewarding and promising branches of nuclear magnetic resonance (n.m.r.) spectroscopy. The complex nature of high-resolution n.m.r. spectra, and the even more complex relations between the spectrum and the molecular structure, make the use of computers very important. Computers are needed not only to control the spectrometer and to acquire and store data, but also to analyze the data in order to achieve deeper insight into spectrum—structure relations.

The present paper describes an attempt to create a highly computerized n.m.r. laboratory as a complex, well organized, and flexible tool for structural elucidation of organic molecules. To achieve this goal, the essential first step is to consider the hardware and software requirements on the basis of a thorough appraisal of present methods and needs.

Description of the problem

Thousands of experimental data acquired during n.m.r. measurements on a given sample have to be transformed, processed, and re-processed several times before the final decision on a chemical structure for the sample can be made. Figure 1 shows a simplified diagram of the multistage process, leading from the raw data to the final information on chemical structure.

Because of its complexity, this process cannot be fully automated at present, but it is possible to accommodate an interactive artificial intelligence system, which can carry the data through the whole process under constant supervision from the operator. The building blocks for such a system are already available: modern Fourier transform n.m.r. spectrometers, relatively inexpensive yet powerful computers, interactive graphics, I/O systems and some basic field-proven software algorithms.

Commercially available up-to-date f.t.n.m.r. spectrometers with built-in

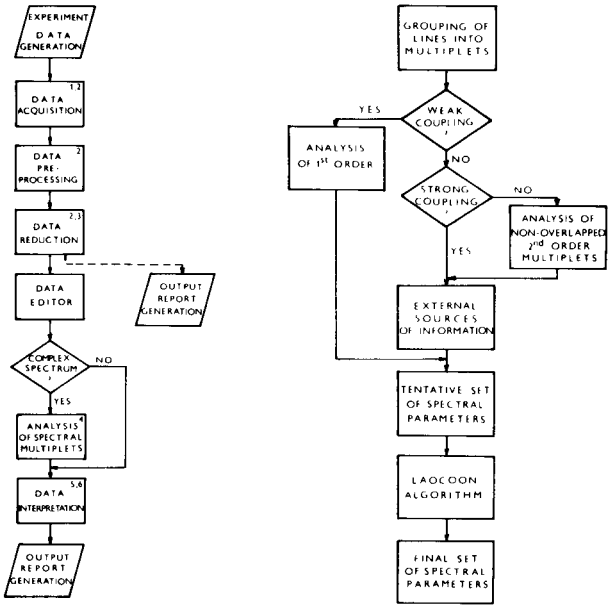

Fig. 1. Generalized diagram of data flow in n.m.r. laboratory. The numbers in the upper right corner denote the relevant literature references.

Fig. 2. Block diagram of analysis of spectral multiplets in a complex n.m.r. spectrum.

dedicated minicomputers, mass storage devices, and interactive graphic display systems, perform satisfactorily at the first stages of the process shown in Fig. 1. Corresponding software and hardware requirements are well known [1—3]. The main emphasis is placed here on flexible interaction between the operator and computer. The resulting data are available in the form of tables of peak positions and relative peak heights.

At present the data flow is discontinued at this point, and the spectroscopist (with occasional partial recourse to computers) is responsible for finishing the work. Though some experts do this interpretation excellently, comments about black magic are not unknown.

Generally, the first and simplest step is to use the data editor routine to transform the data to a suitable scale, delete irrelevant lines (e.g. lines pertaining to solvent) and add any auxiliary information from other measurements (e.g. integral intensities of separated multiplets, multiplicities, etc.). This brings the data to the point where the real problems challenge the spectroscopist's imagination, experience, and ingenuity. Analysis of spectral multiplets, undoubtedly the commonest source of errors in the data evaluation process, leads to extraction of the spectral parameters (i.e. chemical shifts and coupling constants) from the recorded spectra [4]. A self-explanatory block diagram of this procedure is given in Fig. 2.

In work with spectra which do not show line splitting caused by indirect

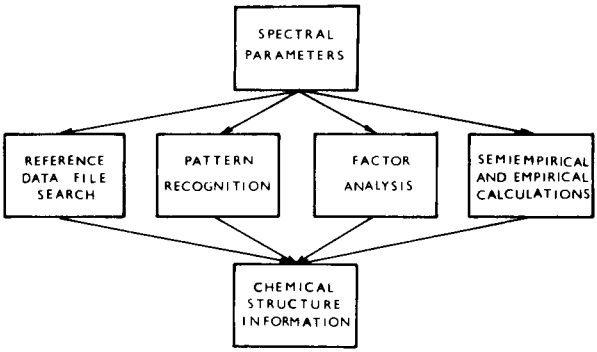

Fig. 3. Generalized data interpretation methods in n.m.r. laboratory.

spin—spin coupling, which is fortunately the case in wide-band proton-decoupled ^{13}C spectra, this procedure can be bypassed and the properly edited data can be used directly by different data interpretation routines, as shown in Fig. 3.

Nowadays, the commonest method of structural elucidation is to compose the structure from individual substructures which have been estimated by consulting the tables of averaged chemical shifts of individual chemical functional groups [5, 6].

Hardware and software requirements

Figure 4 presents a block diagram of a universal artificial intelligence system tailored to the needs of an n.m.r. laboratory. There are two main criteria which will determine the power of such an installation. One is the capacity of the available internal as well as external memory; the other is the flexibility and efficiency of the I/O devices used for interaction of the operator with the system.

Storage-space requirements for the internal memory to accommodate the largest modules of the application software amount to at least 32K words of 16 bits. In addition to this, at least another 16K words are required by the system software, resulting in 48—64K words in total. The last two stages of the data evaluation process, i.e. the analysis of spectral multiplets and data interpretation routines, are the most memory-demanding procedures. A mass storage device with a capacity of at least 1M words will be appropriate to accommodate a modest file of reference data. A link to a large computer would be handy for number-crunching operations.

The problem of human interaction with the application software can be reasonably solved only by means of interactive graphic I/O methods. An intelligent graphic display terminal equipped with a light-pen and a proper hard-copy device is the best choice. Alternatively, a storage CRT dumb terminal can be used. In both cases, the display should be on a large, high-resolution screen, with 1,000 addressable points in the X-axis being desirable.

Analysis of the requirements given in Figs. 1—3 indicates that the applica-

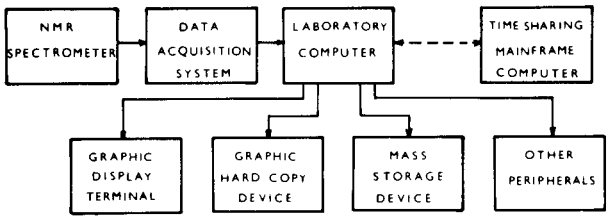

Fig. 4. Hardware block diagram of an n.m.r. laboratory artificial intelligence system.

tion software has to be modular, with individual modules not exceeding 32K words. Because of the diversity of the required functions, which span from data acquisition to interactive I/O operation and from file sorting to heavy number-crunching, a powerful macro-assembler and a high-level language (preferably FORTRAN compiler) must be available for software development. A real-time interrupt driven disk-based operating system is a prerequisite.

CONSTRUCTION OF THE COMPUTERIZED N.M.R. LABORATORY

A few years ago it was decided to build an up-to-date n.m.r. laboratory with a very high sample through-put at the Slovak Technical University. The inadequacy of common off-line and predominantly manual methods of analysis and/or interpretation of n.m.r. spectra became obvious when the expected figures for annual spectra production were estimated. The idea of a fully computerized n.m.r. laboratory integrated into a flexible and powerful artificial intelligence system was quickly adopted.

It was found that the built-in dedicated minicomputers used in n.m.r. instruments, despite their really powerful features, e.g. interactive I/O graphics, disk systems, foreground/background real-time operation, etc., cannot be used to perform all the functions of the desired artificial intelligence system without seriously degrading the operation and sample through-put of the spectrometers. They are, however, perfectly suitable for the first few stages of the process outlined in Fig. 1. Furthermore, the well-known advantages of distributed processing, e.g. increased processing speed, versatility, and the possibility of maintaining some system functions even in the case of partial hardware malfunction, may bring further benefits to the user.

Hence it was decided to compose the system from the dedicated computers used for data acquisition and pre-processing routines, and from an additional computer for the rest of the required system functions. Flexibility and economy were the main criteria here.

Hardware

Figure 5 shows a block diagram of the proposed system. The basic concept of the system can be described best in terms of hierarchical processing networks, operating in a real-time environment and heavily oriented towards the use of interactive graphic I/O methods.

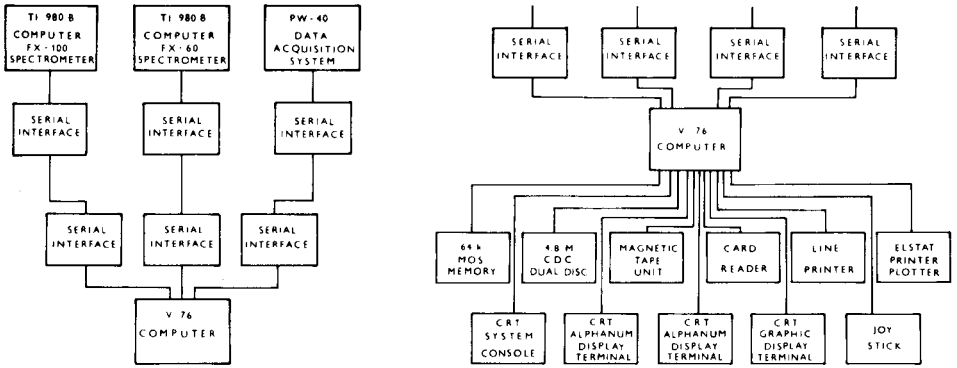

Fig. 5. Distributed processing minicomputer network at STU Central n.m.r. laboratory.

The integrated data system serves three n.m.r. spectrometers. Two pulse f.t.n.m.r. spectrometers, generating the data in relatively fast sequence (up to 50 kHz) are equipped with built-in Texas Instruments 980 B minicomputers. The data acquisition system for a slower broad-line n.m.r. spectrometer is based on a commercial transient recorder.

The heart of the network is formed by a Sperry-Univac V76 minicomputer system, equipped with a large variety of peripherals. This computer works in a multi-task foreground/background real-time environment. A Tektronix graphic CRT terminal with a Varian electrostatic printer/plotter for hard copy forms the main means of human supervision of the artificial intelligence system. More data on this minicomputer network can be found elsewhere [7].

Software

A modified version of the commercially available software packages FAFT 50 and FAFT 01/09 is used for data acquisition, pre-processing (e.g. digital filtering, Fourier transforms, phase correction, etc.) and data reduction on the satellite computers. This highly interactive process is controlled by the spectroscopist by means of a graphic CRT monitor with a light-pen. Subsequently, the data are transferred to pre-allocated files on the system disk of the host computer, where they will wait for calls from the application software.

The continuation of the data evaluation process, controlled now by the spectroscopist from the graphic CRT terminal at the host computer, should closely follow the data flow diagram shown in Figs. 1—3. Because of the complexity of the task that has to be solved at the data analysis and data interpretation stages, some alternative algorithms must be available on this level to give the system a wider scope and enhance its utility.

The host Sperry-Univac V76 system comes with the Vortex II disk-based interrupt driven real-time operating software, capable of multi-tasking operation in foreground/background mode. The macro-assembler DASMR and the FORTRAN IV compiler are available for software development.

DISCUSSION

Apart from the data acquisition system for the broad-line n.m.r. spectrometer, the minicomputer network outlined in Fig. 5 has been assembled and tested. Recently, the hardware and software for data communication within the network has been finished.

The proposed artificial intelligence system software is still under development. However, some important results concerning its most critical parts have already been achieved. This is the case for the analysis of n.m.r. spectra, where the program for analysis of first-order spectra is available and where the well-known programs LAOCOON III and NMREN/NMRIT have been adapted for the analysis of higher-order spectra. Up to 6-spin spectra can be analyzed iteratively by these programs.

For data interpretation, a $^{13}C/^{1}H$ reference data file search system has been built. The system has been found workable in the given hardware and software environment; even though the data files comprise only a few hundred spectra at present, the capacity of one disk cartridge is about 10,000 spectra.

The process of integration of these independent methods into the proposed artificial intelligence system, as well as the development of some other routines, is now under way. However, thanks to the modular character of both the hardware and software of the system, all the existing parts of the proposed system are in regular use already. Essentially, the process of creation of the system is a stepwise replacement of temporary substitutes (i.e. off-line and/or manual operations) by newly developed routines.

Obviously, the proposed artificial intelligence system is not a substitute for a skilled spectroscopist. The vital decisions in choosing the proper steps towards the final structural solution remain a human responsibility. However, this system provides a new dimension in logical problem-solving and in the use of accumulated knowledge. By application of this flexible system, elucidation of the structure of an unknown compound should be accomplished in a few hours rather than days. Preliminary experience with the distributed processing system and the routines available indicates that the integrated on-line data acquisition and evaluation system will be of great help.

REFERENCES

1 J. W. Cooper, Comput. Chem., 1 (1976) 55.
2 T. C. Farrar and E. D. Becker, Pulse and Fourier Transform NMR, Academic Press, New York, 1971.
3 J. W. Cooper, The Minicomputer in the Laboratory, Wiley—Interscience, New York, 1977.
4 P. Diehl, H. Kellerhals and E. Lustig, in P. Diehl, E. Fluck and R. Kosfeld (Eds.), NMR Basic Principles and Progress, Vol. 6, Springer-Verlag, Berlin, 1972, p. 27.
5 N. F. Chamberlain, The Practice of NMR Spectroscopy with Spectra—Structure Correlations for Hydrogen-1, Plenum Press, New York, 1974.
6 F. W. Wehrli and T. Wirthlin, Interpretation of Carbon-13 NMR Spectra, Heyden, London, 1976.
7 M. Vida, Zb. Pr. Chemickotechnol. Fak. SVŠT, 1977—78, in press.

Analytica Chimica Acta, 122 (1980) 47—56
Computer Techniques and Optimization

COMPUTER-AIDED N.M.R. SPECTRA INTERPRETATION
Part 2. Minicomputer-based $^{13}C/^{1}H$-n.m.r. File Search System

V. MLYNÁRIK

Czechoslovak Institute of Metrology, 834 22 Bratislava (Czechoslovakia)

M. VIDA* and V. KELLÖ

Central N.M.R. Laboratory, Slovak Technical University, 880 37 Bratislava (Czechoslovakia)

(Received 19th July 1979)

SUMMARY

Use of a medium-sized minicomputer equipped with a medium-sized disk storage unit for n.m.r. spectral file searching is described. The system is based on two independent reference data files for ^{13}C- and ^{1}H-n.m.r. spectra. Coding of chemical structure is based on a modified linear notation system. With this file search system, mutual assignment of subspectra and substructures can be achieved effectively.

Comparison of spectral data obtained experimentally with reference data collections is the traditional method for structural elucidation of organic compounds. The success of this method depends mainly on the quality and quantity of the reference data. Handling of endlessly growing collections of reference data by conventional means is, of course, very time-consuming. Computer-aided interpretation of n.m.r. spectra has developed rapidly in recent years. Generally, reference spectral data, together with properly coded information on the corresponding chemical structures, are stored in an external memory device of a computer, and sophisticated algorithms are used to search these files for spectral and/or structural features similar to the data to be analyzed. Originally, in n.m.r. spectroscopy, such computerized search systems were built for proton n.m.r. spectra [1—3]. Today, with the increasing importance of carbon n.m.r. spectroscopy, ^{13}C-n.m.r. file search systems are of great interest to practising spectroscopists [4—6].

The common feature of the above-mentioned computerized file search systems is the use of big mainframe computers for this purpose, with the reference data on chemical structure requiring the largest memory storage. Two implementations of ^{13}C-spectral files on small minicomputers have been described [7, 8], but the sacrifices in structural information output from file searches were substantial. The present paper describes an attempt to build an n.m.r. file search system around a medium-sized minicomputer.

SYSTEM DESCRIPTION

The main parts of the system are two reference data files (RDF) and two search programs, for ^{1}H- and ^{13}C-n.m.r. spectra, respectively. Each entry in these data collections contains a reference number, a formula for chemical structure, and chemical shifts of spectral lines together with their intensities (^{1}H RDF) or off-resonance multiplicities (^{13}C RDF). A linear notation is used for encoding chemical structures.

Data retrieval can be achieved with two different search keys, spectral and structural. In the spectral search mode, all spectra exhibiting a reasonable degree of similarity to the input (sample) set of spectral parameters will be retrieved. The output list of the best "hits" gives the respective chemical structure codes and is arranged according to decreasing degree of similarity. In the structural search mode, all the structures having reasonably large structural fragments (substructures) in common with sample the structure will be retrieved. The output list of the best hits includes the respective spectral data and is arranged according to the size of the common substructure.

Structure coding

After a thorough examination of different chemical structure coding methods, with minicomputer implementation in mind, the linear notation system proposed by Skolnik [9] was chosen. The notation is outlined in Table 1. This notation system works similarly to the way in which structural formulae are drawn, accepting even the IUPAC ring-numbering rules. Each notation is unambiguous, yet short and simple. An important feature is the possibility of using structural fragments, so that substructure search becomes effective.

However, practical use of this notation system showed that minor modifications to the system were necessary to make the transformation between structure and notation really unambiguous [10]. Some examples of modifed notations are given in Table 2.

Search algorithm

In the spectral search mode, the main criterion for selective data retrieval is agreement between the chemical shift values of the unknown (sample) spectrum δ_u and the reference spectrum δ_R according to the equation $|\delta_u - \delta_R| \leqslant T$, where the tolerance T provides for all the uncertainties based on structural, solvent, instrumental, and other effects. In ^{13}C-n.m.r. file searches, the corresponding line multiplicities (if they are given) must be identified. In ^{1}H-n.m.r. file searches, the line intensities are consulted, but are of only marginal importance.

To be stored in the hit buffer, a particular reference spectrum must show agreement with the unknown spectrum in a given minimum number of lines L. This criterion and the tolerance T are automatically manipulated by the software. If the hit buffer overflows, the search will be repeated automatically with improved values of the T and L parameters. Finally,

TABLE 1

Notation

CARBONS

Single-bonded		Double-bonded		Triple-bonded		Fused or bridgehead	
$-CH_3$	A	$=CH_2$	E	$\equiv CH$	U	$>CH-$	J
$>CH_2$	C	$=CH-$	B	$\equiv C-$	V	$>C<$	T
$>CH-$	Y	$=C<$	D			$=C<$	R
$>C<$	X	$=C=$	X				

OTHER ELEMENTS AND CARBONYL

Carbonyl		Halogen		Oxygen		Nitrogen		Other	
$>C=O$	K	$-F$	F	$-O-$	Q	$-NH_2$	MH	$-H$	H
		$-Br$	G	$=O$	Q	$>NH$	M	$-S-$	S
		$-I$	I		W	$>N-$	N	$=S$	S
		$-Cl$	L			$\equiv N$	Z	P	P
						$=N-$	Z		

CHARACTER SYMBOLS

.	.	Cyclic structure
:		Atoms between bridgeheads in a cyclic structure
*		Fused or bridgehead atom other than carbon; placed after notation symbol
#		Ionic form
@		Symbol for condensed rings
¬	¬	Polymer repeating unit
&		Used to denote atoms (other than above) with atomic symbol, e.g. &NA for sodium
↑		*Cis*, beta, *exo*, and axial designation
—		*Trans*, alpha, *endo*, and equatorial designation

the hits are arranged according to their similarity, S, to the unknown spectrum; S is calculated by the equation proposed by Bremser et al. [5].

In the structural search mode, the search key is Skolnik's linear notation of the given structure (or substructure) together with the number C of consecutive notation characters which have to be equal to the search key to classify the retrieved structure as a hit. On overflow of the hit buffer, the search will abort and a message will appear on the console.

In Skolnik's notation system, the notation character(s) for a substituent atom (or group) is given in parentheses immediately after the character specifying the atom at which the substitution took place. Thus, the notation characters for directly connected skeleton atoms may not be consecutive in the notation (see Table 2). For generalized substructure searches, without exact specification of every substituent group, a simple search algorithm with stepwise comparison of each consecutive notation character is of limited use.

The search algorithm was therefore modified to provide for the possibility

TABLE 2

Examples of notation

Structure	Notation	Structure	Notation
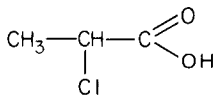	AY(L)KQH	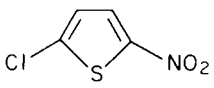	.D(L)BBD(ZW)S.
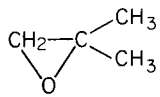	.CX(A)(A)Q.	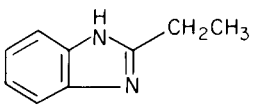	.BBBBRR@ZD(CA

of jumping from any character in the notation of a substituent (i.e., a character placed in parentheses) to the character immediately after the parenthesis to the right. In the search key structural notation, the point of discontinuation is marked by an apostrophe. For example, the notation for the substructure

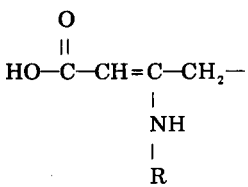

where R is an unspecified substituent, should be either HQKBD(M')C or CD(M')BKQH. When this search key is compared to a suitable reference structure, e.g. ACD(MCA)BKQH, the checking algorithm jumps from the character M to the character B, the notation characters CA of the substituent being ignored. Similarly, the search key .BBD(')BBD('). will retrieve every 1,4-disubstituted derivative of benzene.

Implementation

The n.m.r. file search system was implemented on a Sperry-Univac V76 minicomputer with 64K 16-bit MOS memory. The programs are written in FORTRAN IV and are run under a Vortex II real-time operating system. The reference data files are stored on an IBM 5440-type disk cartridge with a total capacity 5M bytes, sufficient to accommodate about 10,000 references.

Because of the limitations of the available minicomputer system, each compound in the data collection is described by the following parameters only: reference number, structure code (up to 99 characters), chemical shifts (up to 20 or 50 values in the ^{1}H-RDF or ^{13}C-RDF, respectively) and corresponding intensities or multiplicities. Additional information (e.g. the name

of the compound, solvent, concentration, temperature, etc.) can be retrieved by referring to the reference number in a particular RDF manual.

The input to a spectral search run consists of the comparison parameters T and L, and a list of chemical shifts and multiplicities (or intensities in the case of ^{1}H spectra) for all lines of the unknown spectrum. For a structural search run, the comparison parameter C and the linear notation of the query structure (or substructure) is given. The output listing from the ^{13}C spectral search run (Fig. 1) consists of the tables of input values and of the retrieved references with full reference information. The chemical shifts are given multiplied by 10. The chemical shift assignment corresponds to the order of the notation symbols (the first chemical shift corresponds to carbon of the first notation symbol, etc.). The chemical shifts found to be in good agreement with the particular input values are marked by asterisks and their total number is given as the AGR parameter. NUM is the compound reference number in the particular RDF manual. In the case of the ^{1}H-RDF spectral search run, the output listing contains a table of input values and a table of the retrieved structural fragments for individual lines of the unknown spectrum (Fig. 2a) followed by the retrieved references (Fig. 2b). The ^{1}H

```
INPUT CHEMICAL SHIFTS
  95  205 1063 1163 1163 1303 1303 1317 1418 1560
INPUT MULTIPLICITIES
   Q    Q    D    D    D    D    D    S    D    S
LIM= 10      NMIN=  2       AROM. ETHER
TOO MANY OUTPUT STRUCTURES

LIM=  10      NMIN=   3       AROM. ETHER
 AGR  NUM    COMPOUND/CHEM. SHIFTS/MULTIPLICITIES

 10  104   .BBD(A)BBD(QBBA).↑
     1163 1303 1317  205 1303 1163 1560 1418 1063   95    0
        D    D    S    Q    D    D    S    D    D    Q
        *    *    *    *    *    *    *    *    *    *

 SIMILARITY= 1.000
**********************************************************

  8  103   .BBD(A)BBD(QBBA).-
     1165 1302 1316  205 1302 1165 1558 1429 1071  122    0
        D    D    S    Q    D    D    S    D    D    Q
        *    *    *    *    *    *    *         *

 SIMILARITY=  .833
**********************************************************

  7  106   .BBBBBD(QBBA).↑
     1164 1298 1226 1298 1164 1580 1413 1071   95    0    0
        D    D    D    D    D    S    D    D    Q
        *    *         *    *         *    *    *

 SIMILARITY=  .707
**********************************************************

  5  102   .BBBBD(A)D(QBBA).↑
     1147 1272 1226 1313 1275  161 1562 1418 1065   95    0
        D    D    D    D    S    Q    S    D    D    Q
                       *              *    *    *    *

 SIMILARITY=  .544
**********************************************************
```

Fig. 1. An example of the output from the ^{13}C file spectral search run.

```
(a)
INPUT CHEMICAL SHIFTS
  392   800   814  1010
INPUT INTENSITIES
   3     2     2     1
LIM=  15      ILIM=   1      NMIN=   3      4-FORMYLBENZOATE
STRUCTURAL FRAGMENTS
EXP. SH.   LIB. SH.            FRAG.

-------------------------------------
     392         377            (Q  A  ).
     392         378            QC  C  QC
     392         378             L  C  CK
     392         379             .  C  CC
     392         380            D(  M  H)
     392         380                A  KC
     392         380            BQ  C  CQ
     392         380            CQ  C  CQ
     392         382             I  C  BE
     392         387             L  C  CQ
     392         387             G  C  BE
     392         388                E  BQ
     392         391             L  C  BE
     392         394             L  C  CY
     392         399            QB  E  )B
     392         400            QB  E
```

```
(b)
AGR  NUM   COMPOUND/CHEM. SHIFTS/INTENSITIES

   4 518  ./B/BD(/KH)BBD(KQ/A).
          814  800 1010  392    0    0    0    0    0    0    0
            2    2    1    3    0    0    0    0    0    0    0

              *    *    *    *
 AGREEMENT OF INTENSITIES
 SIMILARITY= 1.000
**********************************************************************

   3 311  ./B/B/B/BD(/KH)Z.
          903  788  817  831 1024    0    0    0    0    0    0
            1    1    1    1    1    0    0    0    0    0    0

              *    *         *
 SIMILARITY=  .466
**********************************************************************

   3 477  ./B/BD(KQ/A)/BRR@BBD(KQA)B.
          794  808  397  858    0    0    0    0    0    0    0
            2    2    6    2    0    0    0    0    0    0    0

              *    *    *
 SIMILARITY=  .764
**********************************************************************
```

Fig. 2. Examples of (a) the structural fragment table retrieved for one line of an unknown ^{1}H spectrum, and (b) the output references retrieved in a ^{1}H-RDF spectral search run.

chemical shifts are given multiplied by 100. Their values found in the structural fragments table correspond to protons of the central notation symbol of the given fragment. The ^{1}H chemical shift assignments in the notations of the retrieved structures are marked by a solidus (the first chemical shift corresponds to protons of the first notation symbol found immediately after the first solidus, etc.).

RESULTS AND DISCUSSION

The usefulness of any data collection depends mainly on comprehensive coverage of all classes of chemical compounds. The smaller the number of distinct features per reference, the more reference compounds have to be available in the data file. At present, our data collections contain 600 and 1,000 references in the ^{1}H-RDF and ^{13}C-RDF, respectively; additional references are added frequently. With such small data files, unsuccessful search runs must be expected from time to time, as even the most sophisticated search strategy cannot retrieve substructures or substituents not represented in the data file. However, it was found that these data collections are of adequate size for thorough testing and limited use of the n.m.r. file search system described.

First, it was found that if a compound identical to the subject of query is present in the particular RDF, it will be retrieved with very high probability, despite slight spectral differences caused by different experimental conditions. This is true for both data files. For example, the best assignment for the ^{1}H spectrum of the dimethyl ester of 5-methylisophthalic acid (5% solution in acetone-d_6) was retrieved as the spectrum of the same compound dissolved in chloroform-d_1 (S = 0.855). For these searches, the value T for the tolerance in chemical shift was usually in the range 0.05—0.2 p.p.m. or 1—2 p.p.m., for the ^{1}H and ^{13}C spectra, respectively.

Figure 1 shows the computer output from the ^{13}C file search run. Besides the completely identical structure I (Fig. 3) and its *trans-* isomer II, two additional derivatives of the same basic skeleton indicating *cis-* isomerism and *para-* substitution of the benzene ring were retrieved.

The result of a spectral search generally comprises structures which have important parts in common with the unknown structure. By checking the

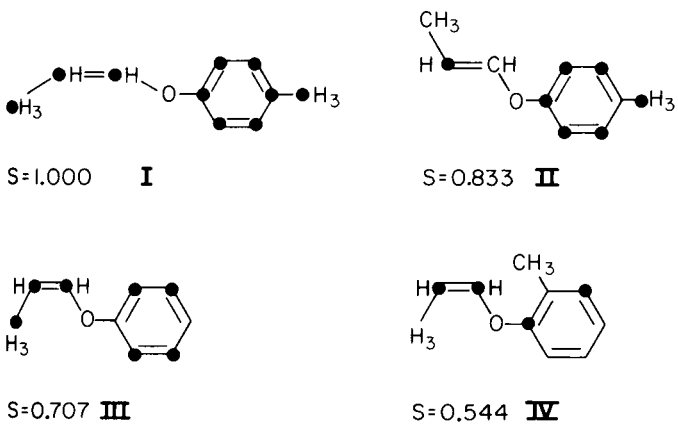

Fig. 3. Output of a ^{13}C file spectral search run for compound I. Corresponding chemical shifts are marked with black circles.

differences between corresponding chemical shifts, the proper placement of substituents can often be inferred directly. If some lines remain unassigned, a second search run limited to these lines may retrieve the missing substituents or parts of the structure not available in the structures retrieved originally.

The ^{13}C-n.m.r. spectrum of an unknown compound (Fig. 4) can be used as a good example of this technique. The spectrum consists of 17 lines, two of which are doubly degenerate. Hence, a monosubstituted or *p*-disubstituted aromatic ring can be expected. Figure 5 shows the structures retrieved. The good agreement of the heterocyclic part of compound V (nine matching lines) and of the aromatic part of structure VI (seven matching lines) is striking. Monosubstitution of the benzene ring and possibly a carbonyl group are indicated by structure VII. The only line assigned neither to structure V nor to structure VI, with a chemical shift of 171.5 p.p.m., might indeed be assigned to a carbonyl group. Actually, a subsequent structural search run for the —CONH— or —CON— group (linear notation KM or KN) found in structures V and VI revealed the possible range of the particular chemical shift to be 162.5—173.5 ppm., thus making structure VIII a possible solution.

A spectral search in the ^{13}C-RDF assigned structures IX and X (Fig. 6) to an unknown derivative of 2-benzylideneindan-1,3-dione. From this result the structure of the indandione part of the molecule seems to be clear. The olefinic proton in the benzylidene part was confirmed by a spectral search in the ^{1}H-RDF (structure XI). Thus, the only remaining uncertainty is the position of the methoxy group. A further search run in the ^{13}C-RDF for the unassigned aromatic signals alone retrieved a few references containing a *p*-methoxyphenyl group. This confirmed *p*-substitution, which was also suggested by the occurrence of two degenerate aromatic lines.

Conclusions

A modern, medium-sized minicomputer equipped with a medium-sized disk storage unit can be used effectively for the storage and operation of ^{13}C/^{1}H-n.m.r. file search systems. Even though the data files are relatively small at present, their use by an experienced spectroscopist is rewarding. Because of the limited number of distinct spectral lines in an average

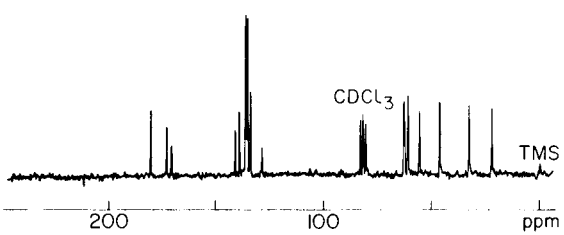

Fig. 4. The ^{13}C-n.m.r. spectrum of compound VIII.

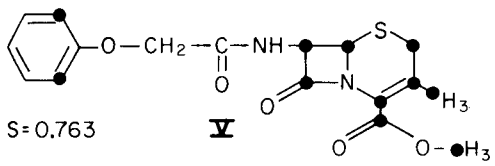

S=0.763 V

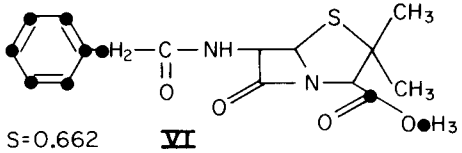

S=0.662 VI

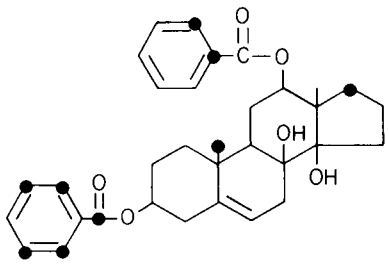

S=0.483 VII

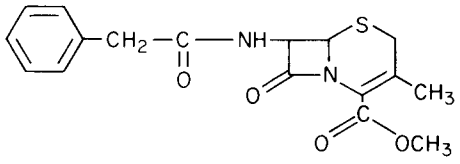

VIII

Fig. 5. Output of the ^{13}C file spectral search run for compound VIII. The corresponding chemical shifts are marked with black circles.

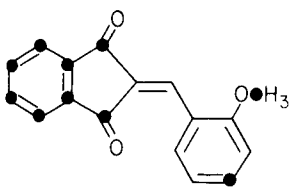

S=0.646 IX

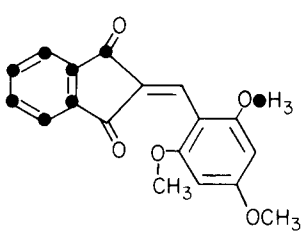

S=0.658 X

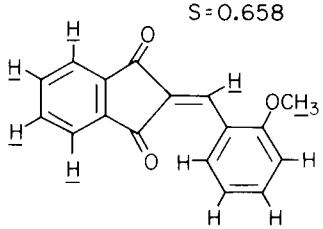

S=0.499 XI

Fig. 6. The structures retrieved by the combined $^{13}C/^{1}H$ file spectral search run for an unknown derivative of 2-benzylideneindan-1,3-dione. Corresponding chemical shifts are marked with black circles or underlined, for ^{13}C or ^{1}H atoms respectively.

^{1}H-spectrum, the independent use of a ^{1}H-n.m.r. reference data file is often rather unsuccessful in attempts to retrieve highly similar compounds selectively. However, in this case the output table of small structural fragments

can be consulted for every unknown spectral line. Furthermore, this data file can often be quite useful as an additional source of information after a ^{13}C reference data file search.

REFERENCES

1 M. H. Jacobs and L. Derslice, Appl. Spectrosc., 26 (1972) 218.
2 S. R. Heller and R. J. Feldmann, J. Chem. Educ., 49 (1972) 291.
3 V. A. Barkhash, S. P. Sokolov, L. F. Sekerina, J. P. Drobyshev and V. A. Koptjug, Izv. Sib. Otd. Akad. Nauk SSSR, 6 (1974) 111.
4 W. Voelter, G. Haas and E. Breitmaier, Chem. Z., 97 (1973) 507.
5 W. Bremser, M. Klier and E. Meyer, Org. Magn. Reson., 7 (1975) 97.
6 J. Zupan, S. R. Heller, G. W. A. Milne and J. A. Miller, Anal. Chim. Acta, 103 (1978) 141.
7 B. A. Jezl and D. L. Dalrymple, Anal. Chem., 47 (1975) 203.
8 R. Schwarzenbach, J. Meili, H. Könitzer and J. T. Clerc, Org. Magn. Reson., 8 (1976) 11.
9 H. Skolnik, Appl. Spectrosc., 26 (1972) 173.
10 V. Mlynárik, Ph.D. Thesis, Slovak Technical University, Bratislava, 1977.

Analytica Chimica Acta, 122 (1980) 57—66
Computer Techniques and Optimization

A MICROCOMPUTER-BASED SYSTEM FOR THE PROCESSING OF SPARK-SOURCE MASS SPECTROMETRY PHOTOPLATES

A. PILATE* and F. ADAMS

University of Antwerp (U.I.A.), Department of Chemistry, Universiteitsplein 1, B-2610 Wilrijk (Belgium)

(Received 21st May 1979)

SUMMARY

A data acquisition system and processing software for spark-source mass spectrometry (s.s.m.s.) with photographic detection is described. The distinctive feature of this system is that data integrity is maintained during the acquisition and real-time reduction. A microprocessor is used to decide whether or not to save the incoming plate blackening data on a digital tape. This results in the selective recording of spectral lines while relatively long fields with only background are neglected. The magnetic tape is then processed on a general-purpose computer. As the complete profile of each peak is recorded, significant improvements can be made for the blackening linearization, the traceback of interferences and the mass calibration. The off-line software makes it possible not only to obtain the elemental sample composition but also to control the instrumental parameters and the photoplate characteristics. This renders the system suitable for research purposes as well as for routine analysis.

Spark-source mass spectrometry is a useful analytical technique whenever survey analyses of complex samples are needed. Many elements can be measured in organic and inorganic matrices with a rather constant detection limit of about 0.5 ppm. For most applications, one is still forced to make use of the ion-sensitive plate as its advantages of integration and simultaneous ion collection are still unequalled by other ion detectors. However, extensive processing of the plates is necessary if good precision and accuracy are needed. Quantitative analysis of the ion-sensitive plates is very time-consuming because of the large data density per exposure and the necessity of using several exposures to cover the entire concentration range from matrix to the sub-ppm region. It consists of the following main steps: densitometry of the spectral lines for a number of exposures; peak detection and linearization of the blackening; evaluation of line intensities; mass calibration; and assignment of an element to each detected mass and calculation of concentrations.

There has been a tendency to use computer-controlled microdensitometers for the measurement and the processing of the blackening data. Several automated systems have been described [1--7]. They are based on the use of either a small on-line digital computer or a large computing facility with practically unlimited data-storage capacity.

Photoplate analysis in this laboratory has so far been done with a commercial JEC-6 system (JEOL, Tokyo) and a JEOL JMA 1340 photoplate-processing dedicated minicomputer [8]. Although this system had been implemented with extensive off-line software [9], several fundamental drawbacks remained untackled, caused by the very limited computer memory available for storing the real-time data. Thus, linearization, peak integration and mass calibration were all done during the densitometry with simplified algorithms and without any possibility of program modification. This results in unreliable data collection and high errors in mass calibration and line-intensity evaluation. Obviously, a more versatile system was needed especially for the analysis of complex samples such as those of environmental origin.

The basic prerequisites of the new system were: (1) the intermediate storage of the digitized blackening data on magnetic tape for off-line peak integration and processing; (2) very limited on-line data processing; (3) substantial real-time data reduction.

Although requirements (1) and (2) suggest a hardware solution, the desired data reduction can be undertaken most profitably by software. As the highest required sampling frequency is 1000 Hz, at least 1 ms of software runtime is available between two data inputs. This lapse of time is sufficient to permit the use of a relatively slow microcomputer if the software is kept simple and straightforward. To realise this, advantage was taken of a characteristic feature of the high-resolution mass spectrum. Indeed, one exposure of the spectrum consists typically of 200 lines, each about 20-μm wide, scattered over the 38-cm long photoplate. Thus most of a spectrum is made up of background so that the selective sampling of only the spectral lines would yield a considerable reduction of the amount of tape storage required. If the selected areas are somewhat wider than the peaks, sufficient background information remains available and a highly versatile off-line processing becomes possible. This selective method was chosen as it allows rather simple algorithms that can be executed by a microprocessor within the timing constraints of the system.

EQUIPMENT

Ilford Q2 plates are exposed in a double-focussing Mattauch—Herzog spark-source mass spectrometer (JMS-01 BM2, JEOL, Tokyo). The developed plate is then measured on a single-beam microdensitometer (JEOL JMD-2C) with a slit width of 3—10 μm. The densitometer delivers a 1-kHz clock signal derived from a crystal oscillator which after further division drives a synchronous motor shifting the photoplate by a screw under the light source and detector. When synchronized on this clock, the blackening is sampled every μm. Experiments have shown that the repositioning precision of the microdensitometer is 2 μm on 30-cm scans. The relatively high sampling rate permits later processing without peak reconstruction or interpolation. Special attention is necessary when dealing with low mass peaks on high re-

solution photoplates. As such peaks have a width of less than 10 μm, profile distortion occurs when the densitometer slit is not adapted. This results in severe errors because of the linearization function used to convert plate blackening to ion intensities and concentrations.

The analog blackening is digitized by an 8-bit AD-converter and fed to the microprocessor. The latter is a commercial board (MOS Technology, KIM-1) containing a 2K byte monitor program in ROM. This monitor allows software development in hexadecimal machine language. About 1K byte of user memory is on the board along with a 22 key-pad and a 6-character 7-segment display. The Rockwell 6502 processor allows the execution of 56 instructions with a cycle time of 1 μs. An audiocassette interface with adequate firmware is included for program storage and retrieval. Other features of this module, e.g. the RS 232 interface and interval timers, are not used in the present application. An asynchronous digital recorder (Kennedy 9832) is used for recording the digitized blackening data. This unit allows writing at a continuous rate of 10 kHz with bursts at up to 250 kHz. The generation of end-of-record marks is automatic after 1024 characters have been written. However, the dead time during this operation is limited to 20 μs thanks to a dual swapping memory bank. End-of-file marks are written under microprocessor control. For the computer compatibility of the generated tape, a 7-track recorder had to be chosen. Each data word of 1 byte must therefore be divided into two 4-bit parts, each filled with two zeros. A general view of the real-time densitometry setup is shown in Fig. 1. The recorded tape is then decoded and processed on a general-purpose PDP 11/45 minicomputer. This machine is extensively equipped with peripherals including an x--y plotter and three disk drives.

THE MICROPROCESSOR PROGRAM

The microprocessor program consists of three blocks: a mode checking

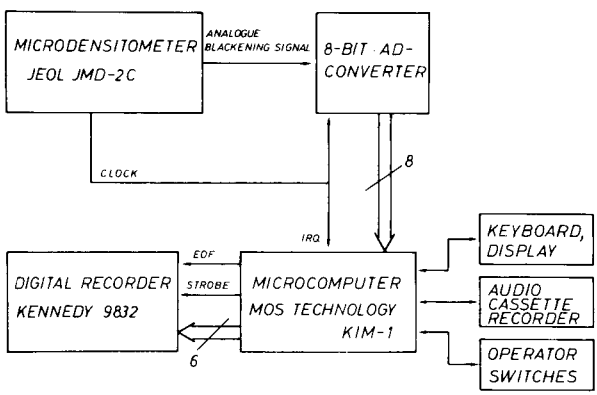

Fig. 1. Data flow in the densitometry setup.

routine, a display routine and a main service routine. The two last blocks are interrupt drives. When an interrupt is serviced, control returns to the mode checking routine, looping typically 20—40 times before the next interrupt is requested. This routine monitors changes of the operator-activated mode switch and manages all initializations, interrupt masks and vectors. In the halt mode, interrupts are vectored to the display routine, while in the run mode they are vectored to the main service routine. When the reading of a new stage is initiated, a user-selected tagword is written on tape. This allows a later reference to be made to the photoplate or analysed sample. The length and the worst-case timing of the routines is shown in Table 1. The display routine is activated only in the halt mode and shows the AD convertor output in hexadecimal code on two 7-segment displays. This is useful to adjust the transmittance scale of the densitometer to 0% and 100%.

The main service routine essentially decides by threshold calculation and comparison whether or not to consider the incoming data from the densitometer as peak information which should be recorded. According to the software decision, the data will be repeated to the magnetic tape recorder, possibly including a protocol for later off-line processing, or deleted. At each interrupt, the data byte from the AD converter is stored in a dedicated memory page. The address within this page is determined by an 8-bit index register. This index is incremented at each interrupt. In this way, the last 256 entries can be accessed for calculation or for output.

Three output triggers are considered by the software: a derivative threshold, a high plate blackening threshold and an operator-activated switch forcing the system to record the area being measured. With these features, both sharp spectral lines and broad hazy peaks are recognised as valid data. The operator also can force the recording of some very faint lines or patterns for special applications. Another switch is used to inhibit the recording of a part of the spectrum, e.g. dust particles or scratches on the plate. This switch overrides all output triggers. When output to the magnetic tape is decided by the system, data are derived from the current input index, I minus 100. One data byte is then written on tape at each interrupt. To ensure a complete recovery of the spectral line on the tape, about 200 bytes are transmitted after the last output

TABLE 1

Software timing and routine length

Routine	Worst-case time (μs)	Length (byte)
Mode check	30[a]	135
IRQ	14	—
Main service	495	280
Display	2000[b]	Monitor firmware

[a]In run-mode. [b]Inactive in run-mode.

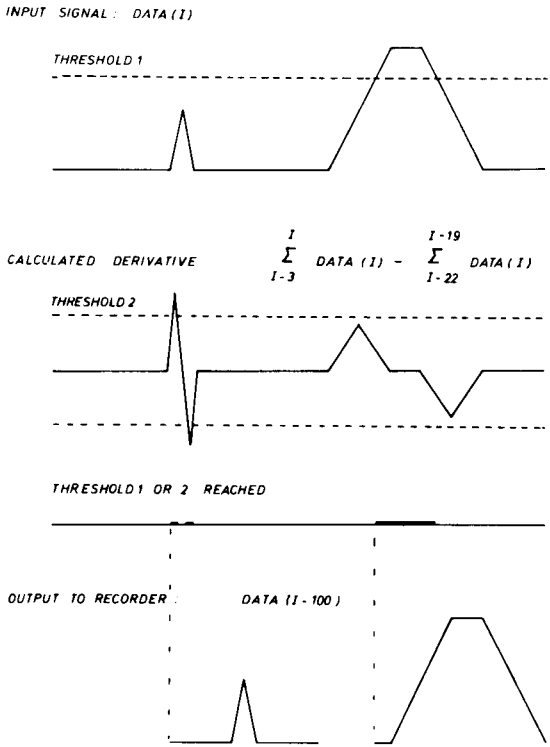

Fig. 2. Threshold activation and algorithms used.

trigger occurred. Figure 2 gives an overview of the threshold activation and of the algorithms used.

As parts of the spectrum of unknown and varying length are deleted on tape, and as the knowledge of the peak position is essential for the correct mass assignation of the spectral lines, trace-back information of the photoplate position must be present. For this purpose, a 24-bit software counter is included in the main service routine. This counter is incremented at each interrupt. When a new peak is detected and before output to tape is generated, this position counter is duplicated at addresses I-99 to I-97. Address I-100 is then filled with a reserved byte, -128, which serves as a beginning-of-peak mark. From this mark, the general-purpose computer used for the subsequent processing of the tape can recognise that the next three bytes are related to the position of the recorded peak. Figure 3 shows a characteristic plot of recorded data. The sharp vertical lines separating the actual spectral peaks are the reserved byte marks and the position bytes. The number at the base of each mark is the numerical translation of the position information expressed in relative distance units with respect to the location where the real-time plate reading was started.

With the data-collecting system, a very sensitive detection of spectral lines

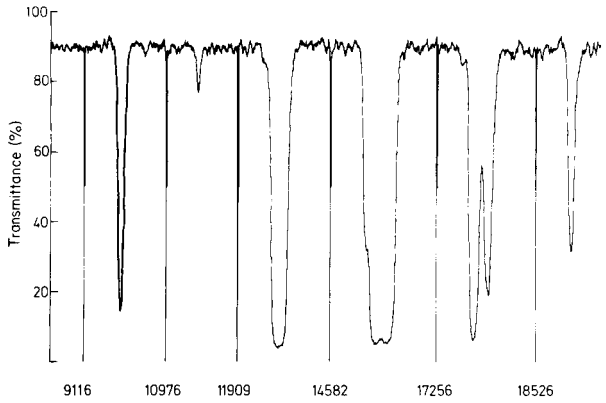

Fig. 3. Typical plot of the data recorded on tape.

is obtained. Even barely visible lines under a photoplate projector are recognised and recorded under software control. Normal working thresholds permit the detection of lines with a transmittance of 3—10% above the background level. The higher figure corresponds to a desensitized condition made necessary by a large number of scratches and dust on a particular plate.

As no processing or linearization is involved in the real-time operation, the flexibility of available primary data is maintained while a data reduction by a factor of 5—10 is obtained.

OFF-LINE PROCESSING

The off-line processing consists of several consecutive programs running on a general-purpose PDP 11/45 minicomputer. Programs are written in FORTRAN IV. Four programs are used in sequence with operator intervention inbetween. Intermediate data are stored on disk cartridge for fast access, or on magnetic tape for long-term record keeping. The general flow chart is shown in Fig. 4.

The first program reads the magnetic tape until a reserved byte mark is encountered. At this moment at least one complete peak is present in memory and a peak search can be initiated. As the determination of a theoretical peak profile is not possible, the search procedure is based on the definition of a threshold level. This level is expressed as a transmittance percent above the background and amounts to 20% in typical working conditions. Smaller peaks also can be detected as this parameter is under operator control at the program runtime.

Before the integration takes place, the plate blackening must be linearized. Several functions are in common use [8, 10]; the empirical Hull equation was chosen because of its relative simplicity and its ability to fit experimental blackening curves over a satisfactory dynamic range. This equation is of the form

$$\text{Ion intensity} = [(1 - T)/(T - T_s)]^K$$

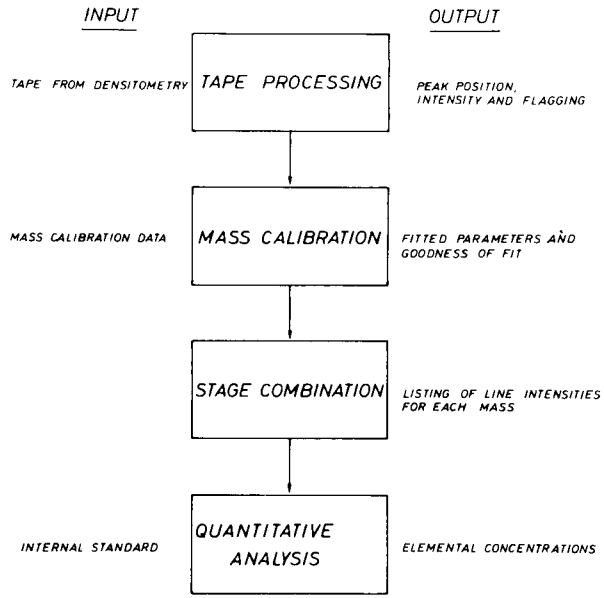

Fig. 4. General flow chart of the off-line software.

where T is the transmittance, T_s the saturation transmittance, and K the reciprocal slope of the calibration curve.

The program at present in use linearizes with constant T_s and K although it would be easy to include mass influence on both parameters. The determination of these parameters is cumbersome but a workable system can be obtained with $T_s = 0$ and $K = 1$. The dynamic range per exposure is then limited to 10 or 20.

Peaks are integrated on both sides down from their maximum until one of the following conditions occurs: (1) a preset percentage, e.g. 20%, of the linearized maximum is attained; (2) the peak tail approaches the background level; or (3) the first derivative (slope) changes sign. Whereas the occurrence of condition (1) is the normal end of a peak integration, condition (2) indicates the presence of a peak of low intensity and condition (3) detects an incompletely resolved multiplet. When the peak is integrated, all corresponding data are zeroed in the computer memory to permit the threshold-based detection of smaller peaks in the same region of the mass spectrum. If no peak is found, the next region is read from the tape and the search is again initiated.

The program delivers an extensive output with individual information on each peak. The output includes peak position (in μm from the initialization point at data acquisition), area, width, maximum blackening, background level, and a complete set of flags indicating, sequentially, peak asymmetry, background characteristics, and the presence of interfering lines. Figure 5 shows results obtained with a doublet at mass 25. The comments are a simple interpretation of the flagging as indicated on the computer output.

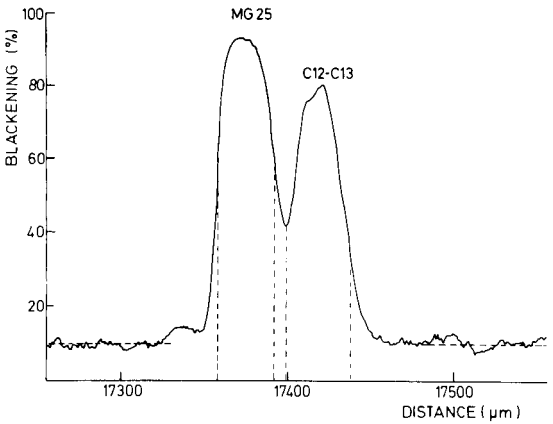

Position (μm)	Area	Width (μm)	Transmittance at maximum	Background transmittance	Comments
17373	288	35	6.2	89.5	No interferences, integration stops at preset percentage (10%) of maximum. Background and peak symmetry OK
17416	83	40	18.7	89.5	Left side interfered, right side reaches the preset percentage. Background and symmetry OK

Fig. 5. Sample output from the tape processing program.

With this output, the operator must identify some characteristic peaks and correlate them accurately to an m/z ratio. The correspondence between positions and masses is used by the second program to perform the mass calibration. The polynomial used for the calibration is

$$\text{Mass} = \left(\sum_{i=0}^{i=N} a_i x^i \right)^2$$

As suggested in Table 2, a degree N of 4—5 gives excellent agreement between the theoretical and experimental masses. For each exposure, the program outputs the fitting parameters and the differences between the tabulated and the fitted masses for the reference peaks used. Up to this point, all plate exposures are processed sequentially. However, the intensity behaviour of spectral lines as a function of the exposure is required. The data recombination needed is carried out by the third program. This program needs no operator input. The output consists of a listing with the line intensity of each ion as measured in all exposures.

The fourth and final program concerns the linear regression of the line intensities versus stage exposure; this involves ion assignation and concentration calculation with respect to an internal standard. A special feature of this program is the determination of calculated exposures, which are found from the ion intensity ratio of each line present in a pair of stages. Equations

TABLE 2

Mass calibration accuracy with varying polynomial degree

Isotope[a]	Expected − fitted mass (milli-a.m.u.)						
	Polynomial degree						
	1	2	3	4	5	6	7
^{24}Mg	0	−1	−2	−1	−1	−1	0
^{28}Si	−11	2	2	2	2	2	1
^{30}Si	−18	0	1	0	0	0	−1
^{41}K	−34	−2	0	−2	−2	−2	0
^{68}Zn	1	1	3	3	3	3	1
^{86}Sr	34	−5	−5	−3	−3	−3	−3
^{100}Mo	67	0	−1	1	1	1	3
^{130}Te	100	1	−2	−2	−2	−2	−1
^{149}Sm	99	9	6	2	2	2	0
^{203}Tl	−107	−4	−3	−3	−3	−4	0
^{207}Pb	−130	−1	1	2	3	3	0

[a]Used as calibration reference.

are found which provide the experimental mean exposure ratio for all possible pairs of stages. A linear least-squares routine then delivers the best-fitting experimental exposures. This method is powerful in detecting any anomaly in the overall procedure, including electrode inhomogeneity, emulsion calibration accuracy and erroneous combination of data. Table 3 gives a typical example of results obtained under optimum conditions. Systematic deviations between calculated and expected exposure data indicate faulty linearization while erratic errors indicate invalid recombination of the different photoplate exposures or that the sample is inhomogeneous. More detailed diagnostic information can be obtained from the ratio equations themselves. Therefore, these are also part of the standard output of this program.

TABLE 3

Sample of output with ratio equations and expected and calculated exposures

Exposure numbers	Number of line pairs	Ratio	S.d. (%)
1, 2	7	0.406	5
1, 3	3	0.134	7
2, 3	6	0.325	8
3, 4	10	0.288	5
3, 5	6	0.312	4
4, 5	24	0.548	2
4, 6	12	0.230	5

Exposures						
From coulometer	0.10	0.30	1.0	3.0	5.0	10.0
Calculated	0.10	0.25	0.75	2.55	4.37	10.56

CONCLUSION

A considerable effort was made to design a setup and to write the corresponding software with all the capabilities required for both routine mass spectrometric analyses and research and development. This end was attained by relatively simple means thanks to the knowledge acquired with the on-line photoplate processing system formerly used in this laboratory.

Using a microprocessor dramatically simplified the hardware requirements since considerable real-time data reduction became possible. This allows for efficient intermediate storage of the densitometry data and for a faster processing on a general-purpose computer.

A relatively simple algorithm based on the binary decision to store or to neglect the incoming data stream was found to be satisfactory both in terms of detection performance and in terms of the data reduction ratio achieved. No acquisition rate or speed penalty is introduced by the microprocessor system and the plate readout time is defined only by mechanical considerations of the densitometer. Having access to the peak profiles also represents an important advantage of this system for many purposes, e.g. spectrometer alignment, emulsion calibration and detection of interferences. Ample control of the operating conditions thus becomes possible.

Comprehensive off-line software further implements the real-time processing described. Highly accurate mass calibration is delivered, greatly facilitating the ion assignation in complex spectra. The modularity of the software also facilitates the assessment of inaccuracies at all levels of the analysis.

The system as presented has been in intensive use for several months with encouraging results in routine analysis of many different standard materials and unknown samples of high complexity.

REFERENCES

1 E. B. Owens and N. A. Giardino, Anal. Chem., 35 (1963) 1172.
2 D. M. Desiderio, Jr. and T. E. Mead, Anal. Chem., 40 (1968) 2091.
3 F. Degrève and D. Champetier de Ribes, Int. J. Mass Spectrom. Ion Phys., 4 (1970) 125.
4 A. Frisch and W. Reuter, Anal. Chem., 45 (1973) 1889.
5 E. J. Millett, J. A. Morice and J. B. Clegg, Int. J. Mass Spectrom. Ion Phys., 13 (1974) 1.
6 R. A. Burdo, J. R. Roth and G. H. Morrison, Anal. Chem., 46 (1974) 701.
7 D. Stuwer, Int. J. Mass Spectrom. Ion Phys., 20 (1976) 387.
8 E. Van Hoye, F. Adams and R. Gijbels, Bull. Soc. Chim. Belg., 84 (1975) 595.
9 B. Vanderborght and R. Van Grieken, Anal. Chim. Acta, 103 (1978) 223.
10 K. D. Shuy and S. Franzen, Z. Naturforsch., 21A (1966) 1479.

Analytica Chimica Acta, 122 (1980) 67—73
Computer Techniques and Optimization

STAIRCASE VOLTAMMETRY AND PULSE POLAROGRAPHY WITH A MICROCOMPUTER-CONTROLLED POLAROGRAPH

P. BARRETT**, L. J. DAVIDOWSKI* and T. R. COPELAND
Department of Chemistry, Northeastern University, Boston, MA 02115 (U.S.A.)
(Received 23rd July 1979)

SUMMARY

A microcomputer, based on the 6502 microprocessor, is applied to the operation and data acquisition with staircase voltammetry and pulse polarography. Results for the reduction of cadmium(II) closely follow theoretical trends, indicating that the approach is a viable alternative to existing analog instruments and more costly minicomputer-controlled systems.

Linear ramp and d.c. voltammetric methods of analysis have largely been replaced by more sophisticated techniques in an effort to enhance sensitivity. These modern methods include staircase, square-wave, and pulse polarography, and various anodic stripping techniques. Because these methods employ complex applied potential functions, there is currently no commercial instrument available with the capability to perform them all. Such an instrument based upon analog circuitry would be expensive, and more importantly, rather inflexible.

Several authors [1—4] have utilized minicomputers to provide this versatility. Moreover, the rectangular shape of these potential functions is intrinsically compatible with digital electronics. While this approach allows the generation of virtually any waveform by means of suitable software, it is certainly not cost-effective because of the expense of the minicomputer. The use of a microprocessor, however, could provide similar advantages at a greatly reduced cost.

The present report is an initial evaluation of such a microprocessor-controlled instrument. Bond and Grabaric [5] have discussed a commercial instrument which is microprocessor-active, but there are severe limitations because of the pre-written software. A microprocessor-based unit, which is open to software manipulations, is a versatile system which should be capable of performing all of the aforementioned techniques. Here, the methods of staircase and normal pulse polarography are presented as a partial example of the capabilities of the system. Two of the most popular voltammetric techniques are differential pulse and square-wave polarography, but these methods

**Present address: Perkin-Elmer Corp., Wellesley Office Park, Wellesley, MA 02181, U.S.A.

were not investigated because of the need for measuring both forward and reverse currents. Since these currents are of opposite sign, their measurement requires a bipolar analog-to-digital converter (ADC) arrangement. The system described here is capable only of unipolar operation. A bipolar ADC is under construction.

To minimize problems arising from changes in the electrode surface area, a stationary electrode (hanging mercury drop) was used in all experiments. Scan rates up to 50 mV ms^{-1} were employed and data acquisition was performed by the microcomputer.

EXPERIMENTAL

Instrumentation

Figure 1 shows a block diagram of the apparatus used. The kit-form microcomputer (Western Data Systems, Santa Clara, CA) is based on the MOS Technology 6502 microprocessor. The complete system is present on two printed-circuit boards. The central processing unit (CPU) board is a stand-alone, eight-bit microprocessor with provision for 1000 bytes of random access memory (RAM). Recording and recovery circuitry for interface to a cassette recorder is present on this board. The CPU board also contains an addressable 8-bit parallel input port and a similar output port. The output port is not presently employed, but can be used for various operational functions such as stirring of solution, flow of purge gas and drop knocker. The input port is connected to a standard ASCII keyboard. This keyboard (G. Risk Industries) is necessary to allow expansion to higher level languages. To allow for system expansion, an S-100 bus is available on the CPU board. A memory expansion board is interfaced to the CPU board via the S-100 bus. The expansion board provides 16 K bytes of RAM and 8 K bytes of read-only memory (ROM). Contained in ROM is the operating system for the microcomputer. This board also contains a processor-active video output to a Wang monitor.

The interface circuitry between the microcomputer and the potentiostat includes a 10-bit DAC (AD7520) and a 10-bit ADC (AD7570). An AD518

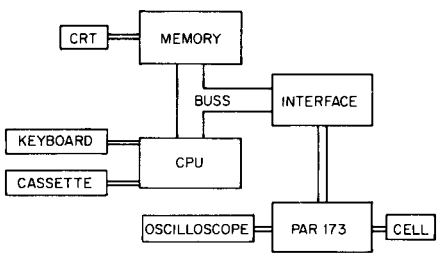

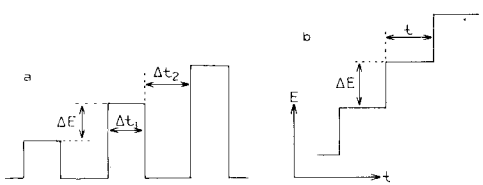

Fig. 1. Block diagram of microprocessor-controlled electrochemical instrument.

Fig. 2. Potential-time waveforms: (a) normal pulse; (b) staircase.

operational amplifier is used as a voltage follower on the DAC output which in its present configuration yields a range of 0 to −1.275 V by increments of 5 mV. The DAC is tri-stated to the data bus by two 74367 integrated circuits; 8212 I/O latches are used to transfer from the data bus to the DAC, and from the ADC to the data bus. The ADC is presently configured for unipolar operation only, with a full scale response at 10 V. Control logic for the ADC is designed such that a memory-write operation at its address will initiate data conversion. A conversion requires ca. 24 μs. This wait-time is provided by software. Data are then transferred to the 8212 and I/O latches are latched onto the data bus with a memory-read operation. The potential-current output (1-V f.s.d.) must be multiplied by ten before introduction to the ADC.

The potentiostat used was a Princeton Applied Research Corp. (PAR) model 173; a PAR model 176 provided the current measurements. The cell was equipped with a hanging mercury drop electrode, a platinum wire auxiliary electrode and a Ag/AgCl reference electrode. All solutions were prepared with water from a Milli-Q system (Millipore Corp.). Acetate buffer (pH 4.0) served as the supporting electrolyte.

Software

In the computer-oriented system described here, software provides the desired versatility of choice between one electrochemical technique or another. The primary element of software in the microcomputer is the operating system which is present in ROM. The operating program has four instructions: load, store, go, and modify (write). The load-and-store commands are used for cassette interface. The go-and-modify instructions execute a program stored in memory and can read or write data into memory.

To expand to a higher-level language, a 2K Tiny BASIC Interpreter was purchased from Peoples Computer Co. (Menlo Park, CA). The program is present on tape whch must first be read into RAM before use. Future plans call for a 6K resident BASIC on ROM which would therefore not occupy RAM locations.

It is well known that the interpreter approach to higher level languages is very time-consuming. For example, the highest-frequency square-wave that a BASIC program can generate is 250 Hz, whereas an assembly language program can produce a square-wave of 10^5 Hz. For this reason it became necessary to write experimental programs in machine code. A new approach was taken which combines the speed of assembly language with the convenience of using BASIC. The concept is to allow a BASIC program to interact first with the user to obtain the desired operating parameters for the experiment. Then, based on this information, the BASIC program writes a tailored machine level program to run the experiment and store the data in memory. The BASIC program retrieves the data and presents it in tabular form on the video monitor. This is currently the only means of data output. The feature of the interpreter which allows for the switching between BASIC and assembly

languages is the USR statement. This USR function is actually a call to a machine language subroutine which can then either transfer control to a certain memory address, write one byte of data into memory, or read one byte of data from memory. The BASIC program is allotted 4K of memory and the machine language program is mapped to 8K. An additional 2K is needed for the interpreter, which leaves 2K available for data storage and video display.

RESULTS AND DISCUSSION

The major limitation of classical d.c. polarography is the presence of double-layer charging current. At low analyte concentrations the charging current becomes an appreciable fraction of the total current, thus limiting sensitivity. Modern polarographic methods achieve high sensitivity by maximizing the ratio of analytical (faradaic) current to charging current.

Pulse polarography

Normal pulse polarography applies a potential scan as a series of pulses, each successive pulse greater in magnitude (Fig. 2a). When a pulse is applied to a potential region where a reduction occurs, there is a sharp increase in both faradaic and charging currents. The rate of decay for charging current is faster than that of the faradaic current, therefore discrimination will result if sampling is performed after the charging current has become negligible. Figure 2a also shows the parameters of the waveform which may be varied, the pulse width (Δt_1), pulse increment (ΔE), and off time (Δt_2).

As theory predicts [6], the polarograms obtained for the normal pulse mode are sigmoidal in shape as in d.c. polarography. In initial experiments, the diffusion current reached a maximum and then tapered off. The cause of these maxima was postulated to arise from the fast scan rates employed; thus Δt_2 was not sufficiently long to allow complete re-oxidation of the deposited species, and depletion of the analyte in the vicinity of the electrode occurred. The effect of Δt_2 upon signal shape is shown in Fig. 3. At low values of Δt_2 (3 ms), the depletion of signal is apparent, whereas at longer values the expected sigmoidal curve is reached. Blutstein and Bond [7] also noted this effect at fast scan rates. All subsequent experiments employed a value of 20 ms for Δt_2.

The influence of pulse height increment (ΔE) was investigated with values ranging from 5 to 50 mV. No significant difference in the height of the current plateau was noted, but the resolution of the polarogram suffers as this parameter is increased. All subsequent experiments were done with pulse increments of 10 mV.

A loss of analytical signal occurs as the sampling delay (Δt_1) is increased from 2 to 20 ms. This is due to the decay of the faradaic current and follows the expected exponential form. The background current remains generally constant over the range of sampling delays studied, indicating that Δt_1 values

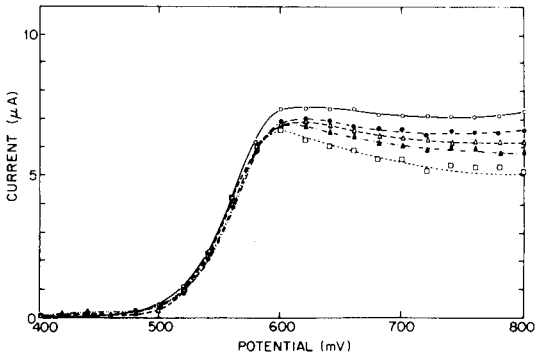

Fig. 3. The effect of off-time (Δt_2) for the normal pulse mode. The curves correspond to off-times of (▫) 3 ms, (▲) 4 ms, (△) 6 ms, (●) 10 ms, (○) 20 ms.

greater than 5 ms are detrimental to the analysis under the afore-mentioned conditions. It should be noted that the current is sampled at instantaneous points, whereas some commercial instruments integrate the current (e.g., PAR 174A over a period of 16.7 ms). A significant increase in sensitivity would be expected if the present ADC were modified to this approach.

Analytical data for cadmium(II) are presented in Table 1. Finally, a mixture of lead and cadmium was analyzed; the polarogram is presented in Fig. 4 to illustrate the resolution obtainable with the technique.

Staircase polarography

The wave form for staircase voltammetry is represented in Fig. 2b. A similar argument for the discrimination against the double-layer charging current applies to this potential function. The step height (ΔE) and step width (t) are variable in 5-mV and 1-ms increments, respectively.

Sweep rates employed frequently exceeded 10 mV ms^{-1} which caused the concentration of analyte to become depleted in the immediate vicinity of

TABLE 1

Analytical data for cadmium(II)

[Cd(II)]		i_p(μA)	
(ppm)	(×10^{-5} M)	Normal pulse[a]	Staircase[b]
2.0	1.78	2.1	2.2
4.0	3.56	4.1	4.9
6.0	5.34	6.0	6.4
8.0	7.12	—	8.4
10.0	8.9	10.0	10.1
		μA mM^{-1} = 1.12 × 10^2	1.13 × 10^2

[a] ΔE = 10 mV, Δt_1 = 3 ms, Δt_2 = 20 ms. [b] ΔE = 10 mV, t = 2 ms.

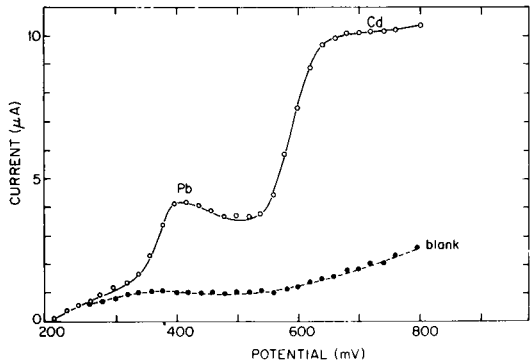

Fig. 4. Normal pulse polarogram for lead and cadmium.

the electrode during a scan. This results in a polarogram which is more peak-shaped than sigmoidal. Christie and Lingane [8] give the theoretical expression for the current at the j^{th} step as: $i = nFC_0D_0^{1/2}t^{-1/2}\Psi(j,\Delta E)$, where Ψ is the current function. The current function is a summation term up to the j^{th} step. It is a function of ΔE, j, $E_{1/2}$, the initial potential, and the point along the step at which the current is sampled. In these studies the current is only sampled at the end of the step. Zipper and Perone [9] have reported the effect of sampling at different points along the step.

As seen in the above equation, the current measured at a particular potential step should be proportional to $t^{-1/2}$. To compare the experimental values obtained with theory, the peak current (i_p) was multipled by $t^{1/2}$. The results (Table 2) show reasonable agreement with theory which states this product should be constant.

Christie and Lingane [8] reported that the ratio $i_p/\Delta E_{1/2}$ is approximately constant. Calculations of this term with ΔE at 10,30 and 50 mV yield 2.84, 2.55, and 2.28, respectively. These results correlate with those of Christie and Lingane in that as ΔE increases, the term $i_p/\Delta E_{1/2}$ decreases slightly. Zipper and Perone [9] reported that the relation between i_p and $\Delta E_{1/2}$ is dependent largely upon the sampling position along the step. These authors also pointed out that the peak potential shifts cathodically as ΔE increases. This trend was also observed in the present study: E_p for ΔE = 50 mV was ca. 602 mV, and E_p for ΔE = 10 mV was 584 mV.

The polarograms for a lead solution and a mixture of lead and cadmium appear in Fig. 5. Resolution is good for the simultaneous analysis. A trade-off exists between resolution and peak current. As ΔE increases, the position of i_p becomes less well defined because of the decrease in the number of readings along the potential axis. This problem is somewhat alleviated by repeating the same experiment several times after increasing the initial potential by values less than ΔE. The microcomputer could store the data and reconstruct the polarogram. Initial experiments have shown this to be a feasible approach.

TABLE 2

Experimental dependence of $i_p t^{1/2}$ on t in staircase voltammetry (ΔE = 10 mV)

t(ms)	1.0	2.0	3.0	4.0	5.0
$i_p t^{1/2}$	16.65	15.41	15.93	16.80	16.51

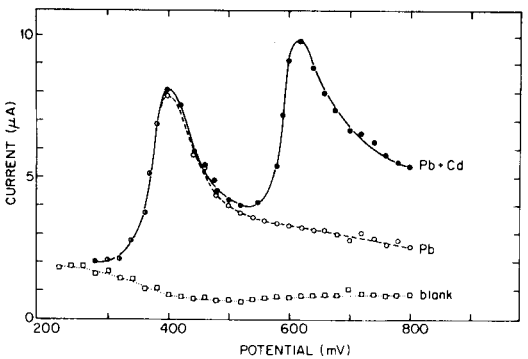

Fig. 5. Staircase polarogram for lead and cadmium.

A calibration study for cadmium(II) by staircase voltammetry is presented in Table 1.

The cost of the complete microcomputer ($750) represents a substantial saving over that of a minicomputer. Detection limits were not studied because it is probable that work at the ultratrace level would require a higher-resolution ADC or a sample-and-hold amplifier.

Possibilities for further work are many. Square-wave polarography and anodic stripping techniques, employing various stripping waveforms, should be amenable to this system with a bipolar ADC. Also, because a computer is an integral part of the instrument, data reduction methods such as ensemble averaging, digital smoothing, derivatization, and background subtraction are all possible.

REFERENCES

1 R. E. Dessy, P. J. Vuuren and J. A. Titus, Anal. Chem., 46 (1974) 917A.
2 R. E. Dessy, J. A. Titus and P. J. Vuuren, Anal. Chem., 46 (1974) 1055A.
3 S. C. Rifkin and D. H. Evans, Anal. Chem., 48 (1976) 1616.
4 A. M. Bond and B. S. Grabaric, Anal. Chem., 51 (1979) 337.
5 A. M. Bond and B. S. Grabaric, Anal. Chim. Acta, 88 (1977) 227.
6 H. Schmidt and M. von Stackelberg, Modern Polarographic Methods, Academic Press, New York, 1963.
7 H. Blutstein and A. M. Bond, Anal. Chem., 48 (1976) 248.
8 J. H. Christie and P. J. Lingane, J. Electroanal. Chem., 10 (1965) 176.
9 J. J. Zipper and S. P. Perone, Anal. Chem., 45 (1973) 452.

Analytica Chimica Acta, 122 (1980) 75—79
Computer Techniques and Optimization

Short Communication

A METHOD OF DATA PROCESSING FOR IMPROVING PRECISION OF INTENSITY MEASUREMENTS IN INDUCTIVELY-COUPLED PLASMA EMISSION SPECTROMETRY WITH A PROGRAMMABLE MONOCHROMATOR

HIROSHI KAWAGUCHI*, TETSUMASA ITO, AKIYOSHI ITO and ATSUSHI MIZUIKE
Faculty of Engineering, Nagoya University, Nagoya 464 (Japan)
(Received 12th July 1979)

Summary. In the computer program described, a Gaussian curve is fitted to the measured line profile and peak intensity is determined from the calculated curve. Relative standard deviations are improved by 20% compared to normal measurements. Effects of the number of accumulations and slitwidths are discussed.

Since very stable light sources such as microwave-induced plasma [1, 2] and inductively-coupled plasma (ICP) [3, 4] have been developed for atomic emission spectrometry (a.e.s.) of solutions, considerable attention has been given to multielement analysis with computer-controlled programmable monochromators [5—8]. Such systems provide great flexibility in the choice of analysis lines, checks for spectral interferences and background correction, which cannot be attained by conventional direct reading spectrometers.

A programmable monochromator with a repetitive optical scanner, which is capable of recording the profiles of all analysis lines and of accurate background correction, has already been described [8]. In this communication, a new method of data processing is reported for improving the precision of intensity measurements in the ICP-a.e.s. system. The calculation is based on fitting a Gaussian curve to a measured line profile and determining the peak intensity from the curve. This procedure allows relative standard deviations of intensity measurements to be decreased by more than 20%.

Experimental

Apparatus. The spectrometric system used was the same as described earlier [8] except that a variable low-pass filter (NF Circuit Design, Model E-3201) was attached to the signal amplifier. The ICP was generated by using a 27-MHz power generator (Nippon Koshuha, crystal controlled, max. 2 kW) with a matching box (Shimadzu Seisakusho) and a gas-flow regulator (Kojima Seisakusho, GM-2A).

Line profiles. Figure 1 shows an example of line profiles recorded when a sample of cocoa powder dissolved in water (1%) was analyzed sequentially for 9 elements. The gain of the amplifier was adjusted for each profile to

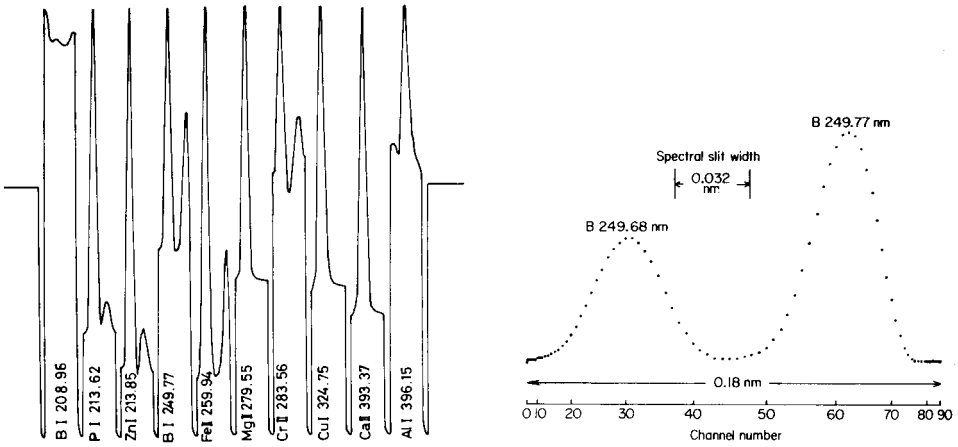

Fig. 1. Line profiles in ICP-a.e.s. Sample: cocoa powder dissolved in water (P 6000; Zn 110; B 17; Fe 55; Mg 4900; Cu 32; Ca 3200; and Al 12 ppm in cocoa).

Fig. 2. Profile of boron lines. Number of accumulations, 416; 10 μg B ml^{-1} solution.

record it within the full width of the chart recorder and the peak intensities corrected for background and amplifier gain were output to a typewriter.

The enlarged profile of a boron doublet is shown in Fig. 2. Ninety data points were acquired during a single scan over a wavelength range of 0.18 nm and each data point was accumulated separately for 416 scans. Though every point in Fig. 2 lies on a smooth curve, the points around the peak are usually more scattered if a weaker line is measured. It was considered, therefore, that the precision of measurement of peak intensity could be improved by fitting a smooth curve to the data points around the peak by the least-squares method and calculating the peak intensity from the equation of the curve. The signal-to-noise ratio enhancement by least-squares polynomial smoothing has been discussed [9].

Preliminary calculations of peak intensity and final procedure adopted. With a mercury hollow-cathode lamp as light source, the intensity of the relatively weak Hg 289.36-nm line was measured repeatedly to optimize the precision. Parabolic, Lorentzian and Gaussian curves were fitted to the 9 data points around each peak of the profile and corresponding peak values were calculated. Mean peak values and their relative standard deviations (RSD) are summarized in Table 1 along with the values for the original data. In the Lorentzian and Gaussian fits, the halfwidth and peak position of each profile were calculated by the corresponding parabolic equation to simplify the calculation in the least-squares method. Obviously, a considerable improvement in precision can be achieved by the Gaussian fit with a fixed halfwidth, especially for narrow slits. Though the line halfwidth must be determined whenever measuring conditions such as the slitwidth are changed, it need not

TABLE 1

Calculation of peak intensity by least-squares method

	Slitwidth 10 μm Low-pass filter 10 kHz		Slitwidth 20 μm Low-pass filter 1 kHz	
	Mean peak value	RSD (n = 9) (%)	Mean peak value	RSD (n = 10) (%)
Original data	0.726	6.6	0.646	2.6
Parabolic fit	0.662	5.9	0.637	2.6
Lorentzian fit				
halfwidth variable[a]	0.704	4.5	0.673	2.7
halfwidth fixed[b]	0.720	3.9	0.665	2.5
Gaussian fit				
halfwidth variable[a]	0.690	4.6	0.655	2.6
halfwidth fixed[b]	0.689	3.8	0.646	2.5

[a]Determined for each profile by parabolic fit. [b]Mean value of parabolic halfwidths used for all profiles.

be determined for each analysis line because the spectral slitwidth of the monochromator is considerably larger than the linewidth.

The halfwidth of the profile can be determined easily by measuring the profile of a relatively strong line (e.g. wavelength calibration line) because a straight line through two adjacent data points closest to the half maximum of the peak represents each side slope of the peak without appreciable error in the measurement of the halfwidth.

As a result of these preliminary calculations, the following procedure was adopted for a computer program:

(1) wavelength calibration with a mercury lamp as light source; (2) measurement of the profile of the calibration line; (3) determination of the halfwidth of the calibration line by using four data points closest to the half maximum of the peak; (4) measurement of analysis lines as described previously [8]; (5) calculation of the peak position of the analysis line in each profile by parabolic fitting of the nine data points around the peak; (6) calculation of peak intensity of the analysis line by Gaussian fitting of the nine data points around the peak by using the halfwidth and peak position already determined; (7) output of the peak intensities of the analysis lines.

Optimum cut-off frequency of amplifier. Since the wavelength is modulated at a frequency of about 100 Hz by a vibrating quartz refractor plate, the cut-off frequency of the signal amplifier cannot be decreased below a certain limit, though the lower cut-off frequency is desirable to reduce the shot-noise. The effect of the cut-off frequency on resolution of spectra is shown in Fig. 3 for a mercury doublet, 313.155 and 313.188 nm. Such resolution tests gave the optimum cut-off frequencies for various slitwidths as follows: 4 kHz for 5 μm, 3 kHz for 10 μm, 2 kHz for 15 μm and 1 kHz for 20 μm. These optimum cut-off frequencies were used thereafter.

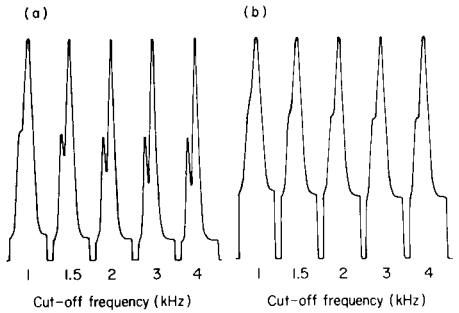

Fig. 3. Effect of cut-off frequency on resolution for the Hg 313.155 and 313.183-nm lines. Slitwidth: (a) 10 μm, (b) 15 μm. Low-pass filter, 24 db oct^{-1}.

Results and discussion

The mercury hollow-cathode lamp was used as the light source in several experiments to examine the improvement in precision and the influence of the slitwidth. A relatively weak line (Hg 289.36 nm) and a strong line (Hg 253.65 nm) were measured, the latter being used as a calibration line. The RSD of peak intensities for the original data and the calculated values are shown in Fig. 4 as a function of the number of accumulations. The corresponding measuring time is indicated on the bottom scale. A 20—40% decrease in RSD by the proposed method of data processing can be observed for almost all data pairs. The slope of the curves for a weak line is about —1/2, that is, nearly theoretical. This means that measuring time can be reduced by 35% for a given RSD when the RSD is reduced by 20% by the data processing.

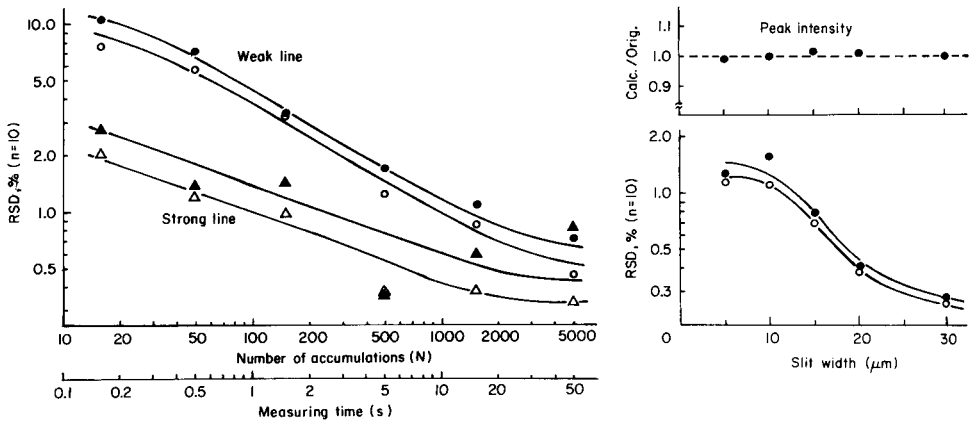

Fig. 4. Improvement in precision of peak intensity measurements for the weak Hg 289.36-nm line (○, ●) and the strong Hg 253.6-nm line (△, ▲). Open symbols represent the calculated results and filled symbols the original results. Slitwidth 10 μm.

Fig. 5. Effect of slitwidth on precision for the Hg 289.36-nm line for the original (●) and calculated (○) data. Number of accumulations, 1024.

Figure 5 shows the effect of slitwidth on the RSD for intensity measurements. The RSD decreases as the slit widens, because of the increased light flux introduced into the detector, and is also decreased by the data processing. The ratios of the calculated peak intensities to the original data (Fig. 5) show that the difference between the two values is less than 1% in the whole range of slitwidth examined.

REFERENCES

1 S. Murayama, H. Matsuno and M. Yamamoto, Spectrochim. Acta, Part B, 23 (1968) 513.
2 H. Kawaguchi, M. Hasegawa and A. Mizuike, Spectrochim. Acta, Part B, 27 (1972) 205.
3 V. A. Fassel and R. N. Kniseley, Anal. Chem., 46 (1974) 1110A, 1155A.
4 S. Greenfield, H. McD. McGeachin and P. B. Smith, Talanta, 23 (1976) 1.
5 D. J. Johnson, F. W. Plankey and J. D. Winefordner, Anal. Chem., 47 (1975) 1739.
6 R. W. Spillman and H. V. Malmstadt, Anal. Chem., 48 (1976) 303.
7 P. W. J. M. Boumans, G. H. van Gool and J. A. J. Jansen, Analyst, 101 (1976) 585.
8 H. Kawaguchi, M. Okada, T. Ito and A. Mizuike, Anal. Chim. Acta, 95 (1977) 145.
9 C. G. Enke and T. A. Nieman, Anal. Chem., 48 (1976) 705A.

Analytica Chimica Acta, 122 (1980) 81—85
Computer Techniques and Optimization

Short Communication

THE DETERMINATION OF HYDROXIDE AND CARBONATE IN CONCENTRATED SODIUM CHLORIDE SOLUTIONS

W. B. ROOLVINK

Akzo Zout Chemie Research, Analytical Department, Hengelo (The Netherlands)

M. BOS

Department of Chemical Technology, Twente University of Technology, Enschede (The Netherlands)

(Received 14th September 1979)

Summary. A computer method for the determination of carbonate and hydroxide in concentrated (2.89 M) sodium chloride solutions is described. The method is based on multiparametric curve-fitting and can also be applied to salts of dibasic acids with unknown equilibrium constants. The systematic error is not more than 1%. The titration and calculation takes less than 20 min.

In the potentiometric titration with hydrochloric acid of hydroxide and carbonate of concentrations less than 0.01 M it is often impossible to determine the equivalence point of hydroxide from the inflexion point or first derivative [1]. The calculation of the hydroxide concentration from the equivalence points of carbonate is not very accurate. Straightforward Gran plots are sometimes curved, while more sophisticated linearization techniques require accurate values of the equilibrium constants [2, 3]. Another method with at least comparable versatility is multiparametric curve-fitting [4—8].

This paper describes the adaptation of the Wentworth method [9], as used earlier by Bos [8] for the titration of mixtures of a weak and a strong acid with sodium hydroxide, for the determination of hydroxide and carbonate in 2.89 M (3.00 m) sodium chloride solutions. Four parameters from the charge-balance equation are adjusted to obtain a least-squares fit, the concentrations of hydroxide and carbonate, and both the equilibrium constants of carbonate.

Theory

The symbols are defined in Table 1.

Charge-balance equations. The charge-balance equation valid for each point of the titration curve of a salt of a dibasic acid and a strong base with hydrochloric acid is given by

$$M_{H^+} + M_{M^+} - M_{Cl^-} - 2M_{Y^{2-}} - M_{HY^-} - M_{OH^-} = 0 \quad (1)$$

TABLE 1

Glossary of symbols

a	activity	K_2	second dissociation constant of th acid
f	activity coefficient	K_1^0	initial estimate of K_1
M	concentration	K_2^0	initial estimate of K_2
C_{OH^-}	concentration of sodium hydroxide at start of titration	K_w	dissociation constant of water
$C_{Y^{2-}}$	concentration of weak acid at start of titration	a_w	activity of water
$C^0_{OH^-}$	initial estimate of C_{OH^-}	T	titer of hydrochloric acid
$C^0_{Y^{2-}}$	initial estimate of $C_{Y^{2-}}$	V	volume of hydrochloric acid adde
K_1	first dissociation constant of the dibasic acid	V_0	volume at start of titration
		F_i	function relating V and a_{H^+}
		H_2Y	weak acid
		MOH	strong base

Combination of this equation with the following relationships:

$$M_{M^+} = C_{OH^-} + 2C_{Y^{2-}}; \; K_1 = a_{HY^-} a_{H^+}/a_{H_2Y}; \; M_{HY^-} = K_1 a_{H_2Y}/f_{HY^-} a_{H^+};$$

$$K_2 = a_{Y^{2-}} a_{H^+}/a_{HY^-}; \; M^2_{Y^-} = K_2 a_{HY^-}/f_{Y^{2-}} a_{H^+} = K_2 K_1 a_{H_2Y}/f_{Y^{2-}} a^2_{H^+};$$

$$K_w = a_{H^+} a_{OH^-}/a_w$$

and (if the activity coefficient of the uncharged a_{H_2Y} is taken as unity)

$$C_{Y^{2-}} = M_{H_2Y} + M_{HY^-} + M_{Y^{2-}} = M_{H_2Y} [1 + (K_1/f_{HY^-} a_{H^+}) + (K_1 K_2/f_{Y^{2-}} a^2_{H^+})]$$

gives

$$F_i = 0 = \frac{a_{H^+}}{f_{H^+}} + \frac{C_{OH^-} V_0}{V_0 + V} - \frac{TV}{V_0 + V} + \frac{V_0 C_{Y^{2-}} (2a_{H^+} + K_1/f_{HY^-})}{(V_0 + V)[a_{H^+} + (K_1 K_2/f_{Y^{2-}} a_{H^+}) + (K_1/f_{HY^-}} - \frac{K_w a_w}{f_{OH^-} a_{H^+}} \tag{2}$$

Multiparametric curve-fitting. Equation (2) relates the experimental data V and a_{H^+} and contains the parameters f_{H^+}, f_{OH^-}, V_0, K_w, T, a_w, $C_{Y^{2-}}$, C_{OH^-}, K_1, and K_2. K_w, T, and V_0 are known previously. The activity coefficients and the water activity are constant during a titration in 2.89 M sodium chloride: $K_w = 0.894 \times 10^{-14}$; $a_w = 0.893$; $f_{H^+} f_{OH^-}/a_w = 0.962$; and $f_{OH^-} f_{H^+} = 0.859$ [10]. In order to calibrate the glass electrode for hydrogen ion concentrations, f_{H^+} is assumed to be 1.000 [4]; this gives f_{OH^-} as 0.859. $f_{Y^{2-}}$ and f_{HY^-} are also assumed to be 1.000.

The parameters to be evaluated by least-squares analyses are therefore $C_{Y^{2-}}$, C_{OH^-}, $K_1 = a_{H^+} M_{HY^-}/a_{H_2Y}$, and $K_2 = a_{H^+} M^2_{Y^-}/a_{H_2Y}$. The Wentworth method requires the partial derivatives of F_i with respect to V, to a_{H^+}, and to the four parameters. These are listed in the following equations:

$$\delta F_i/\delta V = -\{(C_{OH^-} V_0)/(V_0 + V)^2\} - \{TV_0/(V_0 + V)^2\} - \{V_0 C_{Y^{2-}} (2a_{H^+} + K_1)/(V_0 + V)^2 [a_{H^+} + (K_1 K_2/a_{H^+}) + K_1]\}$$

$$\delta F_i/\delta a_{H^+} = 1 + \{a_w K_w/(f_{OH^-} a_{H^+}^2)\} + \{K_1 V_0 C_{Y^{2-}} (1 + K_2/a_{H^+}) (4 + K_1/a_{H^+})/ (V_0 + V) [a_{H^+} + (K_1 K_2/a_{H^+}) + K_1]\}$$

$$\delta F_i/\delta C_{OH^-} = V_0/(V_0 + V)$$

$$\delta F_i/\delta C_{Y^{2-}} = V_0(2a_{H^+} + K_1)/(V_0 + V) [a_{H^+} + (K_1 K_2/a_{H^+}) + K_1]$$

$$\delta F_i/\delta K_1 = -V_0 C_{Y^{2-}} (2K_2 + a_{H^+})/(V_0 + V) [a_{H^+} + (K_1 K_2/a_{H^+}) + K_1]^2$$

$$\delta F_i/\delta K_2 = -V_0 C_{Y^{2-}} K_1(2 + K_1/a_{H^+})/(V_0 + V) [a_{H^+} + (K_1 K_2/a_{H^+}) + K_1]^2$$

Experimental

Chemicals. The chemicals were of analytical grade; sodium chloride (Merck) was used as received, whereas sodium carbonate (Merck) was dried for 2 h at 120°C. Sodium hydroxide and hydrochloric acid solutions were prepared by adding the content of a Merck titrisol ampoule to a calculated quantity of sodium chloride, and diluting with carbon-dioxide-free water to the specified volume.

Equipment. The titrations were controlled and evaluated by a PDP 11-10 computer with 16K core memory RK 05 disk, and a laboratory peripheral system (LPS) comprising a 12-bit ADC and a Teleprint telewriter. The pH was measured with a Schott combined glass—calomel electrode (type N) with a platinum wire diaphragm and a Knick industrial pH meter (type Din). The titrant was added with a Mettler DV 11 automatic burette into a Metrohm thermostatted titration vessel. A Lauda ultra-thermostat (type 43/58/12) was used to maintain 25.0 ± 0.1°C in the titration vessel.

Calibration of the combined electrode. To prevent any effect of a change in the liquid junction potential on the calibration constants, the combined electrode was calibrated in 2.89 M sodium chloride solutions. The pH values of 0.01 M HCl, 0.01 M NaOH, and 0.01 acetate buffer were calculated to be 2.00, 12.03, and 4.79, respectively. These standards were used to calculate the calibration constants in the pH regions 2.00—5.00 and 5.00—12.00.

Titrations. Samples were prepared by mixing sodium carbonate and sodium hydroxide solutions and diluting with 2.89 M NaCl to 50 ml. The electrodes were allowed to equilibrate for 5 min whereafter the titration with 0.1000 M HCl in 2.89 M NaCl was started. The titrations were done under nitrogen at 25.0 ± 0.1°C by addition of constant increments (0.30 ml) of titrant. After each addition, there was a constant time-delay of 30 s to attain equilibrium before pH measurement.

Computer programs. The monitoring program with three real-time tasks divides the memory into four parts, for three real-time programs and the background. The background program runs in the time that is not used for a real-time task. The calibration program calculates the slope and standard potential of the electrode from e.m.f. data for two buffers, taken by the ADC of the LPS from the pH meter and their pH values read from the teletype. Output of the calibration constants is to the teletype. Before each

TABLE 2

Results of titrations of sodium hydroxide and sodium carbonate with hydrochloric acid at different titration speeds

NaOH ($\times 10^{-3}$ M)		Error (%)	Na_2CO_3 ($\times 10^{-3}$ M)		Error (%)	K_w (int) ($\times 10^{-14}$)	Titration time (s)
added	found		added	found			
4.00	4.024	0.6	4.00	4.024	0.6	0.702	990
2.00	1.991	−0.5	8.00	7.964	−0.5	0.680	920
2.00	1.998	−0.2	7.96	7.952	−0.2	0.712	960
4.00	4.016	0.4	6.00	6.024	0.4	0.711	990
2.00	1.978	−1.1	8.00	7.912	−1.1	0.701	690
2.00	1.991	−0.5	8.00	7.964	−0.5	0.758	1380
2.00	2.009	0.5	7.96	7.963	0.5	0.732	1280
2.00	2.001	<0.1	7.96	7.966	<0.1	0.780	1600
10.00	10.040	0.4	5.00	5.020	0.4	0.780	2790
2.00	2.010	0.5	8.00	8.040	0.5	0.818	2970

TABLE 3

Results of titrations of sodium hydroxide and sodium carbonate with hydrochloric acid calculated with an average K_w (int) for series of titrations completed within about the same time

NaOH ($\times 10^{-3}$ M)		Error (%)	Na_2CO_3 ($\times 10^{-3}$ M)		Error (%)	K_w (int) average ($\times 10^{-14}$)	Titration time (s)
added	found		added	found			
4.00	4.022	0.55	4.00	4.026	0.65	0.701	990
2.00	2.004	0.20	8.00	7.956	−0.55	0.701	920
2.00	1.986	−0.70	7.96	7.996	0.45	0.701	960
4.00	4.020	0.50	6.00	6.000	0.00	0.701	990
2.00	1.986	−0.70	8.00	8.012	0.15	0.745	1380
2.00	2.015	0.75	7.96	7.964	<0.10	0.745	1280
10.00	10.060	0.60	5.00	5.013	0.26	0.799	2790
2.00	1.988	−0.60	8.00	8.048	0.60	0.799	2970

titration, the volume of a titrant addition, its number, the time-delay between additions and pH measurements, and the sample identification are entered via the teletype and stored in the disk file. The e.m.f. readings which are measured after each addition are stored in the same disk file as the sample data.

The initial estimates for the curve-fitting program, $C^0_{OH^-}$, $C^0_{Y^{2-}}$, K^0_1, and K^0_2 are obtained from the titration curve. The titration curve, a_{H^+} vs. ml, is calculated from the e.m.f. readings, the calibration constants, the number of additions, and the volume of each addition. $C^0_{OH^-}$ is taken as $K_w a_w/(a_{H^+} f_{OH^-})$ with the a_{H^+} value of the first point of the curve. $C^0_{Y^{2-}}$ is calculated from the volume of titrant when pH 4.0 has been reached. K^0_2, and K^0_1 are assumed

to be equal to the a_{H^+} values at the volumes where half the estimated amounts of Y^{2-} and HY^- have been neutralized.

Results and discussion

To test this method of end-point calculation for the determination of sodium hydroxide and sodium carbonate several synthetic samples were titrated and evaluated. It proved necessary to alter one of the remaining parameters, f_{H^+}, f_{OH^-}, and K_w, to remove a systematic deviation, involving an excessive hydroxide and deficient carbonate concentration. This deviation depended on the total titration time. Variation in K_w or f_{OH^-} had a larger effect on the calculated concentrations than f_{H^+}. Decrease in K_w increased the carbonate result and decreased the hydroxide result. A plot of the relative deviations for these two analytes versus K_w showed two straight lines; the intersection corresponded to a relative deviation of less than 0.5% of both concentrations. When about the same total time was used for titrations of different ratios of hydroxide and carbonate concentrations, the K_w corresponding to the point of intersection, K_w (int), did not vary very much (Table 2). These titrations were also evaluated with an average K_w (int). The systematic deviations were less than 1% (Table 3). An increase in the titration time did not improve the accuracy; a decrease to less than about 15 min seemed to worsen it.

The pH measurements must be accurate to ±0.01 pH unit. The pH of the standards was calculated from literature values for the dissociation constant of acetic acid, K_w, and the calculated f_{H^+} and f_{OH^-}. Separate sets of calibration constants were determined for the pH region 2—5 and for pH > 5. The differences in the constants of these sets can be attributed to the pH influence on liquid junction potentials. The calculations involving a 30-point titration take about 2.5 min.

The initial estimates of the parameters do not have to be very accurate. The calculations of the titrations listed in Table 2 can be started with the same set of initial estimates.

REFERENCES

1 A. K. Covington, R. A. Robinson and M. Garbar, Anal. Chim. Acta, 100 (1978) 367.
2 T. Anfält and D. Jagner, Anal. Chim. Acta, 57 (1971) 165.
3 C. McCallum and D. Midgley, Anal. Chim. Acta, 78 (1975) 171.
4 F. Ingman, A. Johansson, S. Johansson and R. Karlsson, Anal. Chim. Acta, 64 (1973) 113.
5 A. Johansson and S. Johansson, Analyst (London), 103 (1978) 305.
6 D. M. Barry and L. Meites, Anal. Chim. Acta, 68 (1974) 435.
7 D. M. Barry, L. Meites and B. H. Campbell, Anal. Chim. Acta, 69 (1974) 143.
8 M. Bos, Anal. Chim. Acta, 90 (1977) 61.
9 W. E. Wentworth, J. Chem. Educ., 42 (1965) 96.
10 H. S. Harned and B. B. Owen, The Physical Chemistry of Electrolyte Solutions, Reinhold, New York, 1964, pp. 726, 748, 752.

ACA announcements

ANNOUNCEMENTS OF MEETINGS

2nd INTERNATIONAL SUMMER SCHOOL ON DATA PROCESSING IN CHEMISTRY (DPC '80)

DPC '80 organized by the Polish Academy of Sciences and the Technical University of Rzeszów will be held on 24–31 August, 1980. It will cover basic problems of computer application in aiding experiments, modelling and simulating chemical processes, etc. Special attention will be paid to storage and retrieval of spectral data and organization of spectral data bases. Problems of computerized elucidatior of chemical structures through interpretation of spectral data with artificial intelligence will be discussed. Outstanding experts in computer applications will participate as invited lecturers. Further details Professor Dr. habil. Z. Hippe, Department of Physical Chemistry, Technical University, 35-959 Rzeszów Poland.

GERMAN SOCIETY FOR CRYSTAL GROWTH – ANNUAL MEETING, MARCH 1980

The annual meeting of the German Society for Crystal Growth will be held on March 18–21, 1980 in Karlsruhe. The meeting will include a discussion session on striations, and research papers on crystal growth and characterization, together with recent work relating to materials for energy conversion. Further information from: Dr. German Müller-Vogt, Kristall- und Materiallabor, University, Engesserstr. 7, D-7500 Karlsruhe, G.F.R.

33rd CHEMISTS' CONFERENCE – BRITISH INDEPENDENT STEEL PRODUCERS ASSOCIATION

The 33rd Chemists' Conference will be held at the Royal Hotel, Scarborough, England, on 4th and 5th June, 1980. An exhibition of scientific equipment will run concurrently with the Conference. This is the only U.K. conference of its type, devoted solely to Chemical Analysis relating to the Steel Industry, and as such provides a unique forum for Steelworks Chemists.

The conference fee will be £ 20.12.

Further details from: Mr. L.L. Green, The British Independent Steel Producers Association, 4 Melbourne Avenue, Sheffield, S10 2QL, Great Britain.

WORKSHOP ON TCDD AND RELATED COMPOUNDS, October 22–24, 1980, Rome, Italy

The International Association of Environmental Analytical Chemistry organizes annual symposia on "Advances in Environmental Analytical Chemistry" at different locations in Europe and North America. The 9th symposium in 1979 was held in Georgia, U.S.A. and the 10th symposium will take place in Dortmund, Germany, in May 1980. The Association is also organising a Workshop on TCDD and Related Compounds. This meeting will be problem-oriented and will include all aspects of analytical chemistry, environmental chemistry, human toxicology and ecotoxicology as well as case studies. Key areas will be treated by invited speakers. Emphasis will be placed on discussion and exchange of information possibly supported by short research papers and posters.

Attendance to this workshop is limited to a maximum of ca. 80 people. A balance between representatives from Universities, Government and Industry is sought; emphasis will be on maximum interaction between participants. The proceedings of this workshop will be published by Pergamon Press, Oxford.

Further information: Prof. Dr. O. Hutzinger, University of Amsterdam, Nieuwe Achtergracht 166, Amsterdam, The Netherlands.

CALENDAR OF FORTHCOMING MEETINGS

Apr. 17–19, 1980 Athens, Greece	**Balkan Chemistry Days – All aspects of research chemistry** Contact: B.C.D.'s Secretariat, The Association of Greek Chemists, 27, Kaningo Street, Athens (147), Greece.
April 22–24, 1980 London, Great Britain	**Labware 80** Contact: Labware Promotions, 28 Worple Road, London SW19 4EE, Great Britain.
April 23–25, 1980 King of Prissia, Pa., U.S.A.	**ACS – 14th Middle Atlantic Regional Meeting** Contact: Henry C. Beck, P.O. Box 133, Swarthmore, Pa. 19081, U.S.A. Tel. (215) 387-2255.
April 27–29, 1980 Neuherberg/Munich, F.R.G.	**First International Workshop on Trace Element Analytical Chemistry in Medicine and Biology** Contact: Dr. P. Schramel, Gesellschaft für Strahlen- und Umweltforschung, Physikalisch-Technische Abteilung, Ingolstädter Landstrasse 1, D-8042 Neuherberg, F.R.G.
April 29–May 2, 1980 Munich, F.R.G.	**Biochemische Analytik 80 (7th European Conference on Biochemical and Instrumental Analysis)** Contact: Dr. Rosmarie Vogel, Nussbaumstr. 20, P.O. Box 200324, D-8000 Munich 2, F.R.G. Tel. (089) 15 14 19.
May 25–30, 1980 New York, N.Y., U.S.A.	**28th Annual Conference of the Amer. Soc. for Mass Spectrometry** Contact: Dr. H.M. Fales, c/o NIH, Building 10, Room 7N 322, Bethesda, Md. 20014, U.S.A.
May 27–30, 1980 Balaton Lake, Hungary	**4th Symposium on Ion Exchange** Contact: Professor J. Inczédy, Organizing Committee, 4th Int. Symposium on Ion Exch., P.O. Box 28, Veszprém, H-8201 Hungary.
May 28–30, 1980 Dortmund, F.R.G.	**10th Annual Symposium on the Analytical Chemistry of Pollutants** Contact: J. Wendenburg, Gesellschaft Deutscher Chemiker, P.O. Box 900440, D-6000 Frankfurt/Main, F.R.G. Tel. (0611) 791 73 66. (Further details published in Vol. 113, No. 2)
May 30, 1980 Glasgow, Scotland, Great Britain	**High Speed Automatic Analysis** Contact: D.G. Porter, Laboratory of the Government Chemist, Cornwall Hous Stamford Street, London. SE1 9NQ, Great Britain.
June 2–3, 1980 Petten, The Netherlands	**Workshop on Ion-Chromatography – Development of Ion-Chromatography Techniques and Application of Ion-Chromatography** Contact: Dr. J. Slanina, Workshop on Ion-Chromatography, ECN, 1755 ZG Petten, The Netherlands.
June 4–5, 1980 Scarborough, Great Britain	**33rd Chemists' Conference – British Independent Steel Producers Association** Contact: Mr. L.L. Green, The British Independent Steel Producers Assoc., 4 Melbourne Ave., Sheffield S10 2QL, Great Britain.
June 8–11, 1980 Ottawa, Ontario, Canada	**63rd Canadian Chemical Conference and Exhibition** Contact: Don Emmerson, 151 Slater St., Suite 906, Ottawa, Ontario, Canada K1P 5H3, Tel. 613-233-5623.
June 10–13, 1980 Ghent, Belgium	**3rd International Symposium on Quantitative Mass Spectrometry in Life Sciences** Contact: Professor A.P. De Leenheer, Laboratoria voor Medische Biochemie en Klinische Analyse, de Pintelaan 135, B-9000 Ghent, Belgium.

June 16–18, 1980 Milan, Italy	**7th International Symposium on Mass Spectrometry in Biochemistry, Medicine and Environmental Research** Contact: Dr. A. Frigerio, Istituto di Ricerche Farmacologiche "Mario Negri", Via Eritrea 62, 20157 Milan, Italy.
June 18–19, 1980 London, Great Britain	**Nuclear Magnetic Resonance Spectroscopy in Solids** Contact: The Executive Secretary, The Royal Society, 6 Carlton House Terrace, London SW1Y 5AG, Great Britain.
June 23–27, 1980 Birmingham, Great Britain	**Eurochem 80** Contact: Andrew Dedman, Clapp & Polick Europe Ltd., 232 Acton Lane, London W4 5DL, Great Britain.
June 30–July 4, 1980 Cannes, France	**13th International Symposium on Chromatography** Contact: GAMS, 88 Boulevard Malesherbes, 75008 Paris, France.
July 20–26, 1980 Lancaster, Great Britain	**SAC 80** Contact: The Secretary, Analytical Division, The Chemical Society, Burlington House, London W1V 0BN, Great Britain. (Further details published in Vol. 106, No. 2 and Vol. 113, No. 2)
Aug. 4–8, 1980 Denver, Colo., U.S.A.	**Conference on Applications of X-Ray Analysis** Contact: Mrs. Mildred Cain, Denver Research Institute, University of Denver, Denver, Colo.,80208, U.S.A. Tel. 303/753-2141.
Aug. 4–9, 1980 Ottawa, Canada	**7th International Conference on Raman Spectroscopy** Contact: Mr. Ken Charbonneau, Conference Services, National Research Council of Canada, Ottawa, Ontario, Canada K1A OR6.
Aug. 17–23, 1980 Wolfeboro, N.H., U.S.A.	**Gordon Research Conference on Vibrational Spectroscopy** Contact: Dr. Erich Ipsen, Bell Laboratories, Holmdel, N.J. 07733, U.S.A.
Aug. 18–22, 1980 Brighton, Great Britain	**Micro 80** Contact: The Royal Microscopical Society, 37/38 St. Clements, Oxford OX4 1AJ, Great Britain.
Aug. 24–28, 1980 Espoo, Finland	**Euroanalysis IV – Conf. Fed. of European Chemical Societies** Contact: Prof. L. Niinistoe, University of Technology, Dept. of Chemistry, 62150 Espoo 15, Finland. (Further details published in Vol. 109, No. 1)
Aug. 24–29, 1980 San Francisco, Calif., U.S.A.	**ACS 180th National Conference – 2nd Chemical Congress of the North Amer. Continent** Contact: A.T. Winstead, 1155 16th Street, N.W. Washington, D.C. 20036, U.S.A.
Aug. 24–31, 1980 Rzeszów, Poland	**2nd International Summer School on Data Processing in Chemistry DPC '80** Contact: Prof. Dr. Z. Hippe, Dept. of Physical Chemistry, Technical University, 35-959 Rzeszów, Poland.
Aug. 25–29, 1980 Prague, Czechoslovakia	**J. Heyrovský Memorial Congress on Polarography** Contact: Czechoslovak Academy of Sciences, J. Heyrovský Institute of Physical Chemistry and Electrochemistry, Vlasská 9, CS-118 40 Praha 1, Czechoslovakia. (Further details published in Vol. 113, No. 2)
Aug. 25–30, 1980 Graz, Austria	**8th International Microchemical Symposium** Contact: Prof. Dr. A. Holasek, Institut für Medizinische Biochemie, Universität Graz, Harrachgasse 21, A-8010 Graz, Austria. Tel. (0 316) 32 5 32 or 76 5 91. (Further details published in Vol. 109, No. 1 and Vol. 110, No. 2).
Aug. 25–30, 1980 Delft, The Netherlands	**Joint ISMAR–Ampère International Conference on Magnetic Resonance** Contact: ISMAR-Ampère 1980, Postbus 30424, NL.2500 GK Den Haag, The Netherlands.
Sep. 7–12, 1980 Florence, Italy	**IUPAC International Symposium on Macromolecules (Structural Order in Polymers)** Contact: Macro IUPAC 80, Fondazione Giovanni Lorenzini, Via Monte Napoleone 23, 20121 Milan, Italy.

Sep. 8–10, 1980 Oxford, Great Britain	**Photoelectrochemistry Discussion** Contact: Dr. M.D. Archer, Dept. of Physical Chemistry, Univ. of Cambridge, Lensfield Road, Cambridge, Great Britain.
Sep. 9–12, 1980 Eindhoven, The Netherlands	**2nd International Symposium on Isotachophoresis** Contact: ITP 80, Afd. Instrumentele Analyse, Technische Hogeschool Eindhoven, Postbus 513, 5600 MB Eindhoven, The Netherlands.
Sep. 16–19, 1980 Bratislava, Czechoslovakia	**6th International Symposium on Advances and Application of Chromatography in Industry** Contact: Dr. Ján Remeň, Analytical Section ČS VTS,pri n.p. Slovnaft, 82300 Bratislava, Czechoslovakia.
Sep. 22–26, 1980 Paris, France	**European Conference on Chemical Pathways in the Environment** Contact: Dr. C. Troyanowsky, Société de Chimie physique, 10, rue Vauquelin, F-75005 Paris, France. Tel. 707-54-48.
Sep. 23–25, 1980 Cardiff, Great Britain	**Chemical Society/Analytical Division – CS Autumn meeting: Trace and Ultratrace Analysis** Contact: The Secretary, Analytical Division, The Chemical Society, Burlington House, London W1V 0BN, Great Britain.
Sep. 24–28, 1980 Hamburg, F.R.G.	**EMBO-EMBL** **Workshop on X-ray and Neutron Scattering of Biological Structure** Contact: Prof. H. Stuhrmann, EMBL c/o DESY, Notkestrasse 85, D-2000 Hamburg 52, F.R.G.
Sep. 28–Oct. 3, 1980 Philadelphia, Pa., U.S.A.	**7th Annual Meeting of Federation of Analytical Chemistry and Spectroscopy Societies (FACSS)** Contact: Mrs. J.G. Graselli, c/o Standard Oil Co., 4440 Warrensville Road, Cleveland, Ohio 44128, U.S.A.
Sep. 29–Oct. 3, 1980 York, Great Britain	**Modern Radiochemical Practice** Contact: The Secretary, Analytical Division, Chemical Society, Burlington House, London W1V 0BN, Great Britain.
Oct. 6–9, 1980 Houston, Texas, U.S.A.	**EXPOCHEM '80** Contact: Professor A. Zlatkis, Chemistry Department, University of Houston, Houston, Texas 77004, U.S.A. Tel. (713) 749-2623.
Oct. 16–17, 1980 Teddington, Middx., Great Britain	**Quantitative Surface Analysis** Contact: The Meetings Officer, The Institute of Physics, 47 Belgrave Square, London SW1X 8QZ, Great Britain.
Oct. 19–23, 1980 Washington, D.C., U.S.A.	**Annual Meeting of Assoc. of Official Analytical Chemists** Contact: K.M. Fominaya, Box 540, Benjamin Franklin Station, Washington, D.C. 20044, U.S.A.
Nov. 19–21, 1980 New York, N.Y., U.S.A.	**19th Eastern Analytical Symposium** Contact: Norman Gardner, Exposition Manager, 73 Ethel Street, Metuchen, N.J. 08840, U.S.A. Tel. (201) 548 7377.
Dec. 16–17, 1980 Brighton, Great Britain	**Chromatography, Equilibria and Kinetics** Contact: Mrs. Y.A. Fish, The Chemical Society, Burlington House, London W1V 0BN, Great Britain. Tel. 01-7349971.
July 6–9, 1981 Strasbourg, France	**27th IUPAC Symposium on Macromolecules** Contact: Secretariat, Macro 1981, Société de Chimie Industrielle, 28, rue Saint-Dominique, 75007 Paris, France.
Aug. 16–22, 1981 Vancouver, Canada	**28th Congress International Union of Pure and Applied Chemistry** Contact: Congress Secretariat, 28th IUPAC Congress, c/o The Chemical Institute of Canada, 151, Slater Street, Suite 906, Ottawa, Ontario, Canada K1P 5H3.
Aug. 23–28, 1981 University of Auckland, New Zealand	**Golden Jubilee Conference "Chemistry in the Service of Man"** Contact: Dr. D.J. McLennan, Chemistry Dept., Univ. of Auckland, Auckland, New Zealand.

VOL. 122, No. 1 ANALYTICA CHIMICA ACTA March 1, 1980

(Computer Techniques and Optimization, Vol. 4, No. 1)

CONTENTS

Printed in The Netherlands.